Novel Cellulose Based Foam-Formed Products: Applications and Numerical Studies

by

Pouyan Jahangiri

B.Sc. Mechanical Engineering, Amirkabir University of Technology, 2010

A THESIS SUBMITTED IN PARTIAL FULFILLMENT
OF THE REQUIREMENTS FOR THE DEGREE OF

Master of Applied Science

in

THE FACULTY OF GRADUATE AND POSDOCTORAL STUDIES
(Mechanical Engineering)

The University Of British Columbia
(Vancouver)

November 2013

Abstract

A novel methodology using cellulose fibres in foam laid media is proposed in order to produce biodegradable, low-density porous materials called foam-paper. Foam-forming is a process in which paper-making fibres are located among the bubbles created by aqueous solution of surfactant. Finally, the suspension is de-watered and a 3D structure of fibre-network is made. Due to the 3D porous structure, high specific volume and capability of cellulose to participate in chemical reactions, these new products can be applied in heat insulation, sound absorption and aerosol filtration. Simplicity of production, biodegradability and being economically affordable are the most noticeable factors which prefer foam-papers to the other products with similar applications. In the current work, the first set of experiments is done on morphological characteristics of foam-papers. The effect of manufacturing condition (foam air-content) and fibre morphology such as fibre length and coarseness on the characteristics of the final product is studied. The influence of fibre specific surface (by adding valley beaten fibres), fibrillation (by using PFI refined fibres) and different pulp types is also investigated on tensile-index and specific volume (bulk) of the final products. The second set of experiments is run to specify the novel applications of foam-papers in sub-micron aerosol filtration, heat insulation and sound absorption. In order to perceive the physics of the flow though the grossly disordered geometry of foam-papers and also for providing insight into the structure of these novel products, numerical simulations based on Lattice-Boltzmann technique are carried out. For this purpose, 2D micro X-ray tomographic images are taken from the cross-section of some foam-paper samples to reconstruct their 3D structure. Finally, a model based on random cylinders and the frequency distribution of fibres in the thickness of the samples is proposed to reduce the huge amount of memory and large amount of CPU time.

Preface

The current thesis is about proposing a novel methodology using cellulose fibres in foam laid media in order to produce biodegradable, low-density porous materials called foam-paper which has taken place in the period of 2011 to 2013.

The first chapter of the study is about answering to three fundamental questions to inform why this research was carried out. The questions are mainly about ”Why we start making foam-papers?”, ”How we came up with the idea of making foam-papers?” and ”What we did in our research to introduce these new products?”. The need for writing this chapter is identified by Dr. D. Mark Martinez and Pouyan Jahangiri gathered the information to answer these question.

In the second chapter, the major characteristics of foam-papers are studied. The research is conducted on measuring some physical and mechanical properties of the foam-papers. Dr. Ario Madani proposed the need to study the effect of fibre morphology on the properties of the final products. The experiments was continued by Pouyan Jahangiri to understand the effect of fibre morphology foam-papers properties. This chapter is supervised by Dr. James A. Olson and Dr. D. Mark Martinez.

In the third chapter, the applications of foam-papers on sub-micron aerosol filtration, thermal insulation and sound absorption were investigated. Dr. James A. Olson proposed to design experiments to measure the foam-paper properties for these three applications. The experimental work were carried out by Pouyan Jahangiri. The contribution of UBC aerosol lab (Courtesy of Dr. Steven N. Rogak) and UBC research centre for Acoustic Research (Courtesy of Dr. Murray R. Hudgson) were significant. This chapter was authored by Pouyan Jahangiri and supervised by Dr. James A. Olson and Dr. D. Mark Martinez.

In the fourth chapter, the purpose of the chapter was to understand the physics of the flow inside the porous media and finally to simulate the flow inside the geometry of foam-papers (Courtesy of Dr. A. B. Phillion UBC Okanagan campus). The Lattice-Boltzmann method is proposed by Dr. D. Mark Martinez for the flow simulation. Pouyan Jahangiri carried out the numerical analysis and

developed a 3D unsteady solver based on the Lattice-Boltzmann method for parallel machines. A model geometry based on randomly oriented cylinders and fibre concentration in foam-papers were proposed by Pouyan Jahangiri. This chapter was authored by Pouyan Jahangiri and supervised by Dr. D. Mark Martinez and Dr. James A. Olson.

Table of Contents

List of Tables

List of Figures

Nomenclature

A	Area
AC	Air-Content
C	Concentration
c_k	Discrete velocity in k^{th} direction
c_s	Lattice speed of sound
D_p	Pore diameter strength
d_p	Particle diameter Weight
F	External force
f	Probability distribution function (PDF)
f_1	PDF of the first particle
f_{12}	Two particles PDF
f_{123}	Three particles PDF
$f_{1'}$	Post collision PDF
f^e	Equilibrium PDF
f^{ne}	Non-equilibrium PDF
f^*	Superficial PDF in FHM method
f_k	PDF in k^{th} direction
$\tilde{f}_k$	Post collision PDF in k^{th} direction
H	H function
K	Permeability
k	Thermal conductivity
L	Length
L_t	Thickness
Ma	Ma number
m	mass
P	Pressure
Q	Flowrate
Q_H	Heat flowrate
Q_{12}	Collision operator
$\vec{q}$	Flux
$\vec{q}_H$	Heat flux
Re	Reynolds number
Re_P	Pore Reynolds number
Re_d	Reynolds number based on diameter
$\vec{r}$	Particle position in phase-space
S	Entropy
S_s	Specific surface
T	Temperature
TI	Tensile-Index
T_H	Hot plate temperature
T_C	Cold plate temperature
S_s	Specific surface
T	Temperature
V_s	Superficial velocity
V_T	Thermal velocity
V_{rel}	Relative velocity
$\vec{v}$	Particle velocity in phase-space
μ	Dynamic viscosity
η	Filtration efficiency
ϕ	Porosity

$\vec{n}$	Normal unitary vector
$\mathscr{T}$	Tortuosity
ρ	Density
σ	Scattering function
Ω_s	Solid angel
K_B	Boltzmann constant
τ	Relaxation time
w_k	Weighting function in k^{th} direction
Δ	Geometric parameter in FHM algorithm
χ	Extrapolation parameter in FHM algorithm

Acknowledgments

I would like to express my deepest appreciation to my supervisors, Professor James A. Olson and Professor D. Mark Martinez who continually and convincingly conveyed a sprit of adventure in regard to research. Without their guidance and persistent help this dissertation would have not been possible.

I would like to thank Dr. Steven N. Rogak and Dr. Murray R. Hodgson for providing experimental facilities in UBC Aerosol Lab and UBC Centre of Acoustic Research.

I sincerely thank Anupam Biswas for his indispensable support, suggestions and scientific discussions during this project.

I would like to thank Sadaf S. Zeinoddini, Banda Logawa, Yash Sharma, Amin Engarnevis, James Montgomery, Mina Samimi, Mostafa Mohsenvand, Dr. Reza Korei and Dr. Ario Madani for their great help and support during this research.

I would like to thank George Soong and Nici Darychuk for their continuous assistance in UBC Pulp and Paper Centre and other members of the Centre for all the social activities that helped to maintain a positive atmosphere.

I would like to thank the Natural Science and Engineering Research Council of Canada (NSERC) and all members of Green Fiber Networks society for their help and support.

Finally, I would like to thank my family and all my friends for their unconditional support.

Pouyan Jahangiri

Dedication

To my mother, the best person I have ever met.

Chapter 1

Introduction

Climate change and pollution caused by use of non-renewable fossil fuel products has deleterious impact on human health, in addition, continuously increasing price of oil raises the need of substituting the oil based products by green renewable ones. As the world's environmental consciousness and knowledge about the importance of the green products is progressing, the demand for these materials is increasing. The first and the oldest eco-label certificate, is awarded by the Blue Angel, launched in Germany[1] in 1978 for services and products which are environmentally compatible. Blue Angel covers about 10000 products in 80 different categories[1]. After this revolutionary idea, many countries started issuing their own national and international certificates. Today, numerous countries like Japan, India, Malaysia and so many other Asian countries have their own certificates and standards for green products (up to 50 different types of different green certificates and labels). The main message of these certificates is to inform the customers about the importance of the final products being environmentally compatible as it helps in local and global contamination reduction. Biodegradable substances are materials which are able to be decomposed in natural environment. One of the most important sub-branches of biodegradable materials is called green-renewable which can be derived from existing plants and trees. These substances can be recycled and reproduced again. Cellulose is one of the most abundant, cost effective renewable resources that can be used as an initial substance for making green products. In 2009 printing grade paper comprised the largest (up to 66% of the whole pulp and paper industry) share of all paper grades consumed in the North-America followed by container-board (used for packaging applications), followed by tissues as illustrated in Figure 1.1.

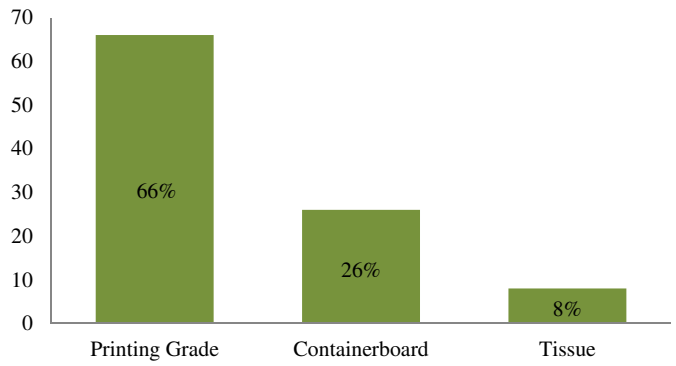

Figure 1.1: Total paper consumption by Paper Grade, North America (2009) [1]

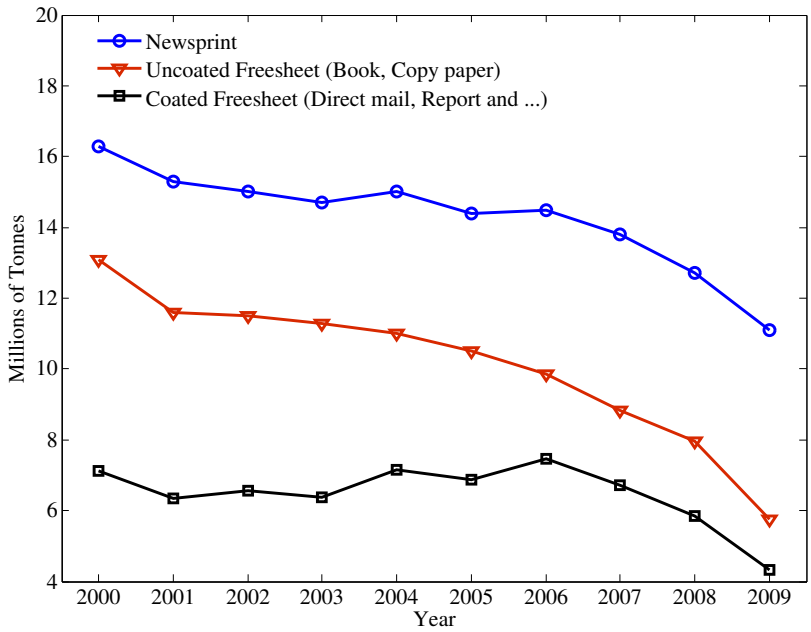

Figure 1.2: Total paper consumption by Printing Grade, North America (2000-2009) [1]

From 2006 to 2009, total North America paper consumption in printing grades (Newsprint, Uncoated Freesheet and Coated Freesheet) decreased by 24% as depicted in Figure 1.2 . Based on this information, it can be concluded that the profitability of traditional markets of paper grades (mainly printing grades) as a major part of North America's forest and pulp and paper industries,

are diminishing and regaining seems improbable. The renovation in forest and pulp and paper industries in North America (especially in Canada), will take place if the production line policies are revolutionized. One way for getting closer to this purpose is to switch from the current paper production lines to more profitable and innovative ones.

1.1 Foam-paper research: a brief introduction

In follow up to one of the major missions of the Canada's strategic network for the development of innovative green wood fibre products, this research is conducted on production of novel eco-friendly lignocellulosic fibre-based materials in foam medium. In this process, the honeycomb three dimensional geometry of foam is used as a template in order to obtain an open structure. Since the final product has a 3D porous structure, has extremely low density and is uniquely soft, it can be applied as aerosol filters, heat insulators, impact resistors and sound absorbers.

The Procedure of making foam-paper looks almost similar to regular paper-making process. In the process of making handsheet, first a suspension of pulp and water in a specified consistency (between 0.5% to 1.0%) is made. After that, a specified volume of pulp slurry for target grammage of 100 g/m^2 based on TAPPI standard procedure is de-watered under vacuum. At this stage, fibres are deposited on one layer of forming fabric and eventually, the handsheet is oven dried. In foam-paper making procedure, the pulp slurry is prepared by adding up a percentage of standard surface active agent (surfactant) under strong shear force which results in uniform bubbles in mixture. This uniform bubble medium plays the role of a 3D template for the fibres that are already located in between the bubbles. The resulting shear thinning suspension is de-watered under vacuum and the sample is air dried without pressing for 24 to 48 hours in CTH [1] room. The final product has open 3D structure, high porosity, high permeability and is extremely light.

In the first study, an attempt is made to comprehend general characteristics of foam-papers. For this purpose, two different pulp types, NBSK[2] and CTMP are used to make the samples in different foam air-contents. It is generally figured out that by increasing foam air-content, bulk and porosity of samples increased which can be considered as the main advantage of the method. However, it has to be mentioned that the disadvantage of the current method is noticeable loss of some mechanical properties like tensile-index. To overcome this problem two different fibrous

[1] Constant Temperature and Humidity
[2] Northern Bleached Softwood Kraft

strengthening additives are added to the structure of foam-papers (valley-beaten NBSK fibres and PFI refined NBSK) and effect of fibre specific surface and freeness are studied. Improvement in results of tensile-index is observed in both cases. It is shown that high specific surface valley-beaten fibres show much more improvement (up to 70% tensile-index of the standard handsheet) but bulk reduction is the penalty which is paid for this achievement. In order to be more precise about the effect of fibre morphology on the final product characteristics, fractionation is applied and the effect of different fibre length is investigated on the bulk and tensile-index of final products.

In the second study, three different applications of foam-papers are studied experimentally. The first one is the application of foam-papers as sub-micron aerosol filters. Pressure drop and permeability of foamed filters are measured using the apparatus in UBC aerosol laboratory as shown in Figure 3.14. Scanning Mobility Particle Sizer (SMPS) is also connected to the same setup to measure the filtration efficiency of foam-papers in sub-micron particle range (between 10 *nm* and 600 *nm*). Effects of fibre type (using different pulps: NBSK and CTMP), fibre specific surface and freeness (using NBSK valley beaten fibres and PFI refined NBSK respectively) and morphological characteristics of fibres such as fibre length and coarseness (using fractionated NBSK pulp) on filtration efficiency of foam-papers are studied. To understand the effect of crowding number, a brief study is done on some new samples of foamed filters made up of nanofibrillated fibres in pretty high foam air-contents (50% to 70%) using freeze-drying technique. Finally the results are compared to some available data of commercial aerosol filters.
The second one is the application of foam-papers in heat insulation. Samples of the same grammage (100 g/m^2) but different porosities of NBSK foam-paper made up of NBSK pulp is used in the experiment. Thermal conductivity of samples is measured using TPS[3] standard analysis method at three different temperatures and the results are compared to some available results of commercial heat insulators. The third one is the application of foam-papers in acoustics. Samples of NBSK pulp made in three different foam air-contents are used for sound absorption coefficient measurement in low frequencies. The experiment is also done for multi-layer foam-papers and foam-papers made up of nanofibrillated fibres. The results of absorption coefficients are compared to commercial acoustic materials.

In the third study, the physics of the flow inside grossly disordered geometry of foam-papers is the matter of interest. For this purpose, micro X-ray tomography technique is used to take 2D

[3]Transient Plane Source

images of the cross-section of sample. Initially, some image processing techniques are applied to de-noise and binarize 2D images. After that, 2D images are reconstructed to a 3D matrix for making the actual geometry of the foam-paper. Other useful information such as density distribution in the thickness and porosity of foam-papers is also computed based on the results of the micro X-ray tomograph. After reconstructing the geometry, a 3D parallel flow solver based on Lattice-Boltzmann method (LBM) is developed using C/C++ language on Linux platform. At the beginning, the code is validated for some well-known 2D and 3D problems and the results are compared to some CFD [4] results of FLUENT simulations and some available literature for low and moderate Reynolds numbers. Then the results of permeability of the simulation for some fibrous porous geometries made by 3D random cylinders are compared to some previous LBM simulations and mathematical models. Finally, a model for the geometry of foam-papers based on the data from micro X-ray tomography (density distribution function in thickness) using 3D random cylinders is proposed and used instead of using the actual geometry for reducing the large amount of CPU time. The flow is solved for the computer generated geometry of a foam-paper and values of permeability are computed.

[4] Computational Fluid Dynamics

Chapter 2

Background

2.1 Foam structure, characteristics and rheology

Before discussing about foam forming process and its application in paper making, it seems appropriate to have a brief review on rheology and characteristics of foam, dynamics of foam, foam drainage and foam flow in porous media.

2.1.1 Structure

Most of the time, the word “Foam” is used for aqueous foam i.e. a substance that encompasses uniform or non-uniform concentrated dispersion of gas bubbles (non-continuous phase) in a volume fraction of water (continuous phase) which contains a percentage of surfactant[2]. Usually, in aqueous foams, volume fraction of bubbles called foam air-content is greater than volume fraction of water. Foams are broadly divided into ”wet” and ”dry” based on volume fraction of water. The air-content of wet foams is normally less than 80% and the shape of the bubbles is very close to a complete sphere as it is shown in Figure 2.1 but the air-content of dry foams is greater than 90% (the volume fraction of liquid part is less than 10%) and the shape of the bubbles is very similar to polyhedral.

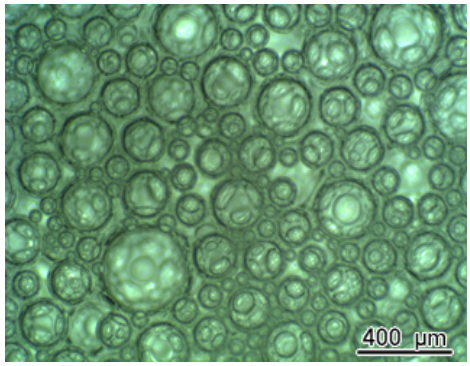

Figure 2.1: Image of a wet foam. (UBC Pulp and Paper Centre)

The 3D random cellular morphology of the foam is long matter of interest for mathematicians. In fact, foam mathematics is a multi-scale system in many cases. The first scale is bubble scale. In this scale foam is studied as "idealized foam", the geometry of foam is a good candidate for mathematical problems of 3D tessellations and minimal surfaces problem. In 1887 Lord Kelvin asked his famous question which was "What is the most efficient bubble foam?". Indeed, dividing a 3D space into equi-volume cells using minimum surface area between them is the matter of question and is referred to as "Kelvin's Problem". Kelvin proposed his famous model based on bi-truncated cubic honeycomb, which is called "Kelvin's Structure"[3] which is accepted as the solution for this problem until it is disproved by Denis Weaire, German physicist and his student Robert Phelan in 1993[3] and the model was called Weaire – Phelan structure. This model is known to be the most optimal unit cell of a perfectly ordered foam (ideal foam). In mid 19th century, Belgian physicist, Joseph Plateau describes the structure of soap films based on his experimental observations. Many other different examples with almost the same pattern in nature also conform Plateau's law[4]. In the second scale which is smaller than size of a bubble, the continuum liquid that splits the flat faces between two bubbles is called the lamella. The area that three lamella intersect is called Plateau border of the foam. The third scale, is the scale for gas-liquid interface at the film separation surface which most of the time is occupied by surfactant molecules to stabilize the foam at larger scale.

Major properties of foam such as stability and viscosity is specified by bubble diameter, bubble size distribution and air-content (related to foam density). Numerous experimental and numerical studies have been carried out on the effect of bubble size and bubble size distribution on characteristics of the final foam. It is important to study the effect of these parameters since they have

significant effect on the final product's quality. For instance Isarin *et al.*[5] mention in their article that in textile technology, the quality of final product is strongly dependent on the bubble size distribution of foam. Gidoa *et al.*[6] perform an experimental study on measuring bubble size of an aqueous foam in two different foam air-contents which are made by applying high shear force using rotary mixers. They generally measure that increasing the angular speed of the mixer causes a reduction in average bubble radii. They also observe that the mean bubble size is slightly smaller in higher air-content foam than the lower air-content one, however, no result is presented about the bubble size distribution. The experimental study on the bubble size distribution of foam which is produced by the same technique as Gidoa *et al.*[6] is conducted by Kroezen[7, 8]. The author finds that the average bubble radius decreases as the applied mean shear force increases. In follow up to this study, a non-linear relationship between bubble size distribution and mean bubble radius is found for different foam air-contents in various flow regimes (from laminar to turbulence). Hirt *et al.*[9] investigate the effect of viscosity of the liquid phase of foam on the average bubble radius for low air-content foams. The author finds that by increasing the viscosity of liquid phase, the mean bubble size diminishes especially in the foams with lower air-content. An interesting study is done by Chang *et al.*[10] on measuring mean bubble diameter and its distribution by freezing small samples of foam. The author shows that freezing the aqueous foam (foam in solid state) will not affect the bubble size and its distribution. So this can be considered as easier approach for investigating on the foam structure. Isarin *et al.*[5] utilized image analysis techniques in order to compute bubble radii and bubble size distribution in an aqueous foam. This study is one of the earliest studies which used image analysis technique to calculate foam parameters. The author finds a good reproducibility in their results comparing to the other available experimental studies. Many other researchers have done studies on using different imaging techniques such as Diffusing-Wave Spectroscopy (DWS), X-ray tomography, Neutron Scattering and Magnetic Resonance Imaging (MRI) to reconstruct a clear 3D image of foam structure. The internal bubble architecture has been also studied computationally using sequential attempts of evolution of the minimum surface energy both in deterministic (surface evolver technique[11]) or probabilistic methods (Ising model and Potts model[12]).

There are also different types of foams in which the continuous part can be a solid or can be other liquids such as liquid metal or polymeric liquid. Solid foams are made by dispersion of gas bubbles inside a solid medium. These materials are actually solid porous structures which are considered as cellular light and bulky engineering materials with vast applications in different industries. They are categorized into two major divisions, closed-cell foams and open-cell foams.

Closed-cell foams are those which do not have interconnected pores so they normally have more density and less air volume fraction. Open-cell foams are those which have interconnected pores and consequently, this category is more permeable, softer and cheaper (needs less amount of material) than closed-cell foams. Metal foams and polymeric foams are two examples of the most important industrial solid foams. Metal foams are cellular structures containing a large volume gas-fraction which are made by solid metals mainly aluminum alloys. These materials have vast application in making orthopedic tools. Polymeric foams are materials containing a polymeric matrix with interconnected pores or air bubbles (closed pores). They are used in a broad variety of applications such as insulation materials, disposable packaging and ultra soft materials. In this thesis, the word "Foam" points to wet foam which is a result of surfactant agitation in aqueous environment.

2.1.2 Characteristics and stability

Foam stability is capability of foam to persist for noticeable length of time without losing its 3D structure and collapsing into two detached constituent phases. In order to be more accurate, from thermodynamic point of view, aqueous foams are inherently unstable and breaking down happens in the direction of diminishing total surface free energy. Surface active agents can contribute to delaying foam decay to a great extent. Without using surfactant, though bubbles can be generated by applying high shear force on fluid, the final two phase fluid will not last long due to gravity which causes liquid drainage, Laplace pressure which causes mass transfer from smaller to larger bubbles and osmotic pressure which causes an internal drainage in the foam structure from lamella to Plateau borders due to local concentration difference[13]. In the first mechanism, the liquid is discharged due to its own weight. The more fluid is draining, the thinner the lamella is becoming and eventually this will result in rupture of foam bubbles. In the second mechanism, which mostly happens in poly-disperse[1] foams, spontaneous diffusion of gas through the interface from smaller bubbles to neighbouring larger bubbles happens[13, 14]. This phenomenon is already predicted by Young - Laplace equation. Based on this equation, capillary pressure is inversely proportional to the effective radius of interfacial film i.e. smaller bubbles cause higher capillary pressure which eventually results in the inter-diffusion of gas from smaller bubbles to the adjacent larger ones. This procedure spontaneously increase the average size of the bubbles in foam media (by shrinkage of smaller bubbles and expansion of the larger adjacent bubbles) and makes narrower foam film which results in bubble bursting and failure in the 3D structure of foam. In the third mechanism, since the

[1] Non-uniform bubble size distribution

lamella is slightly curved, Plateau border has lower pressure than lamella. The pressure gradient results in liquid drainage from lamella to Plateau border which makes the lamella very narrow and finally the foam structure will collapse.

Both bubble formation and foam stability can significantly be improved by adding surface active agents (surfactants) to the liquid. Surfactants are materials that reduce the surface tension of a liquid or the interfacial tension of two liquids. Surfactants are amphiphilic i.e. their molecules have both hydrophilic (polar) group in the water solution and hydrophobic (non-polar) group away from water. Surfactant molecules are accumulated in the gas-liquid interface and contributes to stabilize the detached dispersed gas phase in the liquid phase. The addition of the surfactant molecules into the interface provides an expanding force against the surface tension[15] which diminishes the existing tension at the gas/liquid interface and finally reduces the effective surface tension. Surfactants contribute to bubble formation by decreasing the total surface energy. The energy required to make a change in surface area is given by:

$$dG = \gamma dA \tag{2.1}$$

where dG is surface free energy and γ is surface tension. The greater the amount of adsorption of surfactant molecules, the greater the decrease in γ. A decrease in γ results in diminishing the total surface free energy, so bubbles need less energy to form. It should be also noted that, increasing the surfactant concentration will not always result in decreasing surface tension. The critical micelle concentration (CMC) is defined as the concentration of surfactant above which the surface tension remains relatively constant due to the formation of micelles. Before reaching CMC, considerable change in surface tension can be observed[2, 16].
Surfactants can also contribute to make more stable foam. As mentioned before, a destabilizing mechanism exists due to the curvature in lamella and pressure gradient between Plateau region and lamella. The continuous liquid phase in lamella is attached to the bubble surfaces by the hydrophilic part of surfactant molecules. Presence of surfactant in this part is very important which can reduce the surface tension in the foam lamella. Reducing the surface tension incur reducing in Laplace pressure as predicted by Young-Laplace equation.

$$\Delta P = \gamma(\vec{\nabla}.\hat{n}) \tag{2.2}$$

By diminishing the Laplace pressure, the amount of fluid which would continuously drain to

Plateau border reduces. This helps the foam to become more stable. DLVO theory[2][17] can explain foam stability in more detail. Based on DLVO theory, the forces which play vital role in stabilizing foam are Van-der-Waals attraction between the surfaces of bubbles and the electrostatic repulsion if the lamella contains ions. In the absence of surfactant (no ions in lamella) the Van-der-Waals attractive force causes bubbles to get closer to each other and the resulting pressure drains the fluid of lamella to Plateau border. Consequently, this will lead to thinning the lamella and merging bubbles, which eventually results in destabilizing the foam. However, increasing the concentration of surfactant incur increasing the charge density in lamella which increases the effect of electrostatic repulsive forces. The final trade off between attractive and repulsive forces increases the stability of the final foam if the concentration of surfactant is sufficient.

2.1.3 Rheology

Although the structure and stability of foam are investigated in general literature, rheology of foam as a complex non-Newtonian fluid is also a matter of concern. By increasing the application of foam in different engineering processes, studying foam flow both from fundamental points of view[18–20] and engineering applications view point becomes more important. For instance Krug[18], Wendorff and Ainley[19] and Lincicome[20] study foam flow and rheology in different pipes and co-centric cylinders. Many other works deal with the application of foam in oil industry such as application of foam to move and displace oil through a granular structure. Experimental studies on foam flow and rheology is started by Sibree[21] and Grove *et al.*[22] on soap-foam and fire-fighting foam. Different types of viscometers and other non-viscometer apparatus have been setup by different researchers to investigate various rheological parameters of foam such as fractional force which delays the foam flow, viscosity and stress-strain relationship by changing the concentration and type of surfactant and different techniques for foam preparation which has a major effect on the rheological properties of the final foam.

The rheology of foam is one of the most interesting fluid mechanics problems due to the specific liquid/gas dispersion structure. Based on the results of the works cited earlier, a single rheological behaviour is not reported. The reason behind it is related to geometrical scale of bubbles which are comparable to the geometrical scales of fluid phase and measuring apparatus.
Thus, a small change in the structure of the foam (for example due to foam drainage and collapse during the test) results in a noticeable change in the measurement of the final rheological parame-

[2]Derjaguin-Landau-Verwey-Overbeek theory

ters, flow behaviours and finally leads to significant statistical fluctuations. The parameters which have main effect on the foam flow and rheology are the ratio of average bubble volume to the flow channel size, bubble size distribution, foam interaction with channel walls, type of fluid and surfactant, isotropy of bubble distribution, absolute pressure and the flow regime (depends on the Reynolds number). It should be noted that in most of surveys, final results are affected by some of the parameters that their influence is not taken into account. Rotational viscometry[14] and capillary tube viscometry[14] are two major methods to measure the rheological characteristics of aqueous foams. Marsden and Khan[23] use a rotary viscometer (modified fan VG meter) to measure apparent viscosity of a continuous flow of foam in the range of 70% to 96% air-content. They find that foam is a shear-thinning fluid and the values of apparent viscosity are between 55 cP and 500 cP. They also investigate the effect of air-content and rotational speed on the foam apparent viscosity. Based on Marsden and Khan[23] results, apparent viscosity increases by increasing the foam air-content at the same rotational speed and decreases by increasing the rotational speed in the same air-content.

Later, Wenzel *et al.*[24] study the effect of slip of foam flow on a smooth surface in a co-axial cylindrical viscometer and later on the cone viscometer. Wenzel *et al.*[24] conduct their experiments for numerous dried foams and plot the growing trend of shear stress by increasing the angular velocity of viscometer. Patton *et al.*[25] utilize the method of capillary tube viscometry by studying foam motion in long capillary tubes at upstream and releasing to atmosphere at downstream. They apply this method due to the utilization and applicability of such rheological results to understand the physics of the foam flow in porous media. Patton *et al.*[25] find that the value of normalized pressure drop (with respect to inlet pressure) is close to 1. This implies that as the foam continues flowing along capillary tubes, it also considerably expands which results in two essential conclusions. First, bubble size distribution changes along the capillary tube (larger bubbles are observed at the outlet). Second, it is found that the foam pressure varies non-linearly along the capillary tube; However, drainage of the liquid part of foam leads to bubble rupture and eventually changing the rheology of foam inside capillary tubes. The latter effect is also depends on the diameter of the test tube and wall slip condition. This geometry dependency of foam rheological parameters (here apparent viscosity) is investigated by many researchers[24–26]. Patton *et al.*[25] also figure out that the relationship between dP/L and the foam flow rate in the same tube diameter is non-linear. Hirasaki and Lawson[26] prove both theoretically and experimentally that the rheological characteristics of foam are strongly dependent on the diameter of the capillary tube at the same flow regime.

Many other researchers studied foam dynamics with a different point of view. Foam can also be viewed as a continuous bulk non-Newtonian fluid. Different non-Newtonian fluid models for the stress-strain relations such as power law and Bingham plastic have been tried to predict the behaviour of foam as a continuous fluid by comparing to the experimental results which are geometry dependent. This dependency of models to geometry seems to arise due to unidentified effect of at least one essential parameter in the experiments as discussed before. This problem is overcome and demonstrated by Kraynic[27] by combining two different theories concerning shear deformation for foam-flow inside a tube. This research motivated scientists to write more general models for shear deformation of flowing foam. For a 2D ideal mono-disperse foam, Princen[28] predict a yield stress which causes a deformation. To be more precise, before reaching this value only elastic deformation could happen; However after reaching the critical value, the cells (represents the bubbles trapped in the fluid phase of the foam) in the row which is closer to the applied shear stress shift their location by one cell in the direction of applied shear force. This situation is dramatically idealized and compared to the 3D poly-dispersed structure of the actual foam but such yield stress can also be predicted for the real foam. Princen[28] also finds a relation for the yield stress of ideal two dimensional mono-disperse foam. He finds that the values of yield stress is proportional to the values of surface tension and inversely proportional to the values of bubble diameter. The dimensionless factor of proportionality is a value close to unity and is strongly dependent on the foam air-content. Hirasaki and Lawson[26] modify Princen's[28] relation for the yield stress to reach a critical capillary number for the two dimensional ideal foam. For this purpose, they use the idea of hydraulic diameter of the wetted perimeter of the foam lamella which osculates the tube wall. They also extend the analysis of single bubble motion to motion of a bubble chain which are split by lamella.

Another interesting topic in foam dynamics is foam flow in grossly disordered and porous structures. This topic is of great concern in many industries especially in oil industry. The major equation that relates the flow rate to the pressure drop of porous media irrespective of the internal geometry of the media is Darcy's equation. Darcy's equation is experimentally determined by Darcy and also can be derived from Navier-Stokes equation for homogeneous media. This equation is valid for the flow in continuum regime and in the range of low to moderate Reynolds numbers. Equation 2.3 represents the Darcy equation.

$$\vec{q} = \frac{-k}{\mu}\vec{\nabla}P \tag{2.3}$$

where k is permeability, μ is dynamic viscosity, $\vec{\nabla}P$ is pressure gradient and $\vec{q}$ is the flux (discharge per unit area). In the case of foam flow in porous media, apparent viscosity is being used in Equation 2.3 and $\frac{q}{\nabla P}$ is called mobility. It is observed that, the mobility of foam flow through porous medium for the foams with smaller average bubble size (cell size) is much lower[14]. The reason for that is experimentally studied by Heller[14] and Hirasaki and Lawson[26]. This is due to the fact that the apparent viscosity of foam is extremely geometry dependent[14, 26]. Hirasaki and Lawson[26] point out that by increasing the average bubble size in a capillary tube, apparent viscosity of the foam decreases dramatically which leads to increasing the foam mobility inside the capillary tube. The same scenario happens in foam flow in porous media.

2.2 Foam-forming and its application in papermaking

Before starting discussing about the application and advantages of foam-forming process in paper-making, it is wise to present a brief introduction on paper-making process. Paper is a universal product with vast applications mostly in writing, packaging, hygiene products and so on. Omitting the details of different paper products, the process for manufacturing of paper is generalized in some steps.

In the first step, after breaking the wood into wood chips and making fibres, the fibres which are useful for paper-making process are separated and beaten down to pulp using various refining techniques. In the second step extra treatment is done on pulp. Mechanical, chemical, biological and other parameters of the final paper is controlled by adding specific chemical premixes to the pulp. In the third step, a dilute suspension of pulp (at low consistency of about 0.5% to 1.0%) in water is prepared and drained though a screen called forming fabric. Forming fabric is mostly made up of mono-filament plastic strands and its weave pattern must be designed in a way that could guarantee the minimum resistance to water drainage and maximum retention of fibre fines. In this step, pulp slurry is drained on a forming fabric under vacuum and a mat of randomly distributed interwoven fibres deposit on the fabric. The size of the final paper sheet depends on the size of the forming fabric. After that, extra moisture of paper is removed first by applying pressure and then drying by passing hot air flow. The third step in paper making is carried out automatically on paper-machines in paper-making mills.

One of the major disadvantages of paper-making process is requirement of the huge amounts of water which are used to transfer fibres from the head-box to the paper-making section in paper-machine. The more amount of water is used for fibre transformation, the more water needs to be drained and consequently more energy is used for the water removal process, which is significant at the industrial scale. One way to reduce this amount of energy is to switch the fibre suspending medium from water to a fluid which can allow less energy consumption for its drainage. Aqueous foam is introduced to pulp and paper industry in 1972 as a good alternative to water[29]. Since more than 70% of foam is air, it needs much less energy to drain the suspension in forming section. The second important advantage of foam is the 3D honeycomb structure which prevents fibre flocculation and also provides the flexibility of making porous, bulky and light papers with open structures for making new products with specific applications. This happens because the fibres locate in between the bubbles during the process.

The idea of applying foam in paper-making initially is proposed by Radvan and Gatward[29] in 1972 and Smith and Punton[30] at 1974. Radvan and Gatward[29] for the first time proposed the idea of using foam as a medium for suspending fibres in paper-making. They find that a uniform dispersion of very long and fine fibres even at relatively high concentrations can be made without fibre flocculation. They also propose a discontinuous foam forming unit attached to a small paper machine and they called it Radfoam process[29]. Tringham[31] applies Radfoam process and explores different new properties of papers made by this process. He finds that papers which are made by Radfoam process are typically very uniform and have more open structures compared to the normal papers. Tringham[31] also finds that The specific volume (bulk) of the hand-sheets using Radfoam process is 20 to 30 times greater than a standard handsheet for softwood kraft pulp. Smith *et al.*[30, 32] use Radfoam process to make new papers in foam media and studied other characteristics of the new products. They confirm that foam forming process is a good method to make uniform paper (without fibre flocculation) using longer fibres. They conclude that surface tension and bubble spacing in foam change the properties of the final material however chemical effects are negligible. Moreover, It is showed in their research that beaten pulp increase the tensile strength of foam paper due to increasing the specific surface of fibres.

Recently, Lappalainen and Lehmonen[33] at VTT Technical Research Centre of Finland study characteristics (like bubble size distribution) and dynamics of foam containing cellulose fibres. They use a high speed imaging technique to collect various images of foam-fibre mixture (foam

bubbles with radius larger than $25\mu m$ can be recognized in their imaging technique). Image processing techniques are combined with Circular Hough Transform for determination and analysis of bubble size distribution of the foam-fibre suspension. Poranen *et al.*[34] at VTT Technical Research Centre of Finland produce new cellulose based 3D porous products in foam environment using an automatized foam handsheet maker in a pilot scale foam forming research environment called SUORA. They use various types of pulps and different basis weights to make their products. They study some morphological characteristics of the foam formed materials and also present an automatized foam paper maker. To our knowledge the last two works done in VTT are the initial works which have been seriously followed and published in the last few decades.

Chapter 3

Foam-paper: experiments and applications

3.1 Production and characteristics

The essential concern of paper-making is all about uniformity of final paper. The source of non-uniformity is related to fibre flocculation in the pulp slurry. Fibre flocculation is the consequence of numerous parameters but the most essential ones are fibre length, consistency of pulp suspension and the viscosity of suspending medium. One way of circumventing this problem is to make a very dilute aqueous suspension of pulp however, energy consumption and production rate limitations regarding water drainage, prohibit using high-dilution processes. Another approach to solve this problem is replacing the aqueous suspending medium by foam. Since 60 to 70 percent of foam that is being used for this purpose is air, much lower amount of water needs to be drained comparing to the high-dilution processes. At the same time, since fibres are located in the foam lamella, fibre flocculation will be prevented even in case of relatively long fibres. Another advantage of using foam is that since the structure of foam is 3D and porous, it is a good candidate to be utilized as medium to make 3D porous paper called foam-paper with specific industrial applications. Before studying various applications, lets initially start explaining the production detail and characteristics of foam-paper.

3.1.1 Production details

In this study, a method very similar to Radfoam process[29] is applied to make the foam suspension of fibres. The suspension of foam and fibre is prepared using a foam maker unit based on the apparatus similar to the one reported by Smith et al.[30, 32]. The foam maker unit has two mixing cell part and each cell has a Caframo Brinkmann RZR1 type mixer to apply shear force in order to reach higher foam air-content[1]. In the first mixing cell, normally 5 *ml* of surfactant is added to 1000 *ml* of the suspension but for reaching higher foam air-content the concentration of the surfactant is increased. The foam air-content is varied from 10% to 50% by changing the mixer angular velocity from 280-2200 RPM[2]. The higher air-contents from 50% to 70% are reached by increasing the concentration of surfactant. Between the first cell unit and the second cell unit there is a vent at the bottom to let the foam pass from first cell to the second one. In the second cell, the foam bubbles get smaller and more uniform since extra shear force is applied and also cellulose fibres are added to the foam simultaneously. The consistency of the pulp solution that are used for making foam-papers was 0.5% based on the TAPPI recommendation for standard handsheet making. Figure3.1 shows a sample of a final product.

Two different methods of drying are applied to make different samples in different foam air-contents for various purposes and also study the effect of different drying techniques on the final products. The first method is air-drying without pressing. In this method, the suspension of foam-fibre is then filtered in a 15 *cm* diameter Buchner funnel under 9.8 *kPa* of vacuum. One layer of regular fabric and two layers of plastic forming fabric is used inside the funnel for making the samples. De-watered samples are then dried without pressing at $24^{\circ}C$ and 56% humidity in CTH[3] room for 24 to 48 hours. In this method of drying, two different pulps are used. Some additives are also used for special purposes which will be explained in the next section. The second method is freeze-drying. In this method, after making the foam-fibre suspension, it will be frozen in liquid Nitrogen ($-196^{\circ}C$) and de-watered using a freeze-drier apparatus. Freeze-drier works by reducing the pressure inside the container to be sublimated from solid phase to gas phase immediately. The desired grammage of both air-dried and freeze-dried samples are $100\,g/m^2$. Table 3.1 shows the detail of the pulp and additives used the make samples for different applications.

[1] Air-Content is the volume fraction of air in foam. It can be measured using a cylinder in lab by subtracting the total volume of foam with the fluid volume per total volume of foam.

[2] Round Per Minute

[3] Constant Temperature and Humidity

Table 3.1: Foam-Paper samples: pulp types and additives.

Pulp type	Additives	Drying method	AC(%)
NBSK	—	Air-Dried	10%-55%
NBSK	10%-50% Eucalyptus(Hardwood)	Air-Dried	10%-55%
NBSK	10%-50% NBSK Valley Beaten	Air-Dried	10%-55%
NBSK	100% PFI refined	Air-Dried	20%-60%
CTMP	—	Air-Dried	10%-55%
NBSK	—	Freeze-Dried	20%-70%
NLF[4]	—	Freeze-Dried	50%-70%

In order to be more precise about the effect of fibre morphology on the foam-papers properties, fractionation[5] method is applied to separate longer fibres from the shorter ones. The effect of fibre length and coarseness are studied on foam-papers properties and aerosol filtration tests. For this purpose, fibres are filtered based on their length in different stages of Bauer-Mcnett fractionator. The screen sizes in this fractionator are 16, 30 and 50 based on ASTM standard (labelled as $L_{W_{M16}}$, $L_{W_{M30}}$ and $L_{W_{M50}}$). The length distribution, average fibre coarseness and the average fibre length are analysed using FQA[6]. Morphological characteristics of the fibres that are used to make the foam-papers are briefly reported in Table 3.2. However more detailed information about the length distribution of fibres will be reported in the next section.

Table 3.2: Morphological characteristics of the pulp used to make foam-paper.

Pulp type	$L_W\,(mm)$	$d_f\,(\mu m)$	Coarseness (mg/m)	Fine(%)
NBSK	2.45	27.6	0.17	2.50
CTMP	1.8	30.3	0.52	6.15
NLF	0.1-0.3	0.2-0.3	—	—
Eucalyptus	0.76	—	0.04	2.72
$L_{W_{M16}}$ - NBSK	3.29	28.7	0.19	25.4
$L_{W_{M30}}$ - NBSK	2.72	27.8	0.14	29.8
$L_{W_{M50}}$ - NBSK	1.81	26.6	0.15	—

[3]Nanofibrillated Lyocell Fibre
[5]Fractionation is a technique to separate long fibres from short fibres.
[6]Fibre Quality Analyser

3.1.2 Morphology and characteristics

The morphological characteristics of the fibres that are used to make the foam paper, are studied. The research in this section is conducted in finding the relation between the manufacturing condition and the final-product condition. Moreover, the effect of fibre morphology on the final-product properties is investigated. In this research, foam air-content is considered as manufacturing condition and parameters such as specific volume (bulk), porosity and tensile index are considered as final-product condition.

The first experiment which is actually one of the main purposes of this research, is done on measuring the specific volume (bulk) of foam-paper samples. Figure 3.2a shows that by increasing foam air-content, the values of bulk dramatically increases, up to 50 times for NBSK and up to 20 times for CTMP, compared to the standard handsheet. CTMP shows increase in specific surface and this can be ascribed to the presence of the fines. Longer fibres create an open structure and fines are placed in this open space and since there has not been a very noticeable amount of water, the hydraulic forces during the drainage do not transfer the fines. This effect contributes to increase of the specific surface and consequently lower bulk at higher air-contents. Generally, the penalty for increasing bulk is losing the mechanical properties (such as tensile-index) to a great extent. Figure 3.2b shows that by increasing the air-content up to 55% the values for the tensile-index diminish down to about 10% of standard handsheet for CTMP and about 4% of standard handsheet for NBSK pulp. CTMP has higher value of tensile-index due to the presence of high specific area fibres compared to NBSK.

Figure 3.1: NBSK foam-paper at 40% air-content.

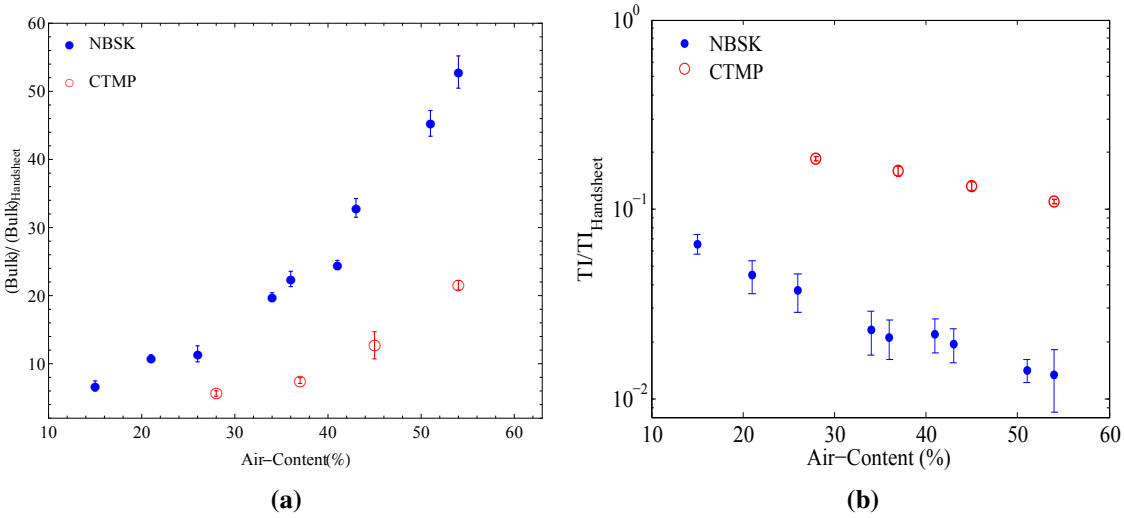

Figure 3.2: (a) Bulk vs. foam Air-Content (b) Tensile-Index vs. foam Air-Content for NBSK and CTMP foam-papers.

In order to solve the strength problem, different weight percentages of refined Eucalyptus (hardwood) fibres is added to the structure of NBSK foam-papers. Figure 3.3b shows that by increasing the weight ratio of hardwood in foam-paper structures, tensile-index increases slightly which also leads to a slight reduction in the values of bulk. It should be noted that a laboratory PFI refiner with 5000 revolution is used to refine hardwood Eucalyptus pulp. The freeness of hardwood pulp after refining is reduced from 417.7 CSF to 335 CSF. PFI refining increase the percentage of external fibrils and fines that contributes to increasing the tensile-index of foam-papers. However both higher amounts of fibrils and shorter fibres lead to lower values of bulk (Figure 3.5a).

To study the effect of fibrillation on both bulk and tensile-index more precisely, PFI refining applied to NBSK pulps and samples with three different values of freeness are made from new refined pulps. Figures 3.3c and 3.3d show the effect of freeness on bulk and tensile-index respectively. It can be concluded that by decreasing the values of fibre freeness (increasing the refining energy), the values of tensile-index increases but this is quite opposite for the values of bulk.

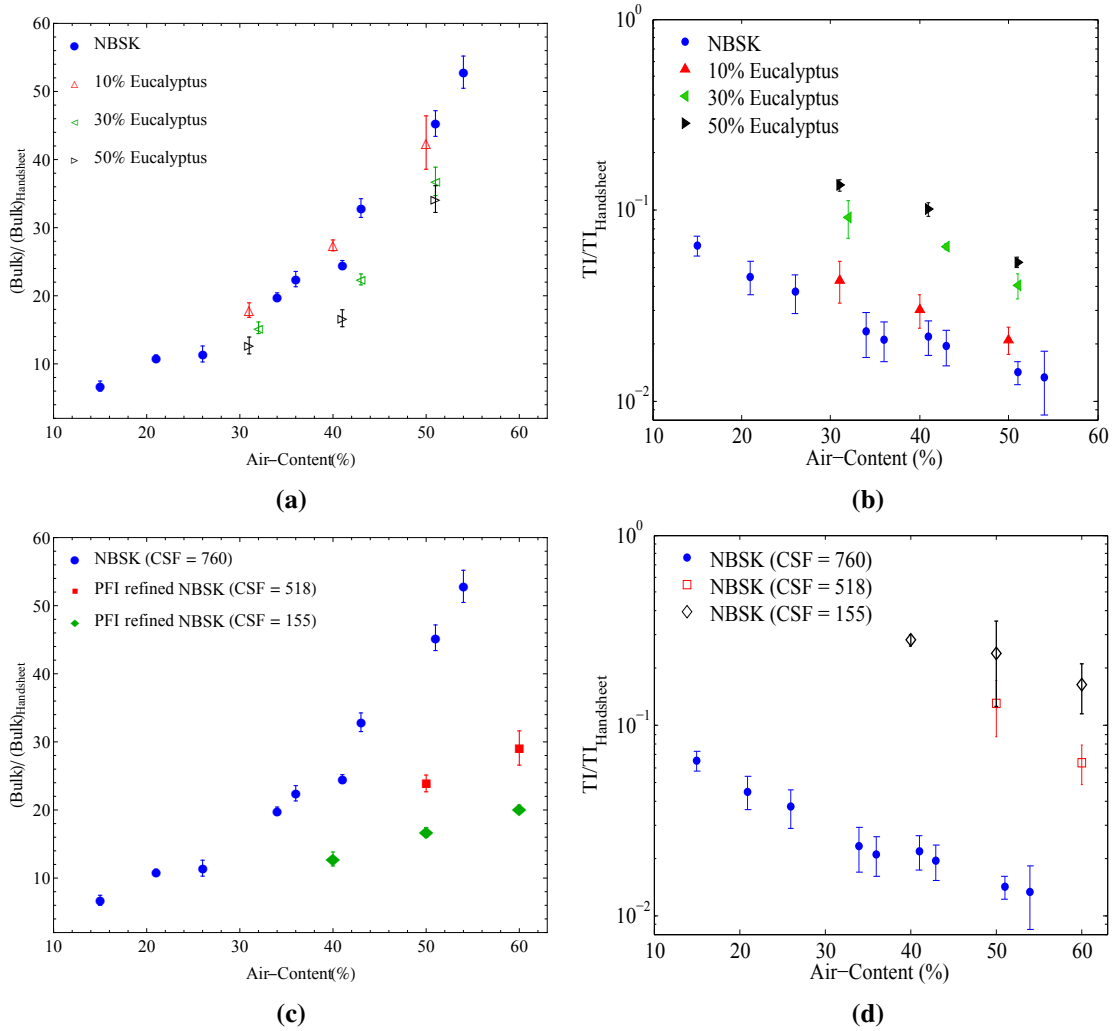

Figure 3.3: (a,c) Bulk vs. foam Air-Content (b,d) Tensile-Index vs. foam Air-Content for various weight ratio of hardwood and PFI refined NBSK samples.

To study the effect of specific surface more rigorously, three different weight ratio of NBSK valley beaten (VB) fibres are added to the structure of standard foam-papers. As shown in Figure 3.4b the tensile-index of the samples improved up to 70% of standard handsheet for 50% weight ratio of VB samples. It is not surprising that the values of bulk is reduced by factor of 2.5 in the same sample. The more amount of VB fibres in the structure of a foam-paper lead to the higher average surface area of the fibres and consequently stronger bondings. At the same time the average fibre length is reducing (Table 3.2). Since longer fibres are able to support the 3D

structure, increasing the percentage of shorter fibres in the structure of samples leads to diminishing the values of bulk (Figure 3.5b). Samples containing different weight ratios of VB fibres are proved to be more effective at increasing mechanical properties of the final foam-papers than hardwood samples as illustrated in Figure 3.4. Since preserving high bulk and high tensile-index is a trade off, samples containing 30% of VB fibres show reasonable bulk and tensile-index simultaneously. The trade off between tensile-index and bulk for various foam-papers is illustrated in Figure 3.6.

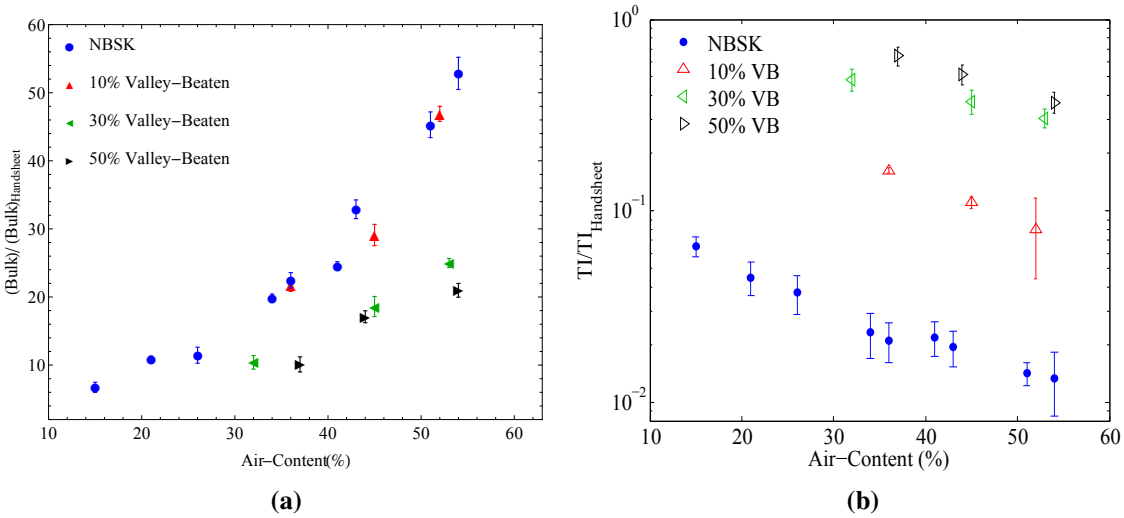

Figure 3.4: (a) Bulk vs. foam Air-Content (b) Tensile-Index vs. foam Air-Content for various weight ratio of NBSK valley beaten foam-papers.

Figure 3.5 shows the average fibre length distribution for both hardwood and VB foam-papers. For samples with additives two maximum points is observed which shows the presence of two frequent fibre length in the mixed samples. It can be concluded that the average length for valley beaten fibres are much lower than the hardwood ones. Other morphological parameters (results of FQA) are reported in Table 3.2.

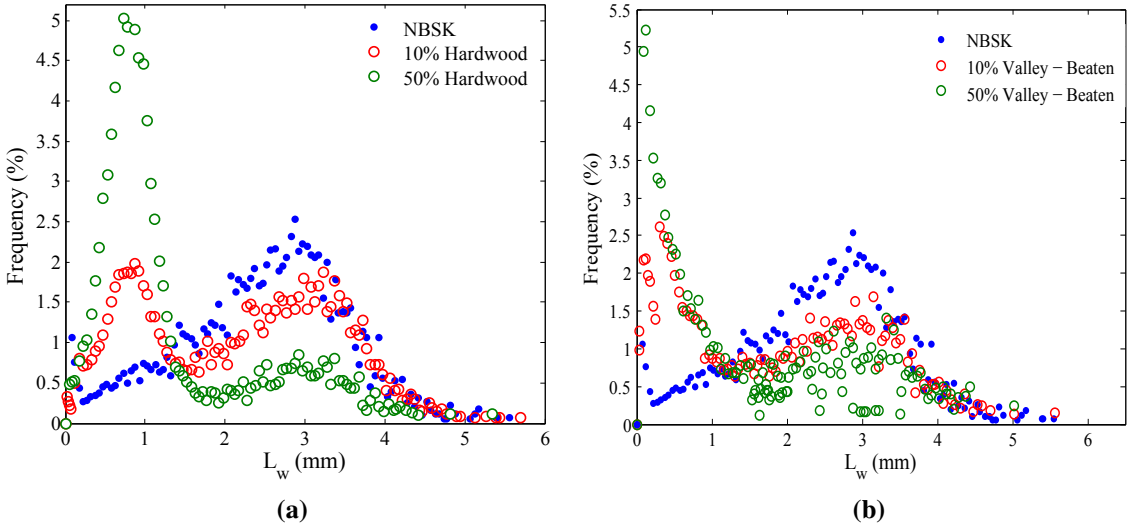

Figure 3.5: FQA results for (a) hardwood foam-papers (b) VB foam-papers

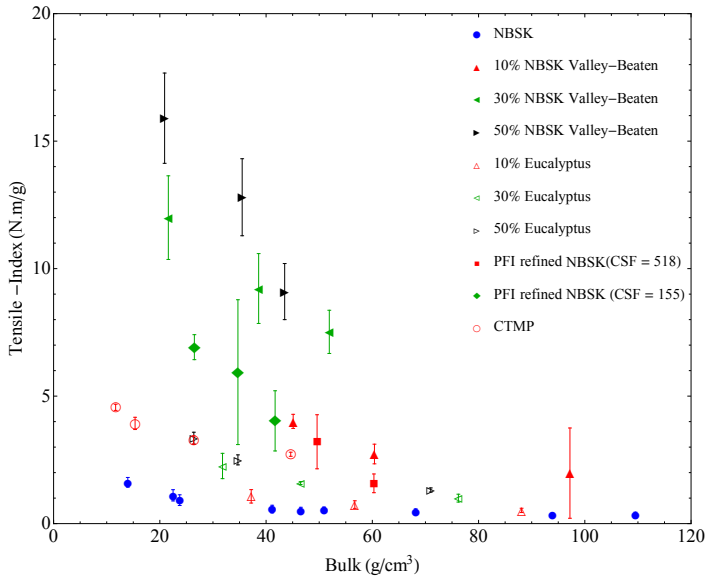

Figure 3.6: Tensile-Index vs. Bulk.

To understand the effect of fibre morphology on the properties of final product, fractionated NBSK pulp is used to make samples with different average fibre length. Figure3.7a shows that by increasing the fibre aspect-ratio, the values of normalized bulk increase at different foam air-

contents at the same grammage. This happens because much more space is required for the same number of longer fibres to locate among each other than shorter ones.

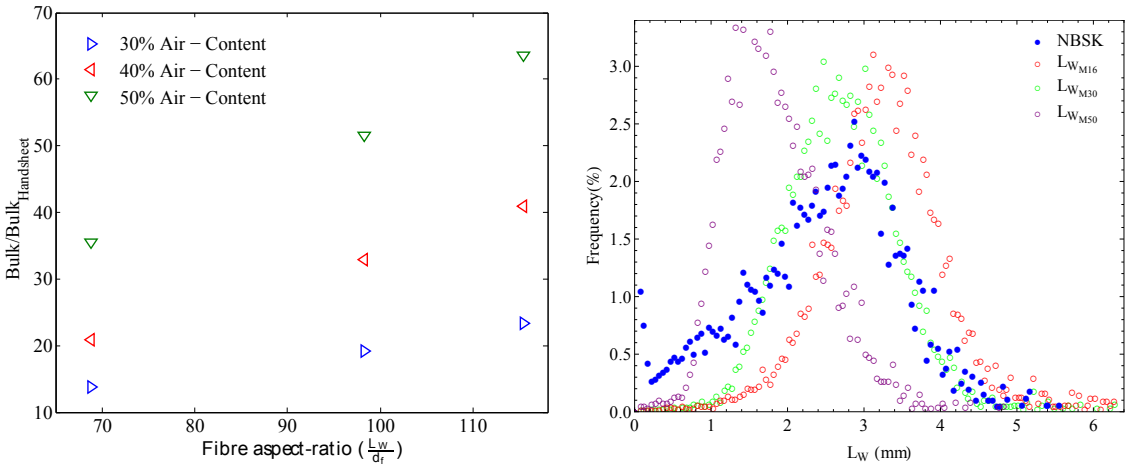

(a) **(b)**

Figure 3.7: (a) Normalized vs. fibre aspect-ratio (b) FQA results for samples made by three different average fibre length (courtesy of Dr. Ario Madani)

The other important parameter is porosity of final product. porosity is defined as the ratio of volume of pores to the total volume of sample. Figure 3.8 shows how porosity of final products changes by changing the foam air-content. Figure 3.8 generally shows that foam-papers are materials with very high porosity. By increasing foam air-content the porosity of final products increases up to 99.7% for NBSK foam-paper.

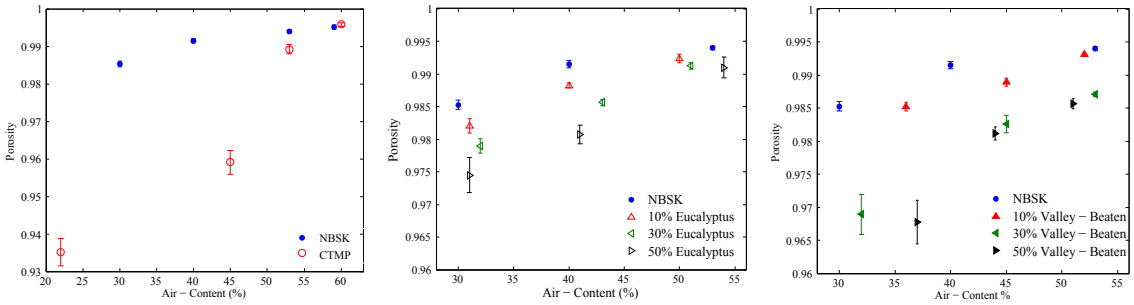

(a) **(b)** **(c)**

Figure 3.8: Porosity vs. foam Air-Content (a) different pulps (b) hardwood additive (c) valley-beaten additive.

3.2 Applications

In this section three potential industrial applications of foam-papers are studied. The 3D porous and filter-like structure of foam-papers let these materials to be applied in filtration of sub-micron aerosol particles. The pressure drop of these products are noticeably lower than the standard hand-sheet and also the filter quality factor of some samples are comparable to the commercial filters. In this section, first the pressure drop, permeability and filtration efficiency of foam-papers are measured and then the effect of different additives on filtration efficiency and filter pressure drop is studied. Since the porosities of foam-papers are quite high, they can also be applied as heat insulators and sound absorbers some of which can compete with their commercial counterparts. The major purpose of this study is to figure out how the essential target parameters vary with different manufacturing conditions. It is also important to study the effect of various additives on these parameters and make efficient foam-papers for that specific purpose.

3.2.1 Aerosol filtration

An air filter is known as a medium composed of fibrous materials which is able to capture and remove airborne particles. The importance of using aerosol filters is raised by increasing the demand for clean air. Controlling the air quality plays a vital role in several industries such as building indoor air quality (for HVAC[7] purpose) and internal combustion engines. Sometimes increasing the concentration of particulates in the air causes very serious health problems, so it is important to make very efficient filters to capture airborne particles in micro and nano scales. Since the internal structure of foam-papers is made up of random orientation of entangled fibres and their specific volume is high (which are associated with low pressure drop), we can assume foam-papers are candidates for aerosol filtration applications. In this section, a research on filtration properties of various foam-papers is carried out.

3.2.1.1 Background

A non-woven fibrous filter media is commonly used to capture airborne particulates. Fibres in the size range between 100 nm and 100 μm criss-cross to form a web of several layers. This structure mostly contains air in order to increase breathability (Reduce pressure drop). Since the particles tend to go through very small holes in this porous structure, they may not become trapped. Rather, while trying to navigate through the layers of filter media, a particle will be attached to a fibre due to a numerous different mechanisms. The main mechanisms are inertial impaction, gravitational

[7] Heating, Ventilation and Air Conditioning

settling, Brownian diffusion, electrostatic deposition, and interception[35, 36]. In order to explain how a particle deposits in the filter media, it is necessary to first consider the flow of air stream. The path of the air around a fibre is described in terms of flow streamlines. Deviation of particles carried by the air from the streamlines depends upon the aerodynamic diameter of particles. The larger the size, the greater the tendency to deviate from air streamlines due to higher inertia of a particle. Several authors investigated that the rate of particle deposition is minimum for the particles of an intermediate size (between 100 *nm* to 200 *nm*)[35, 36]. The deposition mechanisms are more efficient for either very small or very large particles.

Gravitational settling or sedimentation is settling of particles that fall down due to the gravity. This is the dominant mechanism governing the deposition of very large particles particularly those in the range greater than few microns, while Brownian diffusion has the greatest effect on very small particles less than a hundred nano-meter in size[37]. Brownian motion is the process by which aerosol particles move randomly due to collisions with the gas molecules. Smaller particles randomly move across streamlines due to Brownian motion until they touch surface of a fibre. Figures 3.9 and 3.10 show the filtration of very large and very small particles due to gravitational settling and diffusion mechanisms respectively.

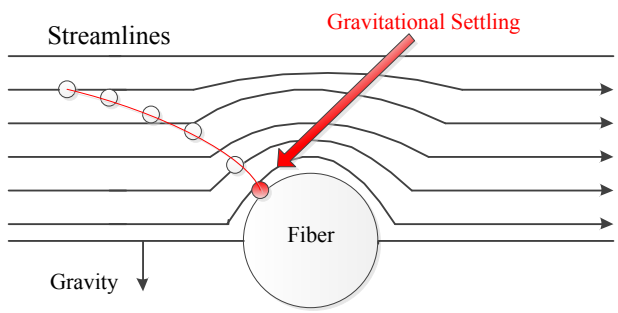

Figure 3.9: Gravitational settling.

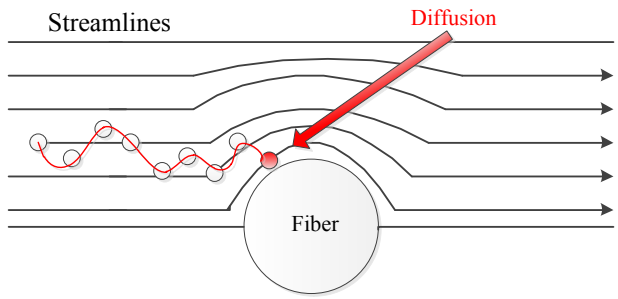

Figure 3.10: Diffusion.

Most of respirable particles are much smaller to be filtered out by gravitational settling. Respirable particles above 400 *nm* in diameter are not likely to be influenced by diffusion mechanism due to very small diffusion coefficients. They may be captured by interception and inertial impaction [38]. Inertial impaction is the deposition mechanism while particles are not able to follow the curved streamlines due to their high values of inertia. Impaction of a certain particle with an obstacle can be predicted by *Stokes number*. Stokes number is a non-dimensional group which depends on particle size, velocity, and drag force exerted by flow, and characteristic size of the obstacle. For the values of Stokes number greater than 1, the particle will collide with fibres[37]. Interception occurs when small particles follow the streamlines, but the streamlines will naturally take the particle close enough to the obstacle to contact the surface of the fibre. If the particle flows too close to a fibre, collision may happen. Figures 3.11 and 3.12 show the filtration mechanisms for impaction and interception respectively.

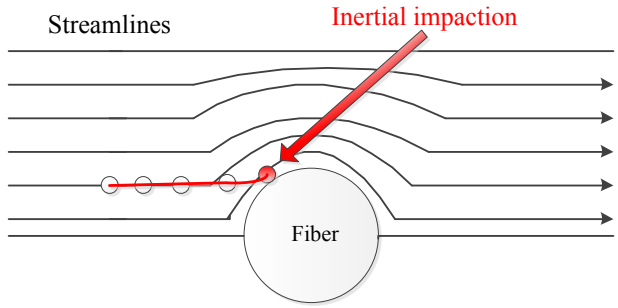

Figure 3.11: Impaction.

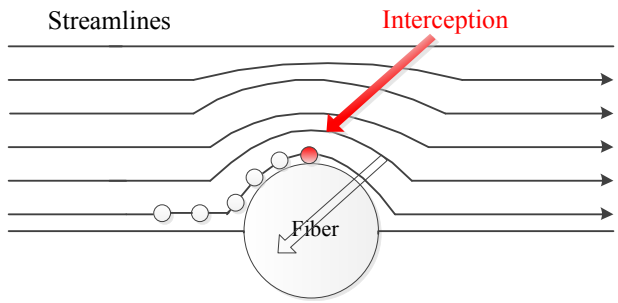

Figure 3.12: Interception.

Electrostatic deposition is an entirely different particulate capture mechanism. By starting producing resin-wool filter in 1930, many of the filters which used in different applications are electrostatically charged[39]. Although it may be difficult to quantify the charge on either the particle or the fibre, electrostatic attraction can be an extremely effective capturing mechanism. A charged particle will be attracted to fibre which has an opposite charge. Figure 3.13 shows the total filtration efficiency of a typical fibrous filter media as a function of particle diameter. As seen in this figure, the efficiency is a strong function of particle size. Air filters are highly efficient at removing particles with a diameter less than $0.1\mu m$ (by diffusion) and greater than $0.6\ \mu m$ (by Impaction). Particles with diameters between 0.1 to $0.6\ \mu m$ have significantly lower filtration efficiency. Particles in this range are too large to be effectively pushed around by diffusion and too small to be effectively captured by impaction. It should be noted that filtration efficiency (which is measured from the concentration of particles before and after a filter), filter pressure-drop (the difference between the pressure in upstream and downstream) and filter quality-factor (takes both the effect of efficiency and pressure drop into account) are three essential parameters that is important to be measured for a filter as it is shown in Equations.

$$\eta = \frac{C_{\text{upstream}} - C_{\text{downstream}}}{C_{\text{upstream}}} \tag{3.1}$$

$$QF = \frac{-\ln(1-\eta)}{\Delta P} \tag{3.2}$$

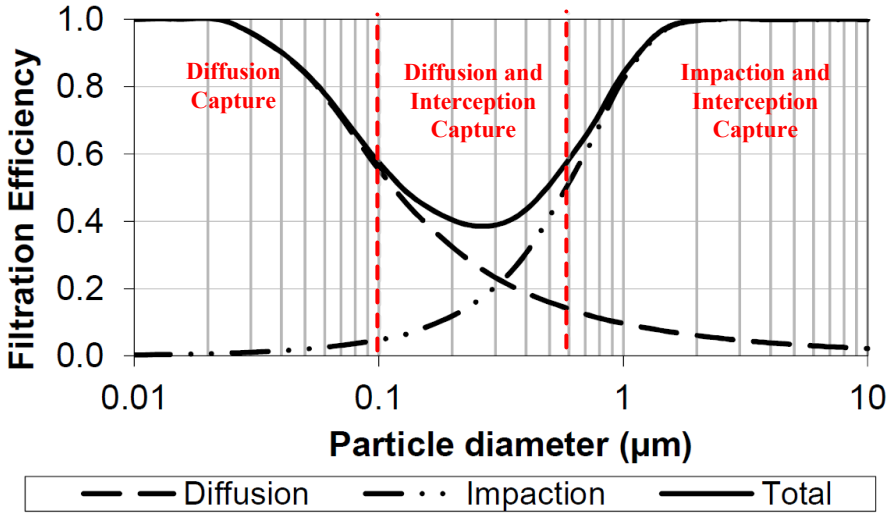

Figure 3.13: Filtration efficiency versus particle diameter. (the picture is made by author.)

In pulp and paper industry, some researchers are trying to make efficient filters out of pulp in order to find a low-cost and biodegradable replacement for polymeric filters. One of the earliest research works in this field is conducted by Rodman and Lessmann[40] in 1988. They review different types of filter media that are commonly used in automotive filtration systems. They also present the filter-papers which their micro-structure constructed by different types of fibres. The effect of different parameters is investigated on the filtration efficiency of the filters and some traditional design approaches for improving the efficiencies are discussed. They did filtration test for paper-filters in the particle diameter range between 5 and 30 μm and concluded that adding micro-fibres in the structure of paper-filters can increase filtration efficiency up to 45%. For the sake of the filtration of sub-micron particles, Mao *et al.*[41] develop a method to make very efficient filters (up to 95% efficiency) using hardwood and softwood pulps with a pressure drop in the range of the commercial filters. They add various percentage of high specific surface valley-beaten fibres into the structure of paper-filters and use freeze-drying technique to retain the surface fibrillation into the dry state. The filter structure made up of this method has very high filtration efficiency(effect of microfibrils) and low pressure drop (long NBSK fibre provide high permeability). Macfarlane *et al.*[42] use similar method to what Mao *et al.* use and carried out a comprehensive research on the the effect of different freez-drying techniques and various parameters of paper-filter on the filtration efficiency and pressure-drop of filters. They find a new parameters in their freeze-dried filters

called filter sectioning and layering. Duo to what they found, a non-uniformity in the fibre packing density is observed in the z-direction of filter-papers because of the effect of cold wall. This non-uniformity is increased by increasing the percentage of valley-beaten pulp in the structure of the paper-filters.

3.2.1.2 Methodology

The filtration efficiency and filter pressure drop of samples are measured in a small aerosol circuit as it is shown in Figure 3.14 . Each foam-paper is cut into the 35 *mm* diameter circular sample to fit into the sample-holder in the circuit. Aerosol particles are generated by the solution of Sodium Chloride (NaCl) containing 0.1% NaCl in the water using a collision nebulizer. The aerosol particles is dried by passing them into a tunnel full of humidity absorber materials (desiccant) and finally dragged through the filter sample using a normal vacuum pump. The flow-rate of the air through the samples are set into 6.66 L/min which is equal to the superficial gas velocity of 11.5 cm/s. The pressure-drop of the samples are measured by sensing the pressure signal before and after filter using a digital pressure sensor. The concentration of particles before and after filter (and consequently filtration efficiency) is measured using scanning mobility particle sizer (SMPS)[36]. The aerodynamic diameter of the particles using for all filtration tests are between 14 *nm* to 670 *nm*[8].

In this survey, the application of the filtration of different foam-papers (variations are due to various pulp types and two methods of drying) is studied. The effect of fibre morphology and foam air-content on the filtration properties and air permeability of the final products are investigated. The experiments are started by measuring the filtration efficiency and pressure-drop of air-dried NBSK foam-papers (standard foam-paper) in different foam air-contents. The effect of fibre length and coarseness on the filtration properties of foam papers studied by using air-dried NBSK foam-papers made up of fractionated NBSK pulp. Filters made by air-dried CTMP pulp are used to study the effect of pulp type on the filtration properties of the products. Freeze-drying technique is applied to make new samples out of Nano-fibrillated Lyocell Fibres (NLF) to find out how nano-fibres change the foam-papers structure and consequently filtration properties of the new products.

[8] http://dustmonitors.ru/d/68562/d/spms_3936.pdf

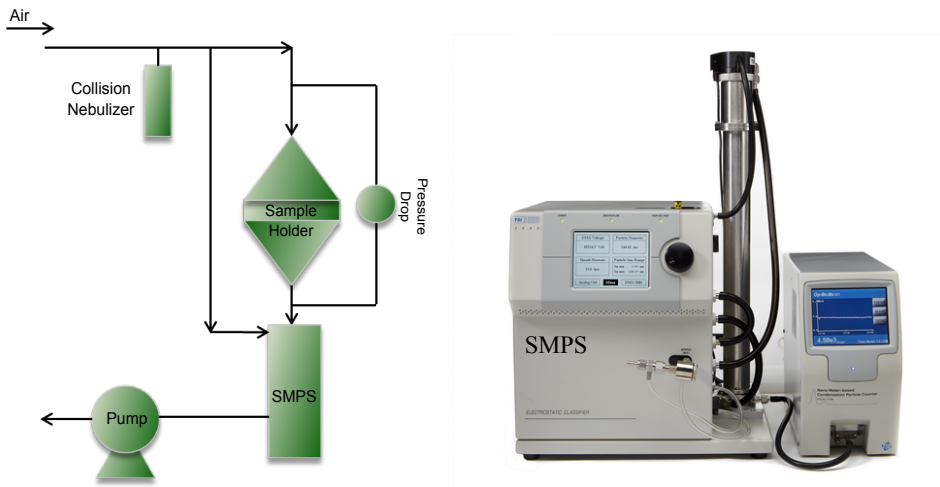

Figure 3.14: The aerosol circuit for measuring filtration efficiency and filter pressure-drop.

3.2.1.3 Results and discussion

Figure 3.15a shows that by increasing foam air-content, permeability of both air-dried NBSK and CTMP samples increases up to 9000 times greater than the standard handsheet at the highest air-content. This high values of permeability of samples are reasonable because of the very large open paths among the fibres which are illustrated in the tomographic images. CTMP samples show lower permeability because of the higher specific surface and more percentage of fines in its structure.

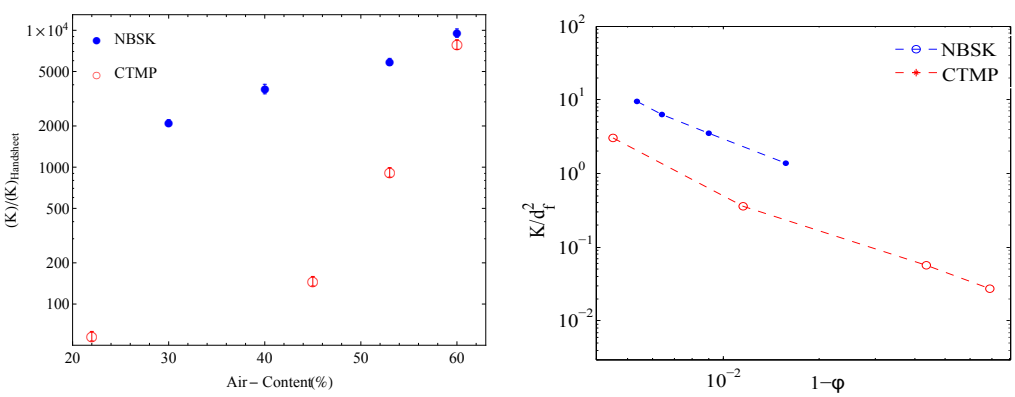

(a) **(b)**

Figure 3.15: NBSK and CTMP (a) Normalized permeability vs. foam Air-Content (b) Darcy number vs. Solidity.

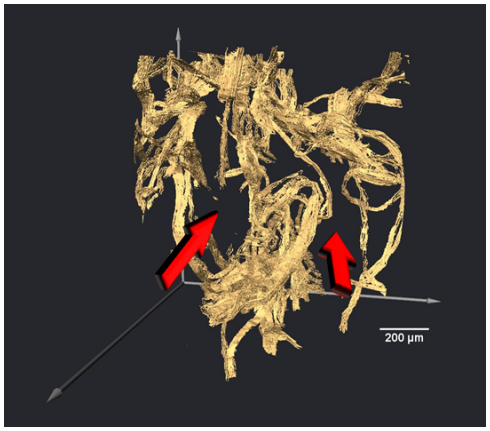

Figure 3.16: Micro X-ray tomographic image of NBSK foam-paper produced in a 50% foam air-content (Courtesy of Dr. Andre Phillion, The University of British Columbia Okanagan campus).

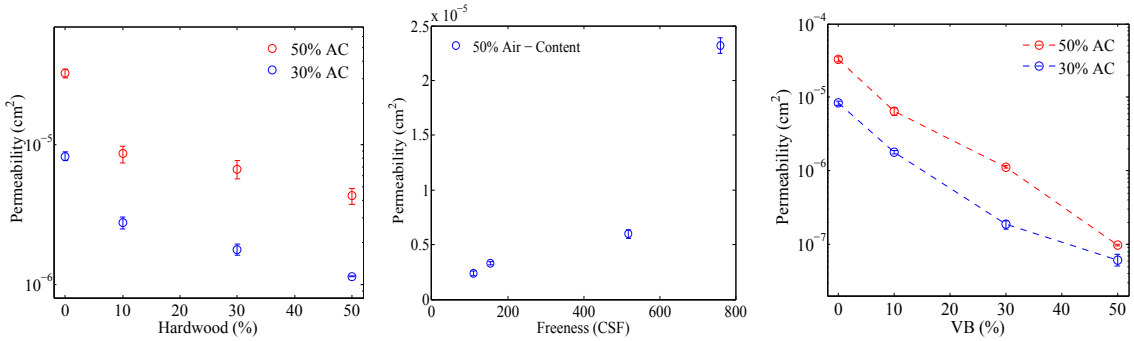

Figure 3.17: (a) Permeability vs. Hardwood weight ratio (b) Permeability vs. pulp Freeness (c) Permeability vs. VB weight ratio.

However, permeability of samples with refined Eucalyptus (hardwood) additives are reduced as is shown in Figure 3.17a. This happens due to two main reasons. First, the average length of Eucalyptus fibres are lower than the average length of NBSK ones (Figure 3.5a). Using longer fibres generally results in samples with higher permeability since longer fibres need more space than shorter fibres to make a fibrous network in the same grammage. Second, the percentage of fibrils in refined Eucalyptus is much more than the NBSK pulp. Figure 3.17b shows the effect of fibrillation on permeability of final samples. The results show that by decreasing the fibre freeness (increasing the amount of fibrils in the structure of foam-paper), permeability of samples decreases

to a great extent. Permeability reduction is much more pronounced for the samples with various valley-beaten weight ratio as illustrated in Figure3.17c. This happens due to the presence of very high specific surface fibres in the structure of these series of foam-papers. The higher the specific surface of fibres, the more they can block the fluid flow and consequently the less permeability will be obtained.

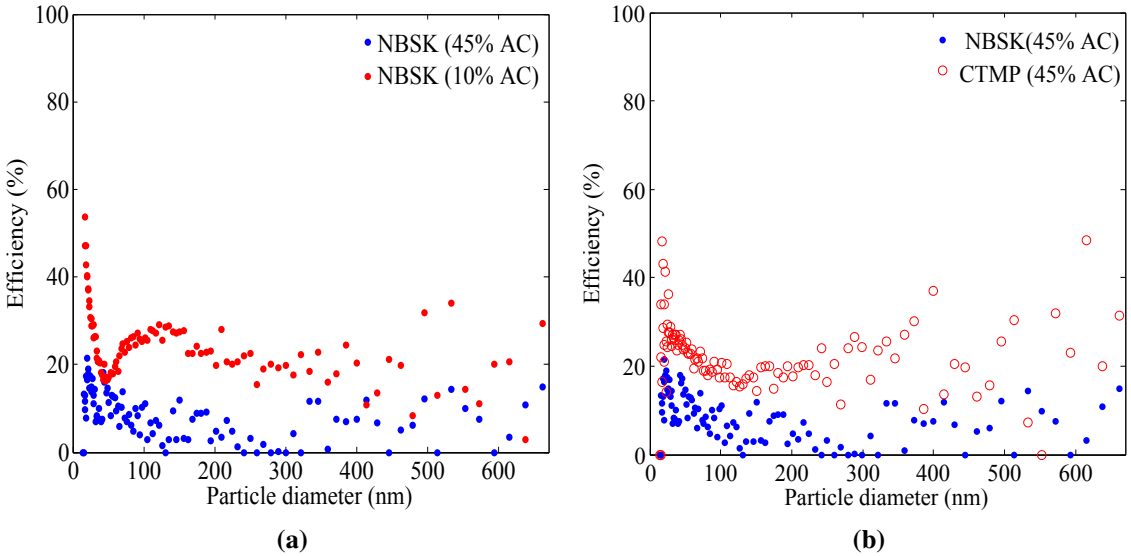

Figure 3.18: Filtration efficiency (a) NBSK in different foam air-contents (b) NBSK vs. CTMP pulp in 45% foam air-content.

3.2.1.3.1 Effect of air-content and pulp type

Figure 3.18a shows the results of filtration efficiency in the range of sub-micron particles for NBSK foam-papers at 10% and 45% air-contents. The results show that by increasing the air-content, the filtration efficiency of standard foam-paper diminishes until it loses its filtration properties at 45% air-content. Though NBSK sample at 10% air-content show reasonable filtration efficiency, it shows much higher pressure drop per unit length which leads to having poor filter quality factor. For this reason, CTMP is used for obtaining better filtration efficiency at higher air-contents. CTMP pulp shows better filtration properties at the same air-content compared to NBSK pulp as shown in Figure 3.18b. Though the values of pressure drop per unit length of CTMP sample at 45% AC are better than NBSK sample at 10% AC, it still shows very low quality factor. The values of pressure drop per unit length are reported in Table 3.3 for these test.

Table 3.3: Pressure drop for the air-dried NBSK and CTMP samples used in 6.66 lpm

Sample	Pressure drop (Pa)	Thickness (mm)	$\frac{dP}{L}(Pa/m)$
NBSK (10% AC)	25.80	1.6	16125.0
NBSK (30% AC)	11.94	4.1	2912.2
NBSK (45% AC)	10.4	9.3	1120.1
NBSK (54% AC)	9.77	11.4	857.20
NBSK (60% AC)	8.76	15.5	565.50
CTMP (45% AC)	125.4	10.9	11504.0

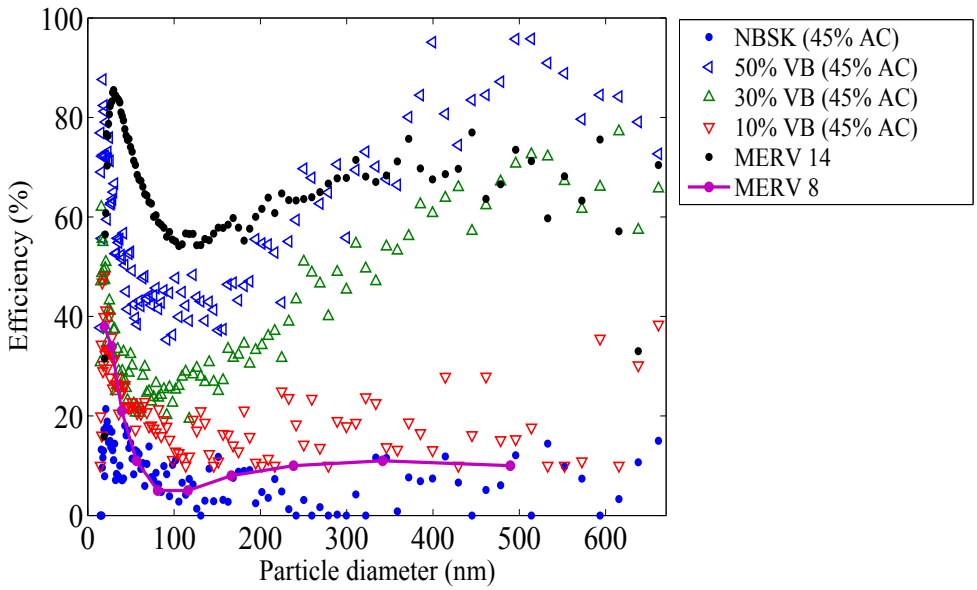

Figure 3.19: Filtration efficiency for different weight ratio of VB pulp in NBSK foam-paper structure.

3.2.1.3.2 Effect of VB weight ratio (fibre specific surface)

Figure 3.19 shows the effect of VB weight ratio on the filtration efficiency of foam-papers. By increasing the weight ratio of NBSK VB pulp in the structure of foam-paper, the filtration efficiency dramatically increases. This happens due to the presence of high specific surface fibres. Micro X-ray tomographic images are also confirm the mentioned claim as illustrated in Figure 3.20. The results also compared to the results of the commercial filters, MERV-8 and MERV-14. According

to the pressure drop per unit length of the VB samples, the results of 10% VB and 30% VB are comparable to the results of MERV-8 and MERV-14 respectively. 50% VB samples show a very high pressure drop and very low filter quality factor.

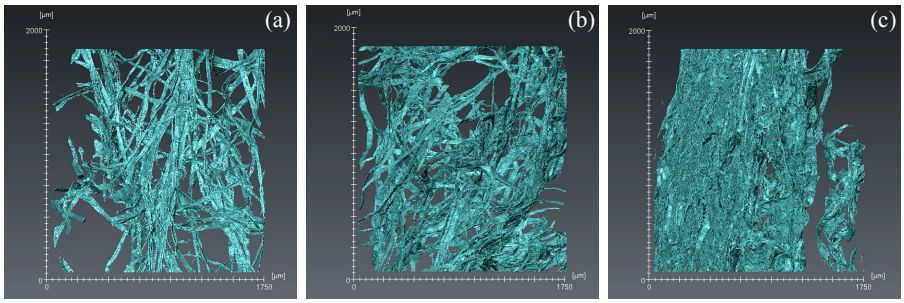

Figure 3.20: Micro X-ray tomographic images for the foam-paper samples at air-content of 40% (a) 0% VB (b) 10% VB (c) 50% VB. (Courtesy of Dr. Andre Phillion, The University of British Columbia Okanagan campus).

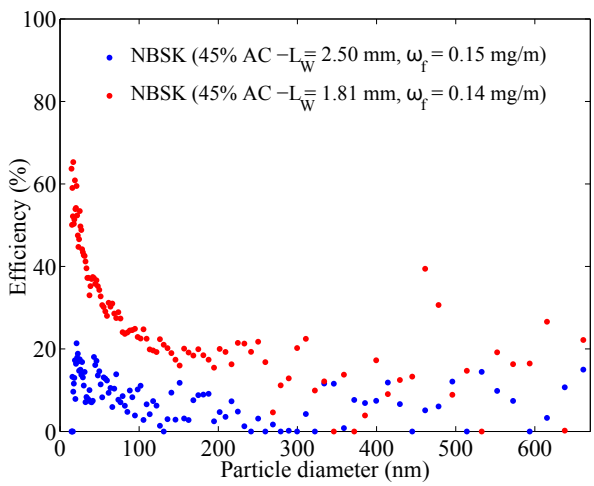

Figure 3.21: Effect of average fibre length on filtration efficiency.

3.2.1.3.3 Effect of average fibre length

Figure 3.21 compares the effect of average fibre length on filtration efficiency of NBSK samples at almost the same air-content (45%), grammage, fibre coarseness[9] and average fibre diameter[10].

[9] 0.14 mg/m for shorter fibres and 0.15 mg/m for longer fibres
[10] 26.8 μm for shorter fibres and 27.6 μm for longer fibres

The results represents higher filtration efficiency for the samples made up of shorter fibres. Since the grammage of the samples are the same, the average number of the fibres per unit volume of the samples made by shorter fibres are greater than the longer ones. This effect contributes to increasing the tortuosity of the internal structure, hence the probability of particle-fibre collisions will increase. Moreover, using longer fibres in the structure of foam-papers leads to having larger open paths as elaborated before. The larger the internal void paths in the structure of foam-papers, the less probability of particle-fibre collisions. Though the filtration efficiency improved using shorter fibres, a slight increase in the pressure drop of the samples is observed. Another problem of foam-papers made by shorter fibres is that the mechanical properties of these samples are very poor. They easily lose their structure at high flowrates.

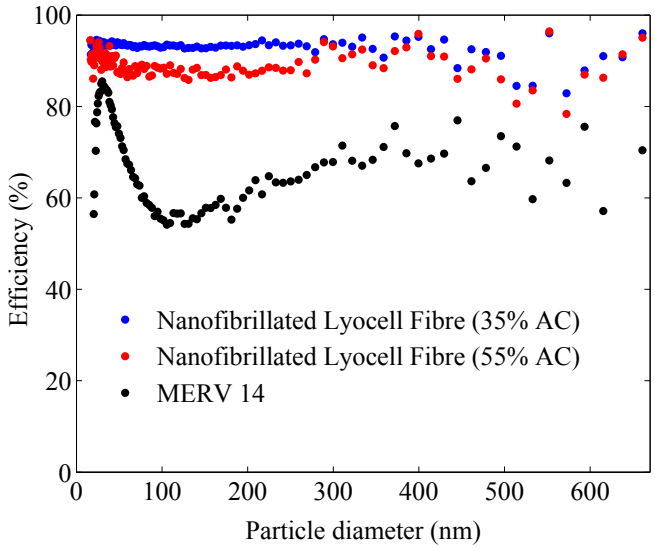

Figure 3.22: Filtration efficiency for NLF in different foam air-content.

3.2.1.3.4 Effect of nano-fibrillated fibres

In this section, nano-fibrillated cellulose is added to the foam-media to make new foam-paper products out of nano-fibrillated fibres. Freeze-drying applied to slurry of NLF and foam in order to preserve the fibre-foam internal structure and avoiding hornification. Figure 3.22 shows fantastic filtration efficiency results for the samples made by NLF in two different foam air-contents. The reason for this can be answered by looking into the morphology of nanofibrillated fibres. The main difference between a actual NBSK fibre and a nanofibrillated cellulose fibre is in the values

of length and diameter of fibres as shown in Table 3.2. The average diameter of NLF is about 300 *nm* (Figure 3.23) and the average length is between 0.1 *mm* to 0.3 *mm*. This means that the number of nanofibrillated fibres per unit volume is much more than the products made up of NBSK macrofibres. Moreover, the large aspect ratio of fibres leads to a very high tortuous fibre networks as elucidated before. These two effects together leads to capturing between 80% to 95% of sub-micron particles in different air-contents. The pressure drop for the samples are a bit high compared to the commercial filters (about 150 *Pa* for 55% air-content and about 320 *Pa* for 35% air-content). However, the results of filter quality factor illustrated in Figure 3.24 are reasonable compared to MERV-14. The lower air-content samples of freeze-dried NFL are not recommended for the filtration purpose because of high values of pressure-drop (For air-content 20% the pressure-drop is more than 750 *Pa*). Figure 3.24 shows that the freeze-dried foam-papers made by NLF in 35% and 55% foam air-contents and air-dried foam-papers with 30% valley beaten fibre weight ratio have reasonable quality factor comparing to the commercial filters. Although the pressure drop values for both freeze-dried NLF foam-papers are high but since these filters have very high filtration efficiency, the quality factors of them are in the rang of commercial filters. Concerning the 30% VB air-dried filters, having low values of pressure drop (about 50 *Pa*) and the average filtration efficiency of about 45% (between 10 *nm* and 670 *nm* particle diameter) incur a reasonable quality factor.

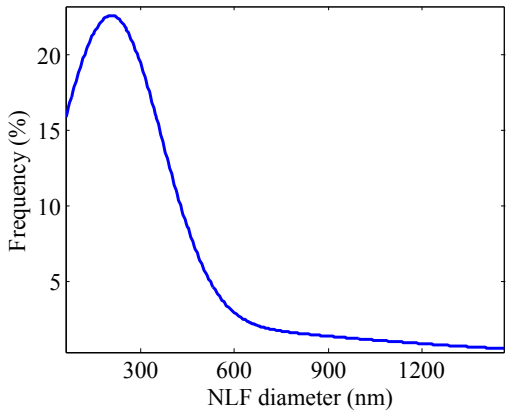

Figure 3.23: Diameter distribution of NLF (The figure is made by author and the data are from: http://www.eftfibers.com)

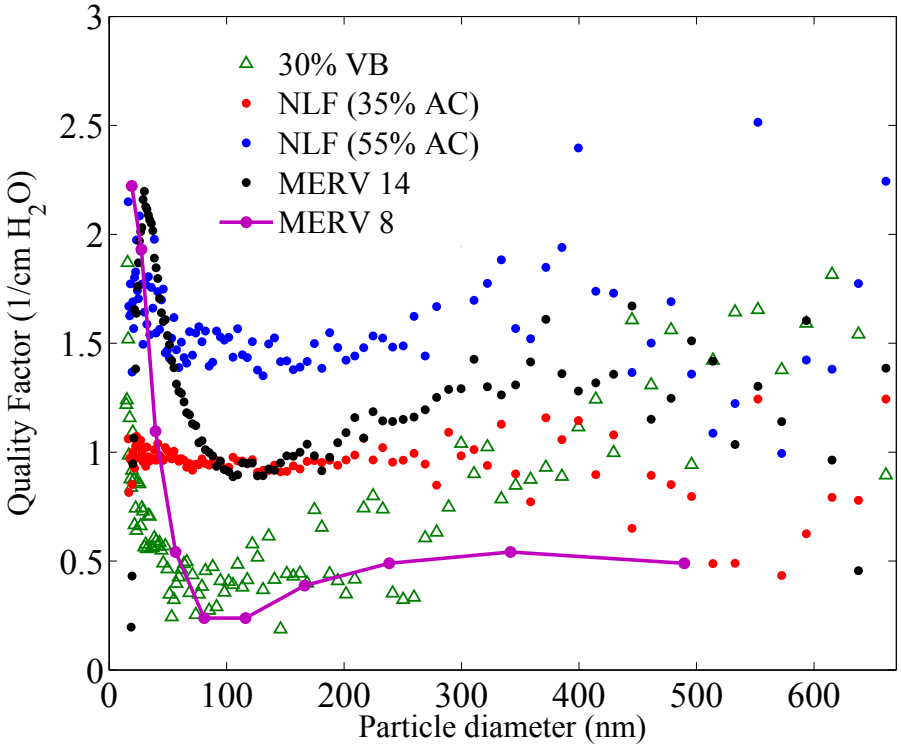

Figure 3.24: Filter quality factor.

3.2.2 Heat insulation

In this section heat insulation properties of foam-papers are studied. Thermal conductivity is measured in a range of working temperature for each foam-paper. Moreover, The relation between manufacturing condition(foam air-content) and thermal conductivity of the final product is studied. Finally, the results of the thermal conductivity of foam-papers made using various air-contents are compared to the results of commercial heat insulators.

3.2.2.1 Background

Thermal conductivity testing is a material property measurement associated with the difficulty in which heat is conducted through a specific type of material. Thermal conductivity is a pure material property independent of other different parameters like area of conduction or the thickness of the

material. Thermal conductivity is defined as the ratio of heat flux to the associated thermal gradient.

$$\vec{q_H} = -k(\vec{\nabla} T) \tag{3.3}$$

In one dimension the equation can be simplified as following. This measurement can be studied as the thermal conduction between two parallel, isothermal surfaces of area "A" and at temperatures T_H (temperature of hot plate) and T_C (temperature of cold plate) separated by a layer of the sample material having a thickness L with a steady state heat power Q. Thermal conductivity, k, is thus defined as:

$$k = \frac{Q.L}{(T_H - T_C)A} \tag{3.4}$$

Owing to recent developments in geological sciences, soil and building technology and oil industry, heat transfer in disordered structures and conductivity of porous materials are becoming very important. As an example, experiment done by Tseng *et al.*[43] can be pointed out. The thermal conductivity of the polyurethane foam is investigated both theoretically and experimentally for the development of liquid hydrogen storage tanks in temperature range of 20 K to 300 K in their research.

The effect of porosity of this sort of materials plays an essential role in their thermal conductivity. The relation between porosity and thermal conductivity is studied by several researchers. The authors try to find a relation between thermal conductivity coefficient and porosity of different porous materials. However some difficulties arise since thermal conductivity of porous materials is not a function of porosity alone. Other parameters such as pore shape and type of the material of the solid state (metallic or polymeric or ...) play important roles in the heat transfer mechanism. The mentioned mechanism is also different for a particular porous material at high and low porosities. So that the model which is accurate for a particular material with low porosity may not be rigorous for the same material with high porosity.

Several models have been proposed for approximating the thermal conductivity of porous materials versus porosity. The simplest model which is also quite rigorous for porosities less than 0.1 and greater than 0.9 is proposed by Loeb[44]. More precisely, for a mono-disperse porous material with closed pores having the porosity less than 0.15, MaxwellEucken[45] model is recommended. This model is not valid for higher values of porosity, since the connectivity of pores (open porosity) change the mechanism of heat transfer. For the high porosity condition, Russells relation[46] is recommended. Russell's relation has been developed based on parallel/series resistor approach used to explain the effect of cubic pores in a medium[46]. Reichenauer *et al.*[47] finds that pore

size is also a very important factor that affects thermal conductivity of porous materials. If the pore size is very small (less than 500 *nm*), thermal conductivity of such a material is less than the thermal conductivity of the same material (with the same porosity) with larger pore sizes. This phenomenon happens due to Knudsen effect.
Recently, Smith *et al.*[48] carried out a complete experimental and numerical research about the thermal conductivity of monolithic porous materials (tin oxide, alumina, and zirconium ceramics) with both high and low porosities. They found an accurate relation between thermal conductivity of a porous material and porosity of the same material based on the thermal conductivity of the solid phase and the gaseous phase (air). Smith *et al.*[48] also figured out that the thermal conductivity models for porosities less than 0.65 and higher than this value should be different in order to have accurate results.

3.2.2.2 Methodology

There are number of possible ways to measure thermal conductivity, each of them being suitable for a limited range of materials, depending on thermal properties, working temperature and other different factors. Steady-state and transient methods are two different classes for measuring thermal conductivity of a sample material. In general, steady-state techniques perform the measurement while the temperature of the sample material doesn't experience any serious variation with respect to time. This makes the signal analysis much more straightforward because of implying a quasi-constant signal. The only difficulty is that a well-designed and engineered experimental setup is usually needed. Transient techniques perform measurement in the condition that the temperature is changing with respect to time (for example in the process of heating up the sample). This measurement is relatively faster compared to the steady-state one since reaching steady-state condition is not required. However, the time dependency of the final signal with respect to time makes the mathematical analysis of the final signal more difficult. The following methods are well known in transient measurement:

- Transient Plane Source (TPS) and Modified TPS (MTPS) methods.
- Transient Line Source (TLS) method.
- Laser Flash Method (LFM).
- Time-domain thermo-reflectance method

In this research we use Transient Plane Source (TPS) technique for calculation of the thermal conductivity of NBSK foam-papers at three different temperatures. The samples were measured at freezing point of water ($0°C$), boiling point of water ($100°C$) and at the standard atmospheric temperature ($20°C$) in different porosities. The ThermTest- TPS-2500-S Thermal Constants Analyser is the instrument chosen for all bulk thermal conductivity measurements. The TPS-2500-S meets the ISO Standard (ISO/DIS 22007-2.2)[11].

Transient Plane Source Method, utilizing a plane sensor and a mathematical model describing the heat conductivity, combined with electronics, enables the method to be used to measure thermal transport properties. It covers thermal conductivity range of at least 0.01-500 $\frac{W}{mK}$ (in accordance with ISO 22007-2) and can be used for measuring various kind of materials, such as solids, liquids, pastes and thin films. In 2008, it was approved as an ISO standard for measuring thermal transport properties of polymers. This TPS standard also covers the use of this method to test both isotropic and anisotropic materials. The TPS technique typically employs two samples halves, in between which the sensor is sandwiched. Normally the samples should be homogeneous, but extended use of transient plane source testing of heterogeneous material is possible with proper selection of sensor size to maximize sample penetration. This method can also be used in a single-sided configuration, with the introduction of a known insulation material used as sensor support. By recording temperature versus time response in the sensor, the thermal conductivity, thermal diffusivity and specific heat capacity of the material can be calculated. Today, many companies like *Thermo Test Inc.* work on producing very accurate machines based on TPS method. One of the very accurate machines for this purpose is ThermTest-TPS-2500-S, the product of *Thermo Test Inc.*.

The Transient Plane Source TPS-2500-S constitutes an industry benchmark thermal conductivity test system. The TPS-2500-S thermal conductivity instrument is designed for analysing thermal transport properties of solids, liquids, paste and powders, including various types of geometries and dimensions. Table 3.4 shows the specifications of TPS-2500-S.

[11] http://www.thermtest.com/

Table 3.4: Specifications of the apparatus(TPS-2500-S) which is used to measure thermal conductivity of foam-papers.

Materials	Solids, liquids, powders and paste
Thermal Conductivity Range	0.001 to 1000 *W/mK*
Thermal Diffusivity Range	0.1 to 100 mm^2/s
Specific Heat Capacity Range	Up to 5 MJ/m^3K
Measurement Time	1 to 1280 seconds
Reproducibility	Typically better than 1%
Accuracy	Better than 5%
Temperature Range	$-160°C$ to $1000°C$
ISO Standard	ISO/DIS 22007-2.2

The basic principle of the TPS System is that the sample surrounds the TPS sensor in all directions and the heat generated in the sensor freely diffuses in all directions. The solution to the thermal conductivity equation assumes the sensor is in an infinite medium, so the measurement and analysis of data must account for the limitation created by sample boundaries. Preliminary measurements are on each sample. This included selection of the TPS sensor to be used, test time and output of power to the TPS sensor. A standard wait period of 10-15 minutes is implemented between successive measurements on each sample to ensure the samples are isothermal prior measurement. Samples for this test are in circular shape and the diameter of each sample is 35*mm*.

3.2.2.3 Results and discussion

Samples of the same grammage ($100g/m^2$) of standard foam-paper made up of NBSK pulp and BiotergeAS-40 surfactant are used for this test. Table 3.5 shows some physical and morphological characteristics of the samples used for this test. Different porosities are because of the different air-content(manufacturing condition) of the foam. The bulk thermal conductivity of the samples made in 21%, 34%, 43% and 54% foam air-contents are measured at three different temperatures (0, 20 and 100 degrees of Celsius) as mentioned before. Bulk Thermal Conductivity was measured using the TPS Standard Analysis Method. This method is used to determine the bulk thermal conductivity of porous materials in the wide range of thermal conductivities ($0.001W/mK$ to $1000W/mK$) and temperatures as shown in Table 3.4.

Table 3.5: Characteristics of NBSK foam-paper samples for thermal conductivity test.

Foam air-content (%)	Bulk (cm^3/g)	Porosity (%)
21	20.15	96.6
34	46.54	98.1
43	50.90	98.7
54	95.21	99.5

The results of thermal conductivity versus foam air-content at different temperatures and thermal conductivity versus temperature for different porosities are illustrated in Figure3.25 and Figure3.26 respectively. The results show that by 3% increasing in porosity of samples, the values of thermal conductivity decrease by about 24% in low temperature and about 15% in high temperature range. This is an interesting result which shows the considerable effect of porosity in thermal conductivity reduction in order to make light thermal insulators out of pulp. As the porosity of the samples increases, the volume fraction of air in the equi-size samples increases. This leads to decreasing the thermal conductivity of the final product since the thermal conductivity of air (about 0.026 at $25°C$) is much lower than thermal conductivity of NBSK fibres (about 0.056 at $25°C$). The results also show that by increasing the working temperature from $0°C$ to $100°C$ the values of thermal conductivity increase since the air convection through the pores (small scale channels) considerably increases. The error bars of the experimental data using TPS-2500-S show outstanding repeatability and reproducibility in measurements. Figure 3.5 also shows that by increasing the working temperature, the thermal conductivity of foam-papers increasing. This is reasonable since foam-papers are porous materials i.e. they consist of a solid phase (fibres) and fluid phase (air). The values of the thermal conductivity of the porous materials depends on both thermal conductivity of solid phase and fluid phase. The thermal conductivity of fluid phase increases by increasing the working temperature which incurs increasing the thermal conductivity of the final material.

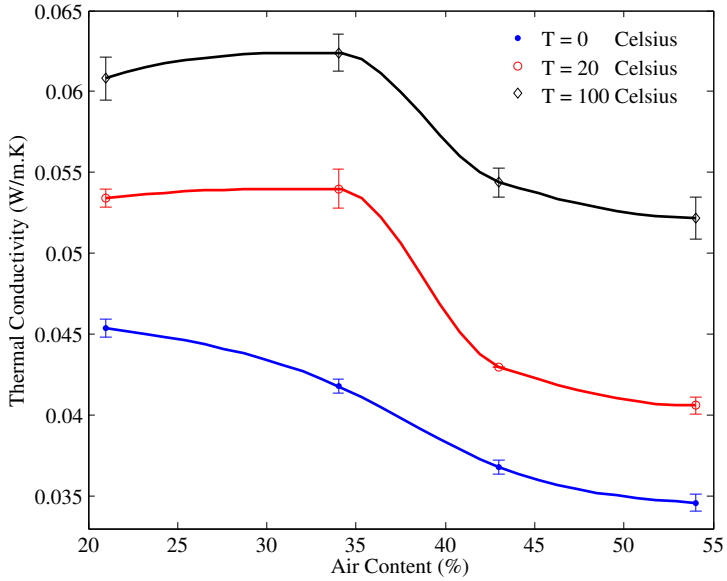

Figure 3.25: Thermal conductivity of NBSK foam-paper vs. foam air-content in three working temperatures.

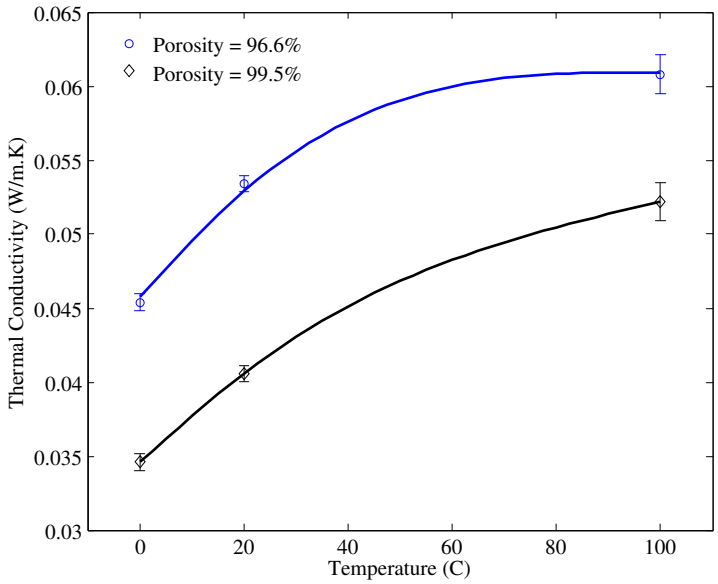

Figure 3.26: Thermal conductivity of NBSK foam-paper vs. working temperature for different porosities.

In the next step the results of the thermal conductivity of our samples are compared to the values of thermal conductivity of commercial heat insulators. The results show that as the porosity of foam-paper increases, the thermal conductivity values of foam-papers get closer to commercial heat insulators. Figure3.27 also shows that the values of the thermal conductivity of the foam-paper made up of 54% foam air-content are in the range of commercial insulators. To summarize, we developed porous papers demonstrated thermal conductivity close to commercial insulators however more research must be done for the commercializing purposes.

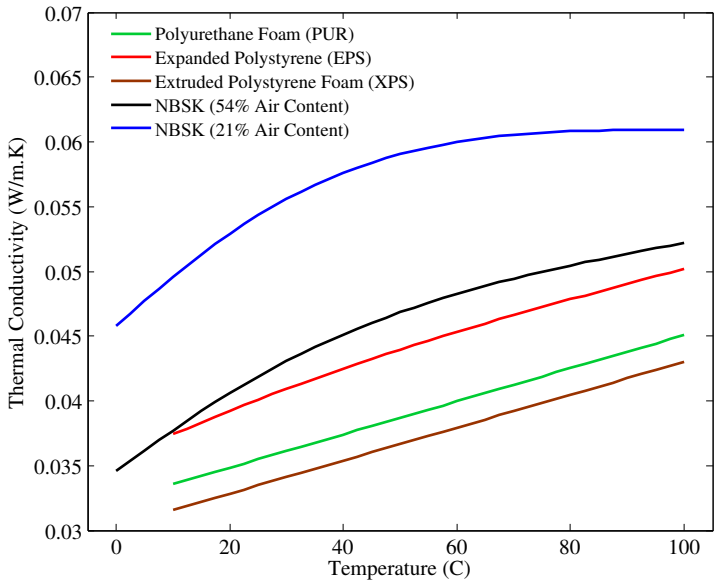

Figure 3.27: Thermal conductivity of NBSK foam-papers vs. temperature comparing to commercial heat insulators.

3.2.3 Acoustics

In this section, attention is focused on measuring the sound absorption (acoustic) properties of foam-papers. Air dried NBSK and freeze-dried Nanofibrillated Lyocell Fibre (NLF) are used to make foam-papers for acoustic tests. The samples are made in both 50% and 70% air-contents in order to study the effect of manufacturing condition on their final acoustic performance. To study the acoustic properties of foam-papers, sound absorption and sound transmission are measured for foam-papers with two different porosities (two different foam air-contents) in the range of low-frequencies. To improve the performance of air-dried NBSK samples, the effect of using multi-

layer foam-papers is investigated. Other non-acoustical parameters such as air-flow resistivity, tortuosity, viscous characteristic length and thermal characteristic length are also measured. At the end of this chapter, the results of foam-papers are compared to the results of some available commercial acoustic materials and also compared to some available mathematical models.

3.2.3.1 Background

All materials have the capability of absorbing sound to some extent but an "acoustical" material or "sound absorber" is a material which is able to absorb most of the sound energy striking its surface. This characteristic can be explained by sound absorption coefficient in a specific frequency range which is defined as the percentage of the incident sound energy which has been absorbed. Acoustical materials have vast industrial applications such as sound absorbers in buildings. They can be categorized in three major groups:

- Porous absorbers: A thick solid that contains cavities, interstices and channels so that sound waves can propagate through them and be converted to heat. Common porous absorbers are fibreglass and generally foams like Polyurethane foam.
- Panel absorbers: Non-porous, thin materials which are usually placed over an airspace, that vibrate in a flexural mode in response to sound pressure exerted by adjacent air molecules. Best examples are thin wood panelling traps at orchestra platforms.
- Resonator absorbers: Perforated materials which have openings capable of absorbing sound in a limited frequency range. A classic example is the Helmholtz resonator used to identify the various frequencies or musical pitches.

Porous absorbers are the most popular and efficient materials in acoustical applications. They generally have a high sound absorption coefficient compared to other materials. In porous materials, essentially closed pores do not contribute in absorbing sound since they do not have a continuous interaction path for friction and viscous forces which are substantially responsible for momentum loss of sound waves. This phenomenon eventually result in sound attenuation as reported by Arenas and Crocker[49]. They explain the mechanism of sound absorption as following. When a porous material is exposed to incident sound waves, the air molecules on the surface of the material and inside the pores, are forced to vibrate. During the time that the vibration is happening, air molecules lose some of their initial energy and simultaneously convert it to heat (viscous losses on the walls of the interior pores). This mechanism is different at low and high frequencies. At low frequencies, the mechanism is isothermal but at high frequencies the same mechanism is adiabatic.

In fibrous materials, much of the energy can also be absorbed by scattering from the fibres and by the vibration caused in the individual fibres. However in granular materials or rigid porous ones the sound absorption mechanism is mainly due to the viscosity of the air trapped among the granules.

Many experimental works and mathematical modelings have been done by researchers on measuring and modeling the acoustic properties of porous materials. A standard technique to characterize these absorbing materials is the impedance tube. In 1976 Seybert and Ross[50] proposed a setup based on random excitation in a two microphone tube to measure the acoustic properties of some available sound absorbers. They claim that the two-microphone random-excitation technique can be used to evaluate the acoustic properties very rapidly since traversing is necessary and random excitation is used. Lauriks *et al.*[51] observe that only free-field technique for the perpendicular surface impedance can give reliable results. They prove that the friction between the screen of the porous sound absorber and the tube causes extra sound attenuation. Allard *et al.*[52] study on the acoustic properties of resonant materials. A very interesting research is done by Vigran *et al.*[53] on the effect of constraints at the tube wall on the absorption coefficient of an elastic porous material. They compare the results of standing wave tube and free field method and figure out that in the case of those porous materials which are influenced by the wall constraints of the tube, the standing tube method should be used carefully since both impedance and absorption coefficient could only be measured inaccurately. Champoux and Stinson[54] carry out an experimental research on the acoustical properties of some simple porous materials. They also compared their results for some available theoretical models between 500 Hz and 4500 Hz. They showed that their results are in good agreement with available theoretical models. Moreover, Champoux and Stinson[54] also study the effect of pore shape factor on the acoustical properties of porous media both in low and high frequencies. Their results show that a single shape factor leads to very good agreement with the exact solutions for all frequencies. Champoux and Stinson[55] investigated on the acoustical properties of porous ceramics both experimentally and theoretically. The Attenborough[56] and the Biot-Allard[52, 54] models are used for the theoretical modeling part of their research. They show that the experimental results of porous ceramics can totally be predicted by Biot-Allard model. The method of three-microphone impedance-tube is first proposed and developed by Izumi *et al.*[57] to improve the two-microphone impedance-tube. By using this method, more acoustical parameters can be measured. This method is improved by Salisuo and Panneton[58] later. Recently, Doutres *et al.*[59] proposed an experimental technique based on a three-microphone impedance tube setup to measure acoustic and non-acoustic properties of porous sound absorbing materials. Based on their new approach, they measure the acoustic properties of

some porous materials such as sound absorption coefficient, sound transmission loss, effective density and effective bulk modulus. In addition to that, they calculate the non-acoustic parameters such as static airflow resistivity, tortuosity, viscous and thermal characteristic lengths using the measure properties by an indirect approach. For calculation of the non-acoustic properties, they used the values of the open porosities of the porous materials.

Besides the experimental studies, lots of mathematical models are proposed by many authors to predict the acoustical properties of porous materials. The final purpose of these mathematical models is to derive the characteristic wave impedance (Z_c) and characteristic propagation constant (k) of a plane wave in a porous material (generally in any sound absorbing media) as functions of non-acoustical parameters. Two approaches can generally be used to model the sound propagation phenomenon in porous absorbers. The first one is empirical approach. The most widely used work for this approach is the work done by Delany and Bazely[60]. However this model has some weak points in predicting the acoustic properties of some porous materials with high flow resistivity in the range of low frequencies. In order to fill this gap, many other researchers such as Miki[61] contributes to Delany and Bazely model. Miki model compensates for the weak points of Delany and Bazely model. The second approach is purely analytical approach based on micro-scale study of the wave equation under specific assumptions for sound propagation in porous media. Biot[62] and Attenborough[56] propose two different models based on the second approach to predict the acoustical properties of a rigid porous sound absorber. The only problem in this sort of models arises when one deals with very complicated internal micro structures. In these structures the final results are highly dependent on how one defines the geometrical parameter called ”shape factor”. Besides these two major approaches, some simple phenomenological approaches are proposed to ignore some complicated details which do not violate the essential physics behind the problem. The models proposed by Johnson *et al.*[63] and Allard-Champoux[64] are in this category.

Some parameters have significant effects on the acoustical results of porous materials. These parameters are investigated by numerous authors. Koizumi *et al.*[65] finds that smaller fibre diameters in the internal structure of a porous material, leads to higher value of sound absorption coefficient. This effect is because using finer fibres in the structure of a porous medium results in having more tortuous medium with the same porosity. The effect of fibre diameter is also investigated by Lee and Joo[66] in a separate research. Ren and Jacobsen[67] studied the effect of air flow resistivity on the acoustical properties of porous medium. They figure out that as the air flow resistivity per unit thickness of the porous material increases, the characteristic impedance

and the coefficient of sound absorption increases. Conrad[68] shows that the current effect happens because when sound wave propagates inside a material with higher resistivity against flow, its amplitude diminishes by friction and its energy of propagation is converted to heat. Another important parameter is open porosity. Shoshani *et al.*[69] show that by increasing the number of pores in the direction of sound propagation, the coefficient of sound absorption of the porous material increases. They also state that the size and the shape of the pore have noticeable effect on sound absorption. Ibrahim and Melik[70] carry out a research about the effect of material thickness on sound absorption coefficient. Coates and Kierzkowski[71] demonstrate that the effective sound absorption in porous media happens when the thickness of the porous material is at least one tenth of the wavelength of the incident sound. Density is another important parameter and its importance is more than other factors as it is directly related to the price of porous material. Koizumi *et al.*[65] show that porous materials with lower density are very good sound absorbers in low frequencies and materials with higher densities are good sound absorbers at high frequencies.

3.2.3.2 Methodology

To measure the acoustic properties of foam-papers, an experimental setup based on the three-microphone impedance-tube method is used in the centre for acoustics researches at the University of British Columbia. Figure 3.28 shows the experimental setup that is used for these tests.
This method is carried out by first measuring two different transfer functions. The first one is the transfer function between the first microphone and the rigid end (the location of third microphone) and the second transfer function is that between the second microphone and the rigid end. By using these two transfer functions, the one between the first and the second microphones can be calculated and eventually the material's impedance and characteristic propagation constant will be calculated. Based on the criteria specified by *ISO CD 10534-2*, the results from the impedance tube that we used to calculate the acoustic properties in low frequency ranges, are valid from approximately 250 Hz to 1750 Hz. The samples for this purpose is made in circular shape with diameter of 10 cm.

Figure 3.28: Three microphone impedance tube for acoustics tests.

The air flow resistivity of the samples is measured using a simple experimental setup similar to what is used before to measure pressure drop in filtration tests. For this purpose, **ASTM C522-03** standard is used to design the experimental setup for the test. The experimental setup induces air-flow through the sample so that the extra pressure drop can be measured due to the presence of the sample. The slope of the air flow-rate versus pressure drop graph is a function of air flow resistivity. Air flow resistivity can also indirectly be calculated based on the results of the impedance-tube. Sometimes, a great difference between the results of these two methods are reported for some materials.

3.2.3.3 Results and discussion

In this section the effect of thickness, air-content and crowding number[12] on the acoustic properties of foam-papers are investigated. The results are also compared with commercial sound absorbers. Figure 3.29a shows the variation of absorption coefficient in the low frequency range for three different thickness of NBSK samples in 50% air-content. By increasing frequency, the values of absorption coefficient increases similar to other typical sound absorbers. It is also shown that at a particular frequency, the absorption coefficient of foam-papers is dependant on its thickness. The larger the thickness of the foam-paper is, the greater the absorption coefficient in that particular frequency will be. In fact, the amount of wave absorption is strongly dependant on the particle velocity of that wave inside the porous material. The higher particle velocity leads to the higher

[12]Crowding number is defined as the expected number of fibres in a sphere of diameter one.

amount of friction and energy loss and consequently higher absorption coefficient. Hence, the higher frequency in the particular thickness provides higher particle velocity and as a result, higher absorption coefficient. The greater thickness at a particular frequency also leads to more energy which can be damped and consequently higher absorption coefficient. That's the reason that multi-layer samples of foam-papers shows better sound absorption performance as shown in Figure 3.29b. Figure 3.29c shows the effect of air-content on the sound absorption performance of foam-papers. Higher air-content leads to having lower absorption coefficient at the same thickness. Higher air-content means lower number of fibres per unit volume and consequently less capability of damping wave energy.

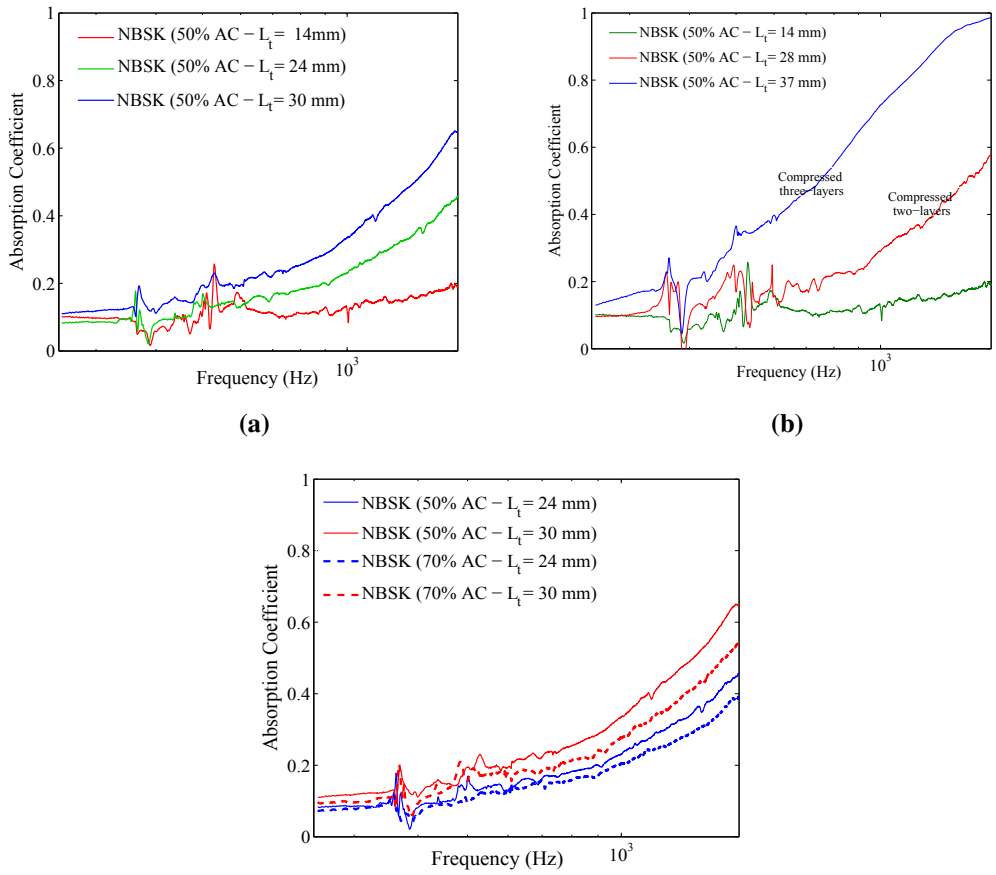

Figure 3.29: Acoustic properties: (a) NBSK (50% AC) in different thickness (b) Effect of multi-layer and compressed samples (c) Effect of air-content.

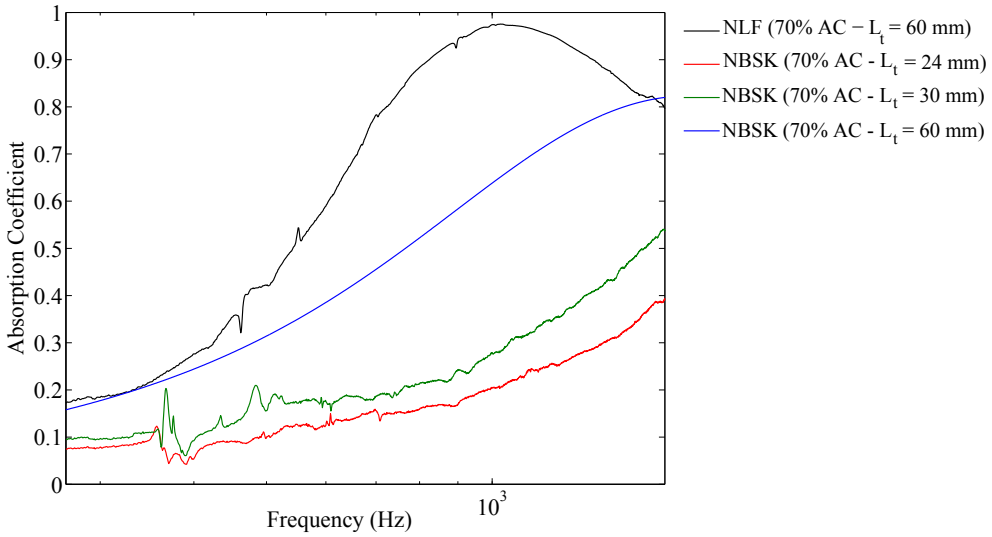

Figure 3.30: Acoustic properties: results of freeze-dried fibrillated fibres (NLF).

Figure 3.30 compares the results of freeze-dried NLF with air-dried NBSK ones at the same air-content and different thickness. Since sample at the thickness of 60 *mm* is not available, Miki's model[61] applied to predict its absorption coefficient. The results show much better sound absorption performance for NLF samples. This happens because of large crowding number and very high tortuous medium which contributes to high wave energy damping.

Figure 3.31 shows the comparison between the results of absorption coefficients of some foam-paper products with commercial sound absorbers. The results show that the absorption coefficients of foam-paper products in low frequency are in the range of commercial acoustic products. The air flow resistivity of the samples are also in the range of commercial sound absorbers at almost the same thickness range. Table 3.6 shows the results of air flow resistivity of foam-paper samples and compared them with commercial sound absorbers.

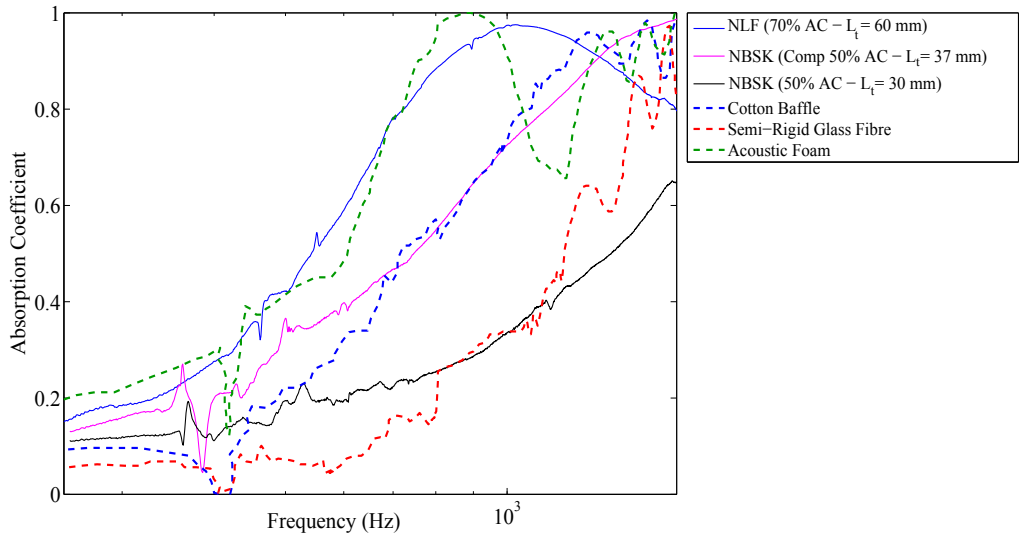

Figure 3.31: Acoustic properties of foam-paper products compared to commercial acoustic materials.

Table 3.6: Air flow resistivity of air-dried NBSK and freeze-dried NLF foam-papers compared to commercial sound absorbers.

Sample	Thickness (mm)	Air flow resistivity ($\frac{Pa.s}{m^2}$)
NBSK (50% AC)	14	2285
NBSK (50% AC)	30	2936
NBSK (50% AC - 2 stacks)	28	5738
NBSK (50% AC - 3 stacks)	37	6913
NBSK (70% AC)	30	2175
NLF (70% AC)	60	28669
Cotton baffle	25.4	52000
Semi-Rigid Glass Fibre	25.5	21000
Acoustic foam	50	22000

Chapter 4

Foam-paper: Lattice-Boltzmann simulation

On of the most usual and interesting phenomena in nature is fluid flow inside grossly disordered geometries. The most common example of this transport phenomenon is the flow of water inside soil. Studying this problem is also important for many industries such as oil industry, membrane technology, fuel cell technology, aerosol filtration technology, tissue engineering and various stages of technical processes in different parts of process industry.
For instance in oil industry, in order to extract the trapped oil in sedimentary rock, another fluid is pumped through the media to force the oil out. In aerosol technology, the goal is to capture sub-micron particles by letting them pass through a fibrous porous media called aerosol filter. The importance of improving our information and understanding of such processes arises because of these type of applications. In the first application (oil industry), the amount of energy consumed to reach the final goal satisfactorily, is high. In the second application (aerosol filtration), filtration efficiency is strongly depend on the dynamics of fluid in filter media.

One of the industries in which comprehending the dynamics of flow in porous structures has a tremendous importance, is pulp and paper industry. The final product of this industry is mainly paper which is made up of compact random orientation of cellulose fibres. The dynamics of fluid in different stages of paper-making process which control the final properties and the quality of paper, is related to the flow characteristics of porous media. For example, fibre deposition on the forming fabric or de-watering the paper in the last stage of paper-making process are good representatives of a very complex fluid flow through a porous structure. Recently, novel developments

in pulp and paper industry along the line of producing porous 3D papers (foam-paper), further increased the significance of this subject. As we know by now, foam papers have applications in different technologies such as aerosol filtration, heat insulation and acoustic technologies. Though a lot of experimental research has been done on characteristics and applications of foam-papers, the mysterious physics of fluid flow through grossly disordered structures of foam-papers has room for research research.

In both theoretical and experimental research works which have been done by now on the physics of flow through porous media, the first and the trickiest part of the research is to find a mathematical correlation between the macroscopic characteristics of the porous material such as porosity and the main macroscopic flow properties. The first study which resulted in finding an empirical relation, is done by Darcy. Darcy, found a linear relation between the flow-rate and the pressure-drop of a porous medium. The slope of the flow-rate versus pressure-drop is a function of a parameter called permeability which can be considered as the indicator of the fluid's conductivity through porous structure. In laminar flow regimes, permeability is defined as the coefficient of linear response of the fluid to the non-zero pressure gradient if the flux is induced[72, 73]. Darcy's law is more generalized for the turbulent flow regimes by contribution of Forchheimer[73, 74]. Another important correlation is the relation between permeability and porosity. The well-known equation for that is empirical Kozeny-Carman equation which relates permeability of the media to porosity, specific surface and tortuosity as represented in Equation 4.1.

$$K = \frac{(1-\phi)^2}{\phi^3 S^2 \mathscr{T}} \tag{4.1}$$

Other mathematical models are also proposed by many authors[75–77] for this purpose which will be discussed in the next section. Another important correlation is between friction factor and Reynolds number called Ergun equation (Equation 4.2).

$$(\frac{\Delta P}{L})(\frac{D_P}{\rho V_s^2})\frac{\phi^3}{(1-\phi)} = \frac{150}{Re_P} + 1.75 \tag{4.2}$$

where $Re_P = \frac{D_P V_s \rho}{(1-\phi)\mu}$ is defined as Reynolds number.
Though the mathematical models are accurate to some extent to predict the behaviour of fluid flow in porous media but the physics is incomplete due to variation in internal geometry, the pore size, shape and scale.

Improvement in computers in terms of both CPU and memory, computational algorithms such as parallel and asynchronous programming architectures and numerical techniques in computational fluid dynamics (CFD) have made it possible to solve very complicated fluid dynamics and heat transfer problems. Recently very huge and geometrically complex fluid dynamics problems are solved utilizing GPU[1] programming. Beside improving the computational facilities and programming techniques, the vital role of fast numerical algorithms for computational fluid dynamics purposes should not be forgotten.

One approach for solving the flow equations is using conventional CFD techniques such as FVM[2] to solve the Navier-Stokes equations. Fluid flow is determined by its macroscopic parameters like velocity and pressure and traditional CFD techniques normally solves them in a discrete domain. For instance in FVM, the domain (which is a complex geometry) should be discretized in finite volumes (which are much simpler geometries) and finally solve the continuum media equations using a numerical algorithm. Though, traditional CFD techniques are considered as a good approach for the vast range of fluid dynamics problems but some serious limitations make one not to consider them for solving the flow problem in random porous structures. The first reason is that the results of CFD techniques are very sensitive to both grid resolution and the method of mesh generation. Practically, one of the most challenging tasks of the traditional CFD approach is generating an appropriate mesh in order to reach a correct solution. Sometimes the geometry is very complicated and randomly structured and it is very time consuming to generate a proper mesh to simulate the flow correctly and sometimes it is totally impractical. The other limitation of FVM methods is that in the rarefied flow regimes, in cases that the mean free path of gas molecules is considerable in comparison to the characteristic length of the control volume, the NavierStokes equations fail to simulate the correct physics of the flow. This phenomenon happens in simulation of flow through some porous structures such as filters made up of micro and nano-fibres. In this case, continuity assumption breaks down and Navier-Stokes equations are not valid.

Another approach for flow simulation is from the microscopic-level point of view. In principle, the modeled flow behaviour can be modeled and simulated based on the direct modelling of the dynamics of fluid molecules. This method is called direct molecular dynamics (MD) and is computationally very expensive. Beside the MD approach, the Lattice Boltzmann Method (LBM) is

[1] Graphical Processing Unit
[2] Finite Volume Method

very promising in terms of ease to simulate the dynamics of fluid and effectiveness is being dealt with distributed computational domains (parallel processing architecture and platform). The models based on LBM are quite different from both accurate microscopic description (MD method) and from a macroscopic description of Navier-Stokes equations in the continuum hydrodynamics limit. The key point is that the macroscopic description is generally quite insensitive to the underlying exact interactions among particles. Because of this reason, a very simplified and idealized microscopic model can be taken into account as long as the basic laws of physics such as conservation laws, are satisfied. For this reason, an "artificial grid-land" can be designed in a way to satisfy all fundamental conditions of flow equations like conservations of mass and momentum, rotational invariance and so on. Indeed, though the LBM known as a finite difference discretized version of the Boltzmann equation, historically it has evolved after realizing that fluid's motion can be simulated with very simple discrete models which were developed based on physics laws (Lattice Gas techniques). Generally, in lattice gas simulation techniques, each node represents probability of the presence of the group of particles in a velocity interval. This probability at each node is evolved by propagation of molecules to their adjacent lattice sites and exchanging their momenta in the next collision.

What has been explained tries to elucidate that there are possibilities to switch from micro-scale to meso-scale simulations since computational cost of micro-scale simulations are much higher. Meso-scale simulations (specifically LBM) also have some advantages compared to the regular computational fluid dynamics techniques even in the range of continuum fluid dynamics. Firstly, LBM is known as a mesh-less technique and so flow problems especially multiphase ones in irregular geometries can be handled with ease. Broadly speaking, easy handling of irregular boundary conditions and mesoscopic forces which drive phase transition, simpler settling the hydrodynamics equations in the territory of soft matter research works when the hydrodynamic equations are not well settled and easier coping with other related complexities hard to describe within a continuum approach, are the advantages of using Lattice Boltzmann method instead of regular CFD techniques. Moreover, lattice Boltzmann method allows solving the problem by massively parallel computing algorithms.

The main objective of this section is to figure out the flow behaviour in uniform and non-uniform (like foam-paper internal structure) porous structures. In order to reach this goal, it is necessary to import the foam-paper geometry to computer and compute the fibre distribution in the thickness of a foam-paper. For this purpose, micro X-ray tomography technique is employed

to take high resolution images from cross section of some samples. The result of the X-ray tomography device is thousands of 2D images containing salt and pepper noise. Image processing techniques for the purpose of noise detection is applied to 2D tomographic images to make the data usable for lattice Boltzmann simulation. All the data are binarized (converted to lattice) using a reasonable threshold. After preparing the 2D data, a 3D image reconstruction code is developed to make the 3D geometry.
Since the size of the 3D matrix is very large, it is decided to make a medium using 3D random cylinder geometry. The cylinders are sampled out of the fibre distribution function which is computed by X-ray tomography technique. Though this is not the exact alternative of the actual geometry, it is very useful to understand the difference between the flow pattern in a non-uniform geometry (such as foam-paper geometry) and a uniform one. Very useful information can be extracted about the difference between the permeability values in above mentioned medium.

4.1 Kinetic theory and lattice gas cellular automata

4.1.1 Kinetic theory

In theoretical physics, intricate dynamics of non-equilibrium systems and their relaxation toward thermodynamic equilibrium was always a matter of question and interest. Kinetic theory is a branch of statistical physics dealing with this topic. The quantitative investigation on the dynamics of the flowing substance can be elaborated in two major levels of description: continuum level (macroscopic) and molecular level (microscopic). Flows in a continuum framework are described in terms of field parameters such as pressure, density and velocity which are both space and time dependant. For most applications, the current view point and description are quite sufficient since the physics of the flow is totally identified. Nonetheless, in some special cases this approach is not able to define the whole picture. For these cases, micro-scale point of view becomes important. In this approach, the motion of individual molecules of the fluid is studied. The final flow will be the result of the collection of molecular motion and interaction. Though this approach directly simulates the flow, it is computationally very expensive. To overcome this problem, statistical mechanics proposed a third intermediate level of description, in which fluid is represented by a distribution function which acts as a representative for collection of particles. In other words, flows are represented in terms of the probability $f(t;\vec{r},\vec{v})$ of the presence of given fictitious ensemble of particles at a given position in space, $\vec{r}$ and time t and velocity $\vec{v}$. The current view point is called mesoscopic approach and is described by kinetic theory.

In 1872 the Austrian physicist, Ludwig Boltzmann derived his celebrated equation for describing the evolution of distribution function ($f(t;\vec{r},\vec{v})$) in terms of micro-dynamics interactions. Although this equation is not an easy approach to a fluid dynamics problem mathematically and computationally, it contains more information due to this fact that f exists in a six-dimensional phase space. The mathematical representation of the Boltzmann Equation (BE) is for the probability distribution function (PDF) $f(t;\vec{r},\vec{v})$ and is as following[78, 79]:

$$[\partial_t + \vec{v}.\partial_{\vec{r}} + \vec{F}.\partial_{\vec{v}}]f(t;\vec{r},\vec{v}) = Q_{12} \tag{4.3}$$

The left hand side of Equation4.3 describes streaming motion of the molecules with the presence of the external force-field ($\vec{F}$) and the left hand side of the equation explains the effect of inter-molecular collisions which diverts fluid's molecules from streaming trajectory. Equation4.3 shows that the collision operator for the evolution of one-particle PDF (f) depends on two-particles PDF (f_{12}) which is concealed inside Q_{12}. It is proved that the evolution of f_{12} depends on the three-particles PDF (f_{123}) and generally, dynamics and evolution of the s-particles PDF depends on $(s+1)$-particles PDF. This chain of equations which imply the dependency of the evolution of $f_{1\to s}$ to $f_{1\to(s+1)}$ is called *BBGKY*[3] hierarchy. BBGKY-hierarchy is first derived from *Liouville* equation for the evolution of an N-particle system[80]. In order to terminate this hierarchy and to close up the mathematical description of the collision operator in Equation4.3, some simplifying assumptions are taken into account[80]. The most important assumption is that the fluid is considered as a rarefied system so that the assumption of binary collision is valid and the probability of ternary (and/or higher order) collisions are practically nil[80]. The final Boltzmann equation for a rarefied fluid regime is written as following:

$$[\partial_t + \vec{v}.\partial_{\vec{r}} + \vec{F}.\partial_{\vec{v}}]f = \int (f_{1'}f_{2'} - f_1 f_2)\vec{v_{rel}}\sigma(|\vec{v_{rel}}|,\Omega_s)d\vec{v_2} \tag{4.4}$$

As shown in Equation4.4 , the mathematical description of collision operator is very complicated even for a simplified binary collision in rarefied regimes.

It should be noted that if all gains and losses in the system are totally balanced the collision term will be annihilated. Explicitly, this means that both rate of change and gradient of change of the probability distribution function is zero and all ensembles are constant. However, constant ensembles does not mean that there is no intermolecular interaction between molecules. This means

[3] Bogoliubov-Born-Green-Kirkwood-Yvon

that every direct intermolecular collisions is dynamically balanced by an inverse collision and vice versa. This condition is called *local equilibrium*. The probability distribution function for the local equilibrium is first proposed by Maxwell and Boltzmann and is known as Maxwell-Boltzmann equilibrium distribution. Equation4.5 demonstrates the celebrated Maxwell-Boltzmann equilibrium distribution. Since $Q(f^e, f^e) = 0$, the Maxwell-Boltzmann distribution for local equilibrium can shown to be:

$$f^e = \rho(2\pi v_T^2)^{-\frac{3}{2}} \exp\left(\frac{-\sqrt{\sum_{i=1}^{3}(c_i - u_i)^2}}{2v_T^2}\right) \qquad \text{and} \qquad i = 1 \rightarrow 3 \tag{4.5}$$

where $v_T = \sqrt{\frac{K_B T}{m}}$ is the thermal speed which is related to the fluid temperature. Another profound contribution of Boltzmann was quantitative discovery of irreversibility. He defined a functional called H-function as represented in Equation 4.6:

$$H(t) = -\int f \ln f d\vec{v} d\vec{r} \tag{4.6}$$

and proved that this function is a monotonically increasing function of the time i.e. $\frac{dH}{dt} \geq 0$. The equality sign happens when the system is in *global equilibrium* and the entropy of the system is maximum.[4] H-theorem is similar to the second law of thermodynamics. By considering the generalized Gibbs entropy into account, it can be easily found that $H = \frac{S}{VK_B}$ which shows that for a system of interest with a fixed volume V, entropy never diminishes.

4.1.2 A brief review of lattice gas cellular automata (LGCA)

Before talking about the idea of lattice gas and application of Cellular Automata for solving the hydrodynamics equations, it will be appropriate to discuss briefly its history and to understand the idea behind it. CA[5] is a discrete novel model and a creative approach for solving physical phenomena in nature and a new smart approach to solve differential equations. The method is studied in vast range of sciences such as statistical physics, computational biology, social science, finance and economics. For the first time, in 1950, CA was developed and introduced by Stanislas Ulam and John von Neumann[81] at Los Alamos National Laboratories while Ulam was working on the

[4]Global equilibrium is a condition that both mean flow speed and the flow temperature is constant. Global equilibrium takes requires much longer time to happen comparing to the local equilibrium. In fact, being in the local equilibrium condition, $Q(f^e, f^e) = 0$, does not put any restriction on the space dependence of temperature and flow speed.

[5]Cellular Automata

growth of crystals, using a simple lattice network and Neumann was working on *self-replicating systems*. In 1969 a German mathematician and computer scientist, Konrad Zuse proposes his celebrated theory, the *Zuse's Theory* that the physical rules of the universe are naturally discrete and the entire nature is the result of a deterministic computation on a cellular automaton[81]. Besides applying the method to hydrodynamics, Zuse applied this model for solving electrodynamics and quantum mechanics problems. Between 1970 and 1985, several scientists such as John Horton Conway[82], Martin Gardner[83–85] and Stephen Wolfram[86] work on the idea of CA and it's different applications. Cellular Automata consists of regular arrangements of single grid of cells of the same kind so that each one of them has a finite number of different states. To start a simulation with CA, a particular state is given to the cells as an initial state at $t = 0$. The new state of each cell is updated synchronously in terms of the current state of each cell and the states of the local adjacent cells according to a determined and fixed set of rules at discrete time steps. The current systematic survey on the algorithm of the one dimensional CA is studied by Wolfram[86].

Lattice Gas Cellular Automata (LGCA) is the first specific Cellular Automata technique developed for the sake of fluid flow simulation in 1973 by Hardy, Pomeau and Pazzis[81]. This method is also called HPP-LGCA which is derived from initials of its authors. HPP technique is able to conserve mass and momentum. However, it is not suitable for the actual macroscopic flow simulation since it is not able to satisfy the other characteristics of Navier-Stokes equations in macroscopic level such as *rotational invariance*[79, 81]. In 1986, Frisch, Hasslacher and Pomeau find that if a CA is run over a lattice with hexagonal symmetry, it leads to satisfy the hydrodynamics equations in macroscopic level. This model is called FHP-LGCA[79, 81].
Though, remarkable progress is achieved in order to make LGCA suitable for simulating flow equations, the interest to use them for this purpose levelled off at early 90s. The major problem was high amount of statistical noise of simulation of high Reynolds number flows. There are also other problems which can be found in the literature[79]. These problems are overcome by the idea of Lattice Boltzmann method.

4.2 Lattice-Boltzmann method: hydrodynamics

In 1988, the idea of Lattice Boltzmann technique to solve the discrete Boltzmann equation for flow simulation purposes is first proposed by G. McNamara and G. Zanetti[79, 87] and then followed by Higuera and Jimenez[79, 88]. They try to minimize and/or escape the major problems in the LGCA approach which are statistical noise and exponential complexity of collision algorithm[79].

Though the main problems of LGCA are lifted by the previous proposed lattice Boltzmann models, the third noticeable limitation is still a matter of concern which is high momentum diffusivity. This limitation is due to the collision operator of the LGCA method which supports very low Reynolds number flows and is also dominated by the works done by Higuera, Succi and Benzi[79, 88].
One of the most serious problems of lattice Boltzmann techniques is raised because of the complex nature of the collision integral in the Boltzmann equation. Several authors propose different models to circumvent this issue. The simplest model which converges to the solution of the Navier-Stokes equations is the model proposed by Bhatnagar, Gross and Krook[79, 89, 90] in 1954 and called *BGK* model. The idea behind their model is to simplify the collision operator which contains huge amount of information about the binary interactions, into a much simpler operator which can preserve the essential physics of the problem. It is proved that most of the of details in the binary collision integral of the Boltzmann equation does not significantly influence the final macroscopic results of the many fluid dynamic problems in the moderate Reynolds numbers[79]. The BGK approximation conserves the collision invariants of $Q(f,f)$ and also expresses the tendency to Maxwellian local equilibrium. These two together are enough to make sure that this model is accurate enough to model the collision integral for a wide flow regimes. The BGK model is represented as:

$$Q(f,f) = -\frac{f - f^e}{\tau} \tag{4.7}$$

Parameter τ is called relaxation time an it defines the time required for the molecules to relax toward local Maxwellian equilibrium. The combination of lattice Boltzmann method with BGK model is called LBGK technique and it is used by many authors[79, 90]. In the lattice Boltzmann technique, the kinetic equation is solved for the probability distribution function, f, in the phase space and the macroscopic parameters such as density, macroscopic velocity and specific internal energy fields can be calculated by evaluating the hydrodynamic moment equations of the distribution functions as following[79]:

$$\rho(\vec{r};t) = m\int f(\vec{r},\vec{v};t)d\vec{v} \tag{4.8}$$

$$\rho(\vec{r};t)\vec{u}(\vec{r};t) = m\int \vec{v}f(\vec{r},\vec{v};t)d\vec{v} \tag{4.9}$$

$$\rho(\vec{r};t)e(\vec{r};t) = m\int \frac{(\vec{v}-\vec{u})^2}{2}f(\vec{r},\vec{v};t)d\vec{v} \tag{4.10}$$

The kinetic model that is used in this survey is the Boltzmann equation with the so called single relaxation-time (SRT) approximation, the BGK model.

$$[\partial_t + \vec{v}.\partial_{\vec{r}}]f = -\frac{1}{\tau}(f - f^e) \tag{4.11}$$

In order to solve the Equation 4.11 numerically, first it should be discritized in the velocity space using the finite numbers of velocity vectors which must obey conservative laws and also preserve other properties of the flow equations.

$$\frac{\partial f_k}{\partial t} + c_k.\frac{\partial f_k}{\partial \vec{r}} = -\frac{1}{\tau}(f_k - f_k^e) \tag{4.12}$$

where $c_k = \delta x/\delta t$ is the kth discrete velocity. The current equation must also be discretized in time and space. The final discrete lattice BGK equation is:

$$f_k(r + c_k\delta t, t + \delta t) - f_k(r,t) = -\frac{\delta t}{\tau}(f_k(r,t) - f_k^e(r,t)) \tag{4.13}$$

The chosen discrete velocity space depicts the type of the lattice model which is selected. A 2D nine velocity square lattice (D2Q9) and 3D nineteen velocity lattice (D3Q19) models are used for simulating two dimensional and three dimensional flows respectively. The discrete velocity set for D2Q9 lattice model is as following:

$$\vec{c}_k = \begin{bmatrix} 0 & 1 & 0 & -1 & 0 & 1 & -1 & -1 & 1 \\ 0 & 0 & 1 & 0 & -1 & 1 & 1 & -1 & -1 \end{bmatrix}$$

The discrete velocity set for D3Q19 lattice model is as following[91]:

$$\vec{c}_k = \begin{bmatrix} 0 & 1 & -1 & 0 & 0 & 0 & 0 & 1 & 1 & 1 & 1 & -1 & -1 & -1 & -1 & 0 & 0 & 0 & 0 \\ 0 & 0 & 0 & 1 & -1 & 0 & 0 & 1 & -1 & 0 & 0 & 1 & -1 & 0 & 0 & 1 & 1 & -1 & -1 \\ 0 & 0 & 0 & 0 & 0 & 1 & -1 & 0 & 0 & 1 & -1 & 0 & 0 & 1 & -1 & 1 & -1 & 1 & -1 \end{bmatrix}$$

The equilibrium distribution function for both D2Q9 and D3Q19 models are:

$$f_i^{eq} = w_k\rho[1 + \frac{\vec{c}_k.\vec{u}}{c_s^2} + \frac{(\vec{c}_k.\vec{u})^2}{2c_s^4} - \frac{\vec{u}.\vec{u}}{2c_s^2}] \tag{4.14}$$

where $c_s = \frac{1}{\sqrt{3}}$ is the lattice speed of sound for both lattices, and pressure can be derived from the

ideal gas equation of state which is $P = \rho c_s^2$. The values of w_k are lattice weighting functions. The lattice weighting functions for D2Q9 is:

$$w_k = \begin{cases} 4/9 & k = 0 \\ 1/9 & k = 1,3,5,7 \\ 1/36 & k = 2,4,6,8 \end{cases} \tag{4.15}$$

and for D3Q19 lattice is:

$$w_k = \begin{cases} 1/3 & k = 0 \\ 1/18 & k = 1 \rightarrow 6 \\ 1/36 & k = 7 \rightarrow 18 \end{cases} \tag{4.16}$$

In order to derive the incompressible flow equations ($Ma = \mid \vec{u} \mid / c_s \ll 1$) (the so-called Navier-Stokes equations) from discrete Boltzmann equations, Chapman-Enskog expansion[92] is applied. The corresponding equation for the dynamic viscosity in the Navier-Stokes equations can be derived as following[79]:

$$\nu = (\tau - 0.5) c_s^2 \delta t \tag{4.17}$$

Since the value for dynamic viscosity should be positive to be physically meaningful, the condition $\tau > \frac{1}{2}$ also must be satisfied.
The lattice BGK equation, Equation 4.13 can be computationally solved in a specific manner. If the physical time step for computation (δt) is sufficiently less than the mean collision time of particles, the **streaming** and **inter-molecular collision** parts of Equation 4.13 can be decomposed into two independent local equations as following:

$$\tilde{f}_k(\vec{r}_i, t) = f_k(\vec{r}_i, t) - \frac{1}{\tau}(f_k(\vec{r}_i, t) - f_k^e(\vec{r}_i, t)) \qquad \text{Collision} \tag{4.18}$$

$$f_k(\vec{r}_i + \vec{c}_k \delta t, t + \delta t) = \tilde{f}_k(\vec{r}_i, t) \qquad \text{Streaming} \tag{4.19}$$

where $\tilde{f}_k$ depicts the post collision probability distribution function.

4.2.1 LBM versus Navier-Stokes solvers

One of the most important questions which is required to be answered is what are the major differences of a Lattice-Boltzmann based solver and Navier-Stokes solvers based on the regular continuum CFD techniques. In other words, it should be answered that who really needs LBM to solve a

fluid dynamics problem. In this section, some advantages and disadvantages of LBM are listed in detail.

- One of the most challenging problems of regular NS[6] incompressible solvers, is to solve a Poisson equation in order to compute the pressure field. This results in global data communication and parallelization is relatively difficult. The condition for the LBM is reverse. The collision step in LBM is completely local and no calculation is happened in the streaming step. The pressure field is also solved using an equation of state (for an ideal gas this equation is a linear function of density field, $P = \rho c_s^2$) [79]. This shows that the data communications in the whole LB algorithm is local making it easy to incorporate massive parallelization.

- Uniform data shifting is another advantage of LB method compared to the conventional NS-solvers. Non-linear convective term in the Navier-Stokes equations ($\vec{u}.\nabla\vec{u}$) is hard to treat. However, in the LB method, due to the linear operator in the Boltzmann equation(Equation 4.4), the non-linear convective term is replaced by linear advective term (Equations 4.18 and 4.19) and hence it is very straightforward to model.

- The value for the lattice time-step and the lattice grid size are both equal to 1. So that the CFL[7] number which is proportional to $\frac{\delta t}{\delta x}$ in lattice Boltzmann method is 1. This implies that the rate of convergence in LB is totally imposed by the acoustic propagation which must be very low in order to take care of the destructive effect of high lattice Mach number. Consequently, LB is considered as a low-speed convergent method for steady-state simulations.

- Handling complex geometries and boundary conditions are matter of concern for both NS-solvers and LB method. In NS-solvers, the boundaries of the objects must be precisely detected and the domain should be discretized with special and careful treatment. However it is not always possible to mesh the domain properly due to the gross disorderedness and complexity (such as random disordered porous structures like the geometry of paper). Moreover, proper handling of normal and tangential shear stress components on the boundaries is required. LB methods also suffer from problems related to curved boundaries and lack of a specific counterpart in micro and meso-scale for some boundary conditions (for example no-slip boundary condition does not have a very accurate representation in micro-scale).

[6] Navier-Stokes
[7] Courant - Friedrichs - Lewy

4.2.2 Applications of LBM

Nowadays the vast applications of Lattice-Boltzmann method in solving fluid dynamics problems has become more common because of the availability of huge computational resources, especially in the domain of parallel computing architectures. Lattice-Boltzmann incorporates complex physics in a very simple and natural way by playing the details of particle-particle interactions or level of expansion of the distribution function in velocity space. In other words, complex physics can easily be added to the fundamental equations of the Lattice-Boltzmann method. What is meant by complex physics are two-phase flow problems(liquid-gas or solid-liquid transitions)[93], physics of the single-component or multi-component flows through random disordered geometries and porous media[94], particle suspensions in fluid (such as sub-micron aerosol filtration)[95], chemically reacting flows and combustions[96], MHD[8] flow[97], fully turbulent non-reactive and reactive flows[94, 98], crystallization and so on.

For simulation of fluid flow through porous media, a lot of reasonable work has been done both purely on understanding the physics of the flow and the applications such as aerosol filtration, oil industry and so on. The works which are done in FP-Innovation by Drolet[95] on the numerical simulation of aerosol filtration in fibrous media are good examples. Rebai et. al.[95] carried out a complete analysis on the effect of different computer-generated fibrous filters. They calculate the effect of filtration efficiency of fibrous filters by changing different parameters such as aspect-ratio of fibres, crowding number and the Reynolds number using Lattice-Boltzmann method. Thomas *et. al.*[99] study the Stokes flow through uni-modal fibrous porous media using LBM. They used coarse numerical lattice technique to predict the permeability of the media in different solid fractions and different fibre diameters. Przekop and Gradon[100] simulate fluid flow and unsteady particle deposition in nano-structured fibrous media using the combination of LBM and Brownian dynamics. They finally investigate the efficiency and the dynamics of deposition on the nano-fibrous media. There are several other papers similar to the presented works investigate different parameters of fibrous filters and their effect on the filter efficiency.

4.2.3 Source of errors in LBM

A matter of concern of every numerical method to solve hydrodynamics equations is about unavoidable errors. In this section, the sources of errors for the lattice Boltzmann technique are introduced.

[8]Magnetohydrodynamics

- *Domain discretization errors:* One of the main error sources in numerical methods is due to the problem's domain discretization into finite number of cells or nodes. The level for accuracy needed in LB simulations determine the largest lattice size that can be used. It is very common to determine the size of the lattice spacing based on the minimum scale length of the geometry. For instance the lattice spacing sizes in the flow simulation inside a 2D channel and around a 2D cylindrical obstacle, are the width of the channel and the radius of the cylinder respectively. In the flow simulation in porous media it is very common to use the minimum pore size as the scale length which sometimes results in very fine lattice nodes spacing near percolation threshold *i.e.* many pores have very small size leading to huge simulation time. Several works are done to circumvent this problem by applying local grid refinement methods[101, 102].
  It has been shown that in LBGK method, smaller values of the BGK relaxation time, decreases the finite size effect. On the other hand very small values of relaxation time (τ close to 0.5) might result in some errors and numerical instabilities[79, 102].

- *Compressibility errors:* Compressibility errors are caused and propagated due to the dependency of the pressure field to density in Lattice-Boltzmann simulation. This is in contradiction with the assumption of incompressible fluid. In order to simulate the incompressible flow equations with LB method which is inherently quasi-compressible, the simulation must be done in low Ma number. The error in the LB due to the compressibility effect is $O(Ma^2)$[79]. The value of lattice Ma must not locally be greater than 0.3 [79].

4.2.4 Boundary conditions

One of the main strong points of lattice-Boltzmann method is its capability of handling different (even very complex) boundary conditions, especially handling boundary conditions according to grossly irregular geometries which can be illustrated by the case of no-slip boundary conditions at solid walls. Two different approaches are applied to model boundary conditions for LBM. One is called *"Distribution Modification"* and the other is *"Distribution Reconstruction"*[103, 104]. The distribution modification approach tries to imply that some physical rules such as conservation laws and bounce-back rules are able to obtain the unknown distribution functions. The distribution reconstruction approach tries to recreate the distribution function on the boundaries by relating them to the macroscopic properties and their derivatives. The half-way bounce-back[79, 102], full-way bounce-back[79] boundary conditions for wall no-slip condition in solid-fluid interactions and the so-called Zou and He boundary condition[105] and Inamuro boundary condition[106] for mod-

elling of the open boundaries are examples of the distribution modification approach. Methods such as finite-difference boundary condition[107], regularized boundary condition[108] and the one proposed by Guo *et al.*[109] for modeling of the open boundaries are categorized in the distribution reconstruction approach.

It should be noted that all the mentioned boundary conditions are developed for the boundaries and geometries which can be described by horizontal and vertical lines in Cartesian coordinates. Special treatment based on the interpolation and/or extrapolation techniques must be taken into account in order to calculate much more precise approximation of those values that must be computed on the nodes away from the walls of the solid geometry in the Cartesian/lattice coordinate system. The interpolation and/or extrapolation techniques must be utilized since the boundary nodes can not locate on the curved boundaries (lattices configuration) as it can for methods like finite difference in regular CFD. The method developed by Filippova and Hanel [110] (FH boundary condition), the modified method developed by Mei *et al.*[111] in continuation of the work done by Filippova and Hanel (FHM boundary condition), the method proposed by Bouzidi *et al.*[112] (BFL boundary condition) and the method proposed by Yu *et al.*[102] (Yu boundary condition) are the examples of distribution modification approach for the curved wall boundaries. However, the method proposed by Verschaeve *et al.*[108] which is based on the regularized boundary conditions for the open curved boundaries is a good example of distribution reconstruction.

4.2.4.1 No-slip boundary condition

In fluid dynamics the no-slip boundary condition is used in the solid-fluid interaction and states that at a solid boundary, the velocity of the fluid is zero relative to the boundary interface. In lattice-Boltzmann method, this can be achieved by implementing an algorithm based on particle's bounce-back on the boundaries[79]. Though the algorithm is simple, it can preserve the particles' momenta. Other techniques for simulating no-slip boundary condition is based on the idea of bounce-back algorithm but they provide more detail in order to diminish the errors on the boundaries.

4.2.4.1.1 Bounce-back algorithm

During the streaming process, the components of the distribution function which are propagating into the solid nodes[9] are bounced-back exactly in the opposite direction to its adjacent fluid-node. This means that the portion of the particle propagated into the solid boundary is reflected back to

[9]solid-nodes are those nodes that are inside the solid geometry and are in contact with at least one node out of the solid geometry (fluid-node)

the adjacent fluid-node in the opposite direction. In this process, the momentum of the particle is reversed. The applied surface force and applied torque are also calculated from the momentum transfer at each boundary node and summed over the whole number of solid-nodes. The *full-way bounce-back* method can be described as following:

$$\tilde{f}_{\tilde{k}}(\vec{r}_b,t) = f_k(\vec{r}_b,t) \tag{4.20}$$

where $f_k(\vec{r}_b,t)$ is the set of the incoming populations from computational domain into solid boundary before collision and $\tilde{f}_{\tilde{k}}(\vec{r}_b,t)$ is the set of the outgoing populations after collision from solid boundary to the computational domain. The full-way bounce back algorithm is a first-order accurate algorithm for no-slip boundary condition.

In order to increase the accuracy of algorithm to second-order algorithm, the idea of *half-way bounce-back* can be taken into account. In this method, the solid boundary locates halfway the link (between a solid node and a fluid node). In this algorithm solid nodes are practically act as ghost nodes so particles bounce back before reaching the actual solid node in halfway the link. From computational point of view, in the half-way bounce-back algorithm, at a given time t the post-collision values which are given by the population in the opposite direction at time $t-1$, are assigned. The collision step takes place after this step. Computationally, this is totally different from the full-way bounce-back method since the full-way algorithm takes place after the collision step. This implies that the half-way bounce-back algorithm keeps the normal collision step but modifies the streaming step quite differently in comparison to the full-way algorithm which modifies the collision step and keeps the normal streaming step. The mathematical description of the half-way bounce-back algorithm is as following:

$$f_{\tilde{k}}(\vec{r}_f,t+\delta t) = \tilde{f}_k(\vec{r}_f,t) \tag{4.21}$$

4.2.4.1.2 Filippova-Hanel-Mei (FHM) algorithm

The current algorithm is developed to take care of the solid-fluid interactions on the curved boundaries by applying a interpolation/extrapolation technique. Two major problems are involved in modeling of the curved boundaries in lattice Boltzmann method. The first problem is that the solid boundary nodes (wall nodes) are not exactly located on the lattice coordinates (or even at the halfway the link between sold nodes and fluid nodes). The second problem is that the field macroscopic parameters cannot be computed by only the conservation laws since the number of unknown populations are more (or sometimes less) than the equations. In this section, the algo-

rithm introduced by Filippova and Hanel and the modification that is done by Mei *et al.*[110, 111] is elaborated. As it can be seen in Figure 4.1, the vertical distance between the wall node and its adjacent fluid node is $\Delta.\delta x$ where $\Delta = \frac{|\vec{r}_f - \vec{r}_w|}{|\vec{r}_f - \vec{r}_b|}$ and obviously $0 \leq \Delta \leq 1$.

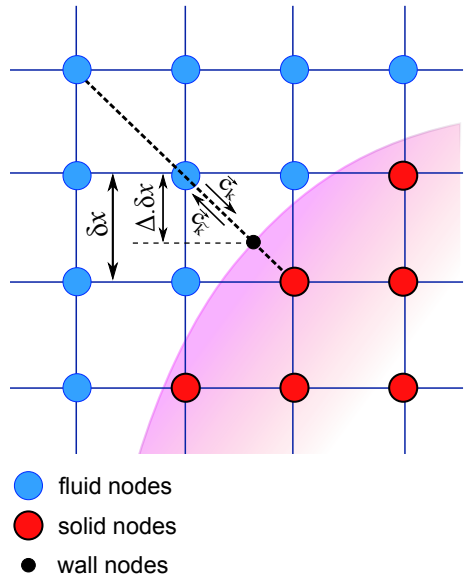

Figure 4.1: Curved boundary condition and lattice orientation.

In this method, after the collision step, the distribution function for the solid nodes which are linked at least with a fluid node should be updated based on an interpolation technique. The solid-to-fluid post collision distribution function can be interpolated by the values of post collision distribution function which is computed in the collision step (referring to Equation 4.18) and a fictitious equilibrium distribution function (f_k^*)[110, 111]:

$$\tilde{f}_{\bar{k}}(t,\vec{r}_b) = (1-\chi)\tilde{f}_k(t,\vec{r}_f) + \chi f_k^*(t,\vec{r}_b) + 2w_k\rho(t,\vec{r}_f)\frac{\vec{u}(t,\vec{r}_w).\vec{c}_k}{c_s^2} \tag{4.22}$$

where $\vec{u}(t,\vec{r}_w)$ is the velocity of the moving wall. The last term will vanish if the walls are stationary. The fictitious equilibrium distribution function is calculated as:

$$f_k^*(t,\vec{r}_b) = w_k\rho(t,\vec{r}_f)(1 + \frac{\vec{c}_k.\vec{u}(t,\vec{r}_b)}{c_s^2} + \frac{(\vec{c}_k.\vec{u}(t,\vec{r}_f))^2}{2c_s^4} + \frac{\vec{u}(t,\vec{r}_f).\vec{u}(t,\vec{r}_f)}{2c_s^2}) \tag{4.23}$$

where $\vec{u}(t,\vec{r}_b)$ is calculated as following:

$$\begin{cases} \vec{u}(t,\vec{r}_b) = & \vec{u}(t,\vec{r}_f) & \Delta < \frac{1}{2} \\ \vec{u}(t,\vec{r}_b) = & (\frac{\Delta-1}{\Delta})\vec{u}(t,\vec{r}_f) + (\frac{1}{\Delta})\vec{u}(t,\vec{r}_w) & \Delta \geq \frac{1}{2} \end{cases} \tag{4.24}$$

In Filippova and Hanel algorithm the interpolation parameter, χ is calculated as:

$$\begin{cases} \chi = & \frac{2\Delta-1}{\tau-1} & \Delta < \frac{1}{2} \\ \chi = & \frac{2\Delta-1}{\tau} & \Delta \geq \frac{1}{2} \end{cases} \tag{4.25}$$

The method proposed by Filippova and Hanel is improved by Mei *et al.*[110, 111] since the stability of their method is weak as $\tau \to 1$. The following formula for χ is proposed by Mei *et al.*:

$$\begin{cases} \chi = & \frac{2\Delta-1}{\tau-2} & \Delta < \frac{1}{2} \\ \chi = & \frac{2\Delta-1}{\tau} & \Delta \geq \frac{1}{2} \end{cases} \tag{4.26}$$

4.2.4.2 Open boundary conditions

Boundary conditions such as inlet/outlet boundaries, boundaries with free-slip condition (lines and planes of symmetry) and periodic boundaries are categorized in the scope of the open boundaries. In this section, algorithms for open boundaries in lattice Boltzmann method are briefly discussed.

4.2.4.2.1 Inlet/Outlet boundary condition

Several methods are proposed to model the inlet/outlet conditions for lattice Boltzmann method. One of the most successful and straight-forward methods to implement the Dirichlet boundary conditions at inlet/outlet is the method proposed by Zou and He[105] based on the general rules of conservation of mass and momentum at boundaries. The idea is derived by applying the bounce-back rule for the non-equilibrium part of the distribution function in the normal direction where the other two unknown functions are derived by the conservation rules. Zou and He boundary dynamics can be considered as extended bounce-back rule for open-boundaries. The probability distribution function can be decomposed into the equilibrium part and the non-equilibrium part as represented in Equation 4.27 .

$$f_k = f_k^e + f_k^{ne} \qquad k = 0 \to 8 \tag{4.27}$$

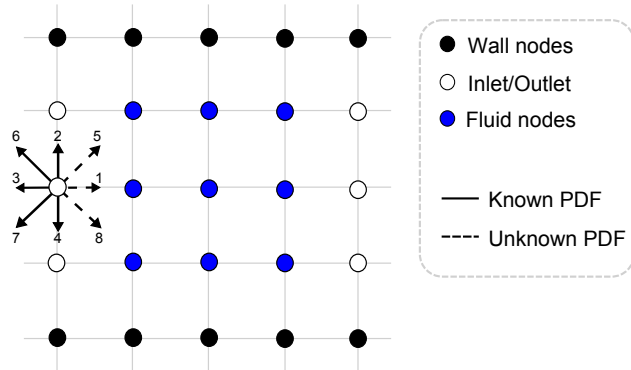

Figure 4.2: Unknown and known probability distribution functions in D2Q9 lattice.

For instance the x-component of velocity at inlet (west boundary) is u_x^{in} and the y-component of velocity is u_y^{in} as it is shown in Figure 4.2 for D2Q9 lattice. Recalling from Equations 4.8, 4.9 and **??** macroscopic field variables can be re-written as:

$$\rho^{in} = \sum_{k=0}^{8} f_k \tag{4.28}$$

$$\rho^{in} u_x^{in} = (f_1 + f_5 + f_8) - (f_6 + f_3 + f_7) \tag{4.29}$$

$$\rho^{in} u_y^{in} = (f_2 + f_5 + f_6) - (f_4 + f_7 + f_8) \tag{4.30}$$

The equilibrium condition normal to the boundary (Equation 4.27) results in:

$$f_1 - f_1^e = f_3 - f_3^e \tag{4.31}$$

where the equilibrium functions in Equation 4.31 can be calculated by Equation 4.14 . Solving Equations 4.31 , 4.28 , 4.29 and 4.30 the four unknowns can be found as[105]:

$$f_1 = f_3 + \frac{2}{3}\rho^{in} u_x^{in} \tag{4.32}$$

$$f_5 = f_7 - \frac{1}{2}(f_2 - f_4) + \frac{1}{6}\rho^{in} u_x^{in} + \frac{1}{2}\rho^{in} u_y^{in} \tag{4.33}$$

$$f_8 = f_6 + \frac{1}{2}(f_2 - f_4) + \frac{1}{6}\rho^{in} u_x^{in} - \frac{1}{2}\rho^{in} u_y^{in} \tag{4.34}$$

$$\rho^{in} = \frac{1}{1-u_x^{in}}(f_0+f_2+f_4+2(f_3+f_6+f_7)) \tag{4.35}$$

The equations for other boundaries (North, East and South) and other lattices (such as D3Q19 and so on) can be derived using the same technique[105].

4.2.4.2.2 Symmetry boundary condition

In many practical problems some geometrical symmetry can be identified. Hence, in order to reduce the computational time, the solution can be found only in one part of the problem and assume that the identical solution is repeated beyond the lines (and/or surfaces) of symmetry. Mathematically, symmetric boundary is usually understood by setting the component of velocity normal to the boundary to be zero:

$$\vec{u}(\vec{r},t).\hat{n} = 0 \tag{4.36}$$

In Lattice-Boltzmann method this condition can be satisfied by setting the unknown distribution functions equal to their mirror images[79] . The mathematical representation of such a condition, for example, for the south boundary(f_2, f_5andf_6 are unknowns) of Figure4.2 is as following:

$$\begin{cases} f_2 &= f_4 \\ f_5 &= f_8 \\ f_6 &= f_7 \end{cases} \tag{4.37}$$

4.2.5 Numerical stability

One of the main issues of different algorithms in fluid dynamics are problems related to the stability of that algorithm. Lattice Boltzmann technique is also not immune to the error dispersions related to the stability problems. Numerical instability in Single Relaxation LBM (SRT-method) are mainly arises due to the poor trade off between the relaxation parameter (τ) and the lattice Mach number (Ma). The problem arises because of inadequate-definition of the initial condition which results in high values of the lattice Mach number and spurious pressure waves. A very comprehensive research is done by Sterling and Chen[113] at Los-Alamos National Laboratories on the effect of different parameters on the SRT-method's stability. The distribution of the mass at a site between the different discrete speeds, the relaxation time in BGK model, the mean velocity and the wave number of perturbations are introduced as parameters on which the stability of SRT-method are depends on them[113]. Another important reason for numerical instabilities in SRT Lattice-

Boltzmann method is singular points in geometries. For instance, in a lid driven cavity problem, the two upper corners are singular points in the geometry which may result in a very noisy pressure field [113]. This effect is reduced by applying multi-block method[102] but, in the case of transient flow at high Reynolds number it is very hard (sometimes impossible by increasing the Reynolds number) to damp the acoustic wave propagated due to the singularity in geometry[102]. This is mainly because in SRT lattice Boltzmann, both bulk viscosity and shear viscosity are relaxed by a single value[102]. It should also be noted that the stability of boundary conditions (specifically open boundaries) is very important. The stability of Zou and He boundary condition is guaranteed in the range of low and moderate Reynolds numbers[102, 105]. However this boundary condition becomes vulnerable (and sometimes totally unstable) in high Reynolds numbers. In the case of no-slip boundary conditions in solid-fluid interaction, Yu *et al.*[102] compare the stability of different boundary conditions in different flow regimes.

In order to circumvent these problems, different algorithms are proposes which are more stable than the SRT-method. D'Humieres[114] proposes an algorithm based on the general collision matrix for collision operator that is called Multi Relaxation Technique (MRT). The idea of MRT-method is to relax different modes with different relaxation times while all modes in the SRT-method are relaxed with a single value of relaxation. A lot of scientific investigations is done on the MRT Lattice-Boltzmann method. Mei *et al.* compare the performance of SRT and MRT Lattice-Boltzmann methods in detail. A comprehensive study on stability characteristics and dispersion on MRT Lattice-Boltzmann method is carried out by Lallemand and Luo [115].

4.3 Results and discussions

This section is divided into two parts. In the first part, some 2D and 3D benchmark problems are solved for code validation purpose. Error and stability analysis of the code are also presented in this section. The results and discussions about the flow simulation inside 3D model geometry of foam-papers will be presented in the second part of this chapter. Codes for all 2D and 3D simulations are developed in C++ language in Linux platform from scratch. In both 2D and 3D codes the memory is dynamically allocated for handling huge data structure. Moreover, both 2D and 3D codes are parallelized for multi-core machines using OpenMP computer architecture. Complementary codes for geometry generation (for example generating a geometry for 3D random fibre medium) is also written from scratch for the simulations.

4.3.1 Benchmark studies

In this section, for the purpose of code validation, flow in a 2D channel at low Re number, flow around a circular cylinder at low and moderate Re numbers and pressure driven flow around bundle of 2D cylinders are solved. For the validation of 3D code, pressure driven flow inside a uniform random orientated cylinders (a model geometry for uniform fibrous porous media) are solved.

4.3.1.1 Flow inside a 2D channel

The first benchmark study is done on a 2D flow inside a channel geometry at a low Reynolds number. Zou and He boundary condition is applied for the inlet and outlet open boundaries. A uniform velocity profile is considered as an inlet boundary condition and a constant pressure is applied to the outlet boundary. No-slip boundary condition is applied to the top and bottom wall boundaries using full-way bounce-back algorithm. The channel aspect ratio is 25, the grid resolution in the width of channel is 80 and the flow solved for $Re = 4.0$.

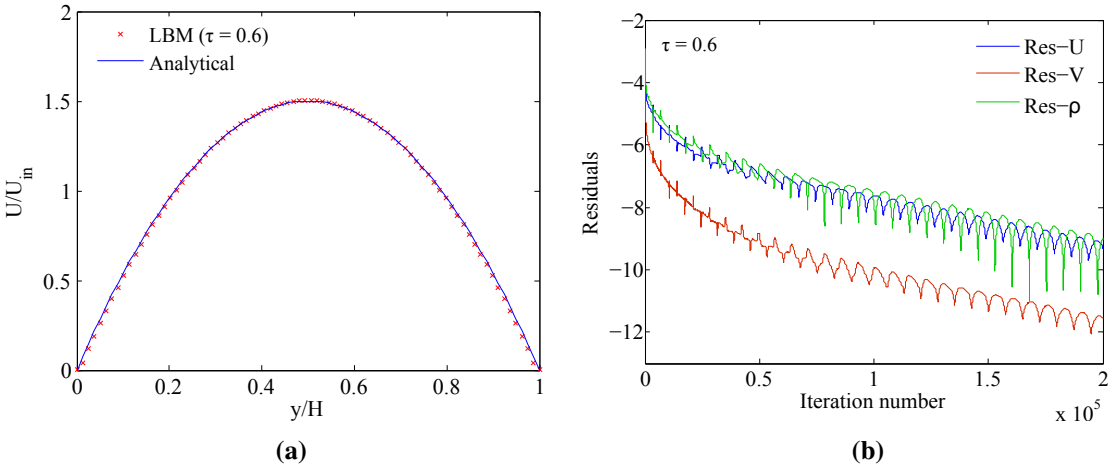

Figure 4.3: (a) Lattice-Boltzmann simulation of a 2D channel flow at $Re = 4.0$. (b) Residuals.

Figure4.3a shows the results of x-velocity in the thickness of the channel at fully-developed region. Comparing the LBM results to the analytical solution of 2D channel flow shows an excellent agreement. The residual plots are shown in Figure4.3b. The residuals are defined based on the maximum difference of a macroscopic parameter between the current and the previous time-step. In order to be more precise about the simulation parameters and source of errors in LB simulations, domain discretization and compressibility errors are studied. Figure4.4 shows how accuracy of the solution changes by increasing the grid resolution in the domain. Beside having a error in by

applying first-order accurate full-way bounce-back method on the channel walls, the other source of error causes using Zou and He algorithm in the simulation of open boundaries as shown in Figure4.5. This algorithm becomes unstable at high Reynolds number flow regimes due to increasing the error overshoot on boundaries by increasing *Re* number.

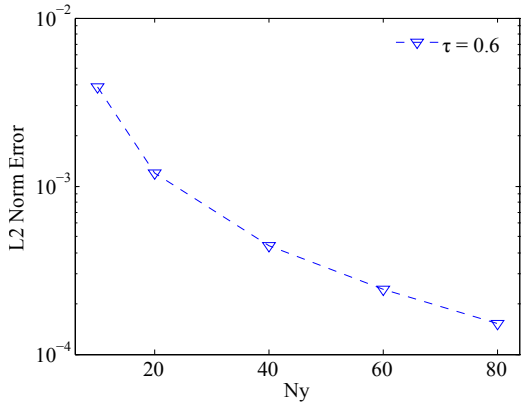

Figure 4.4: L2 norm errors of x-velocity for five different grid resolutions.

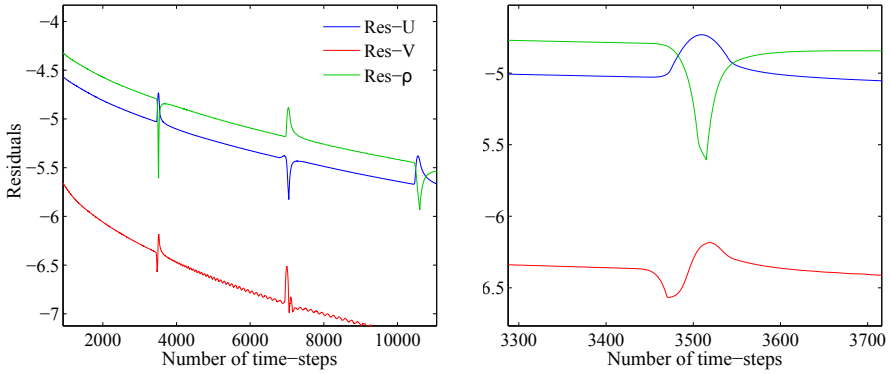

Figure 4.5: Errors made by applying Zou-He boundary conditions

Figure4.6a shows how the solution of the channel flow changes by increasing the lattice Ma number at the same number of iterations, same grid resolution and same Re number. Figure4.6b shows the effect of Ma number on the RMS error of the solution. By increasing the Ma number in the simulation domain the solution loses its accuracy. By increasing the value of Ma number to $Ma = 1.0$ the simulation becomes unstable and divergence occurs as is shown in Figure4.7.

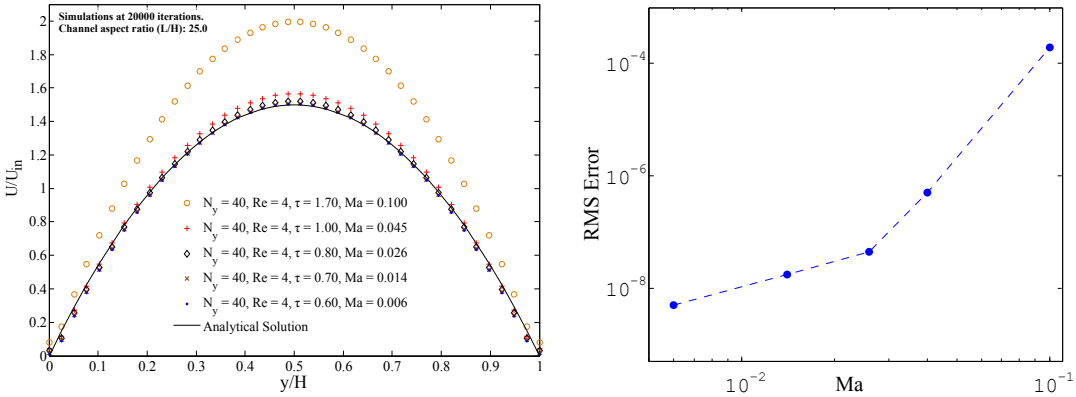

(a) **(b)**

Figure 4.6: Compressibility errors (a) Solution (b) RMS error vs. lattice Ma number.

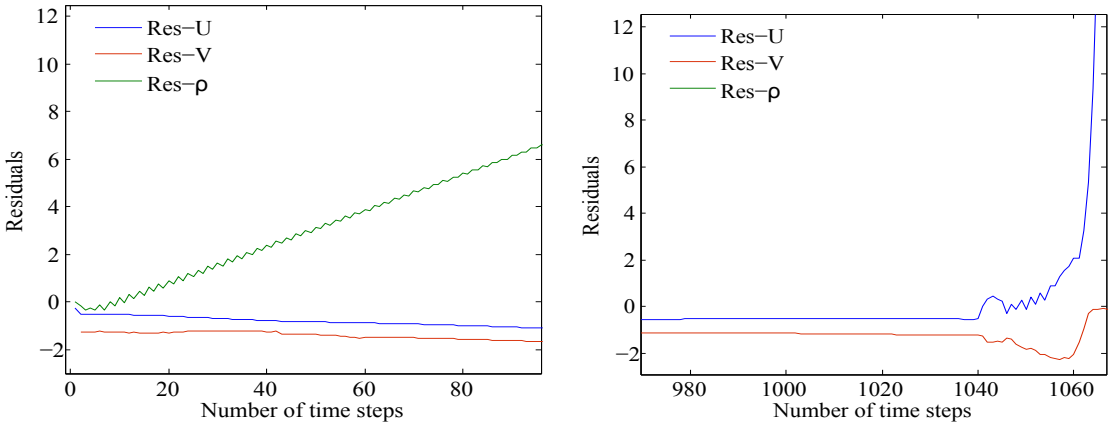

(a) **(b)**

Figure 4.7: Compressibility instability plots at $Ma = 1$.

4.3.1.2 Flow around a 2D circular cylinder

The second benchmark study is done on a 2D flow around a circular cylinder geometry at low and moderate Reynolds numbers. Zou and He boundary condition is applied for the inlet and outlet open boundaries. A uniform velocity profile is considered as an inlet boundary condition and a constant pressure is applied to the outlet boundary. No-slip boundary condition is applied to the top and bottom wall boundaries using full-way bounce-back algorithm. The channel aspect ratio is 6.25, the grid resolution in the width of channel is 160, the blockage ratio (Ratio of the channel

width to cylinder diameter) is 8 and the flow solved for $Re_d = 1, 5, 10, 20$ and 40. Second order accurate FHM boundary condition is implemented to simulate the no-slip condition on the surface of the cylinder more accurately. Figure4.8 a shows how those solid-nodes which are in contact with at least one fluid-node are identified by the code. The values of geometric parameter, Δ, is also plotted in Figure4.8b. This figure shows that the value of Δ is between 0 to 1 as it is predicted in FHM theory. Figure4.9 shows the results of the Drag coefficient in different Re_d numbers for both LB method and CFD. The CFD simulation is done using commercial software ANSYS-FLUENT 14.5. The results show excellent agreement compared to the CFD results. The centre of the cylinder is located at $x_c = N_x/4$ and $y_c = N_y/2$.

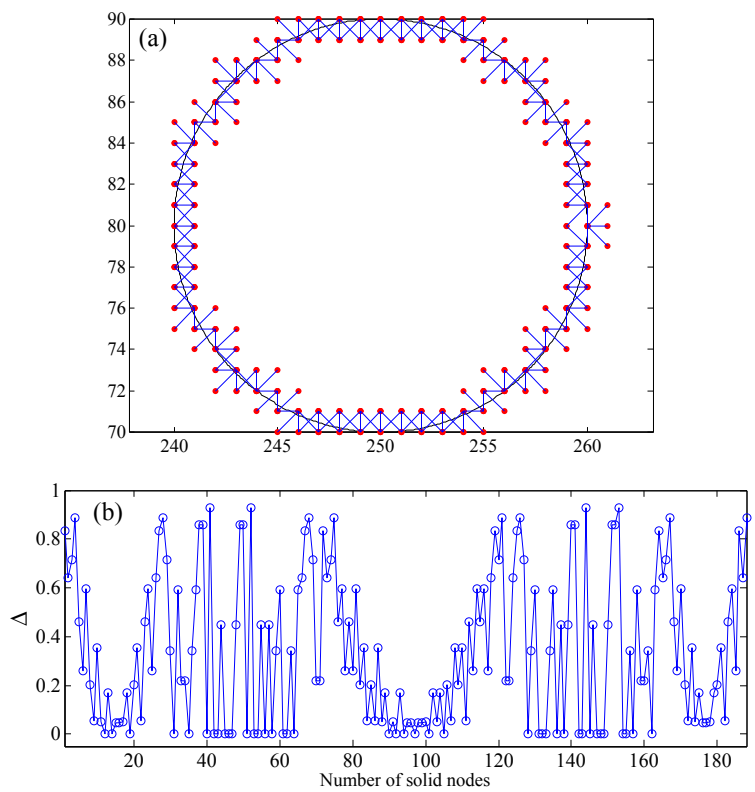

Figure 4.8: (a) Solid-nodes which have a connection at least to one fluid-node (b) Value of geometric parameter Δ.

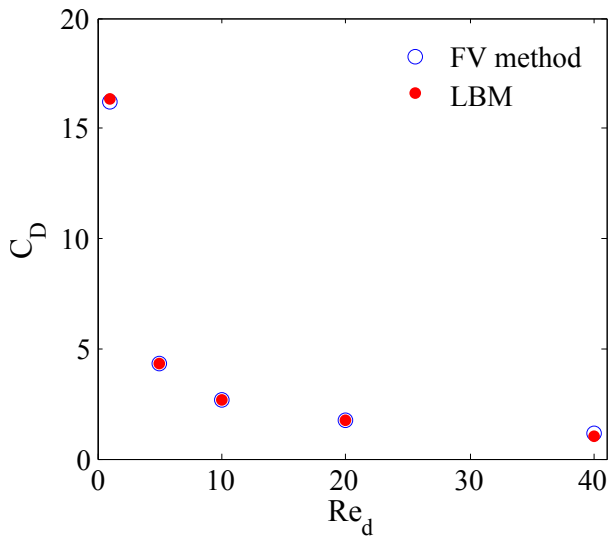

Figure 4.9: Drag coefficient vs. Re_d number.

In order to be more precise about the number of grid resolution which is used to simulate the flow around the cylinder, a sensitivity test study is done. Figure4.10 shows the minimum number of nodes which should be considered for a cylinder in order to have accurate results. Minimum number of 8 nodes per radius of cylinder is required to have accurate results. This number will change by changing the Re_d number (Accurate resolution for $Re = 1$ is $r = 4$).

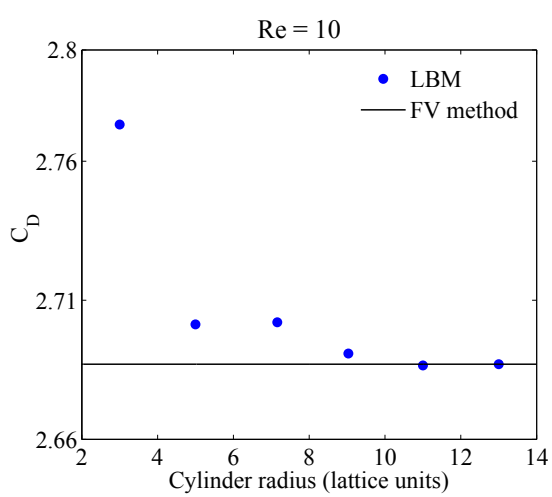

Figure 4.10: Drag coefficient vs. cylinder resolution at $Re_d = 10$.

Figure4.11 shows the contour plot of velocity magnitude around the circular cylinder in $Re_d = 1, 5, 20$ and 40. The result depicts how the flow pattern changes by increasing Re_d number as expected.

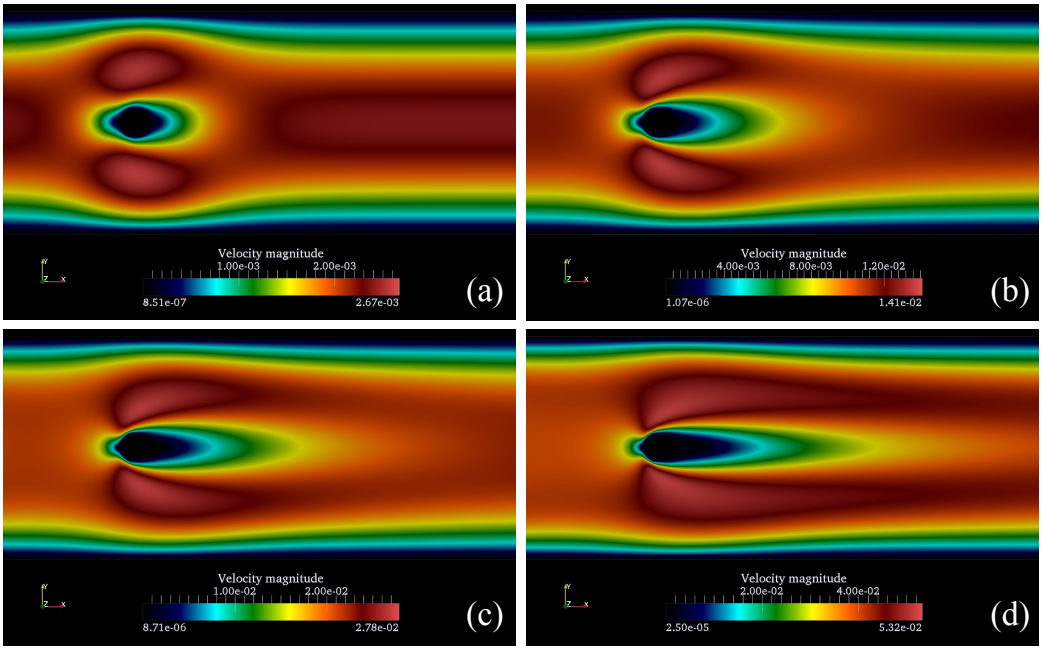

Figure 4.11: Velocity magnitude around circular cylinder at low and moderate Re_d.

4.3.1.3 Pressure driven flow around bundle of 2D cylinders

The third benchmark study is a pressure driven flow around bundle of 2D cylinders in low Reynolds number regime. A periodic arrays of identical cylinders which are oriented perpendicular to the flow are considered. Since the geometry is periodic in this particular case, the solution of the problem is reduced to one cylinder but the boundary conditions is changed to periodic boundaries. The porosity of the geometry can be changed by changing the diameter of the cylinder in the flow domain. Zou and He boundary condition is applied for the inlet and outlet open boundaries. In order to apply the open boundaries, a buffer zone is taken into account before the inlet and after the outlet. This buffer zone must be large enough (in this simulation the size of the buffer zone is $\frac{N_x}{10}$) to minimize the interaction between inlet and outlet of the simulation domain while periodic boundary condition is applied. Second order accurate FHM boundary condition is implemented to

simulate the no-slip condition on the surface of the cylinder more accurately.

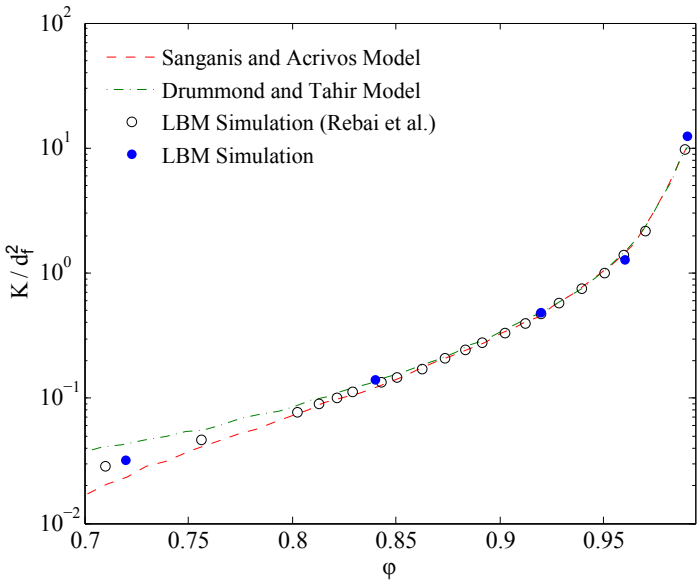

Figure 4.12: Normalized permeability vs. porosity

Results of normalized permeability vs. porosity are presented in Figure4.12. The results are compared to the models presented by[76, 77] and the LBM simulations done by Rebai*et al.*[95]. The discrepancy from analytical models in lower porosities are expected since the models are valid for high porosity media[75].

4.3.1.4 Flow inside a uniform 3D random fibrous structure

The fourth benchmark study is for validation of the 3D code. A uniform distribution of random entangled cylinders are generated to simulate the geometry of fibrous porous media and filter-like structures in different porosities. The geometry made in a way that non of the cylinders can intersect with each other in the simulation domain. Resolution of $r = 4$ is used since the flow is solved in $Re_d < 2$. The aspect ratio of all the cylinders are the same and equal to 5 ($L/d = 5$). For sake of diminishing the huge amount of CPU time and large amount of memory, periodic boundary condition is applied to the side walls of the channel. Zou and He boundary condition is applied for the inlet and outlet open boundaries. In order to apply the open boundaries, a buffer zone is taken into account before the inlet and after the outlet. This buffer zone must be large enough (in this simulation the size of the buffer zone is $\frac{N_x}{6}$) to minimize the interaction between inlet and outlet of

the simulation domain while periodic boundary condition is applied. Second order accurate FHM boundary condition is implemented to simulate the no-slip condition on the surface of each cylinder more accurately. The other details of the simulations is reported in Table4.1. The sample geometry is shown in Figure4.13.

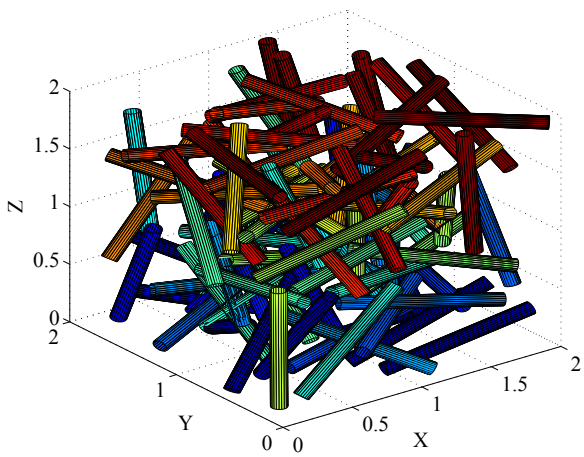

Figure 4.13: Sample uniform 3D fibrous geometry.

Table 4.1: 3D Benchmark test case.

Porosity	No. of cylinders	N_x	N_y	N_z
93.5	340	330	220	220
95.5	234	330	220	220
97.5	132	330	220	220

Results of normalized permeability vs. porosity are presented in Figure4.14. The results are compared to Davies empirical model[75] and the LBM simulations done by Rebai *et al.*[95]. The small discrepancy from empirical model of Davie is expected du to the random nature of the medium and small numerical errors in the LB algorithm and numerical implementation of boundary conditions.

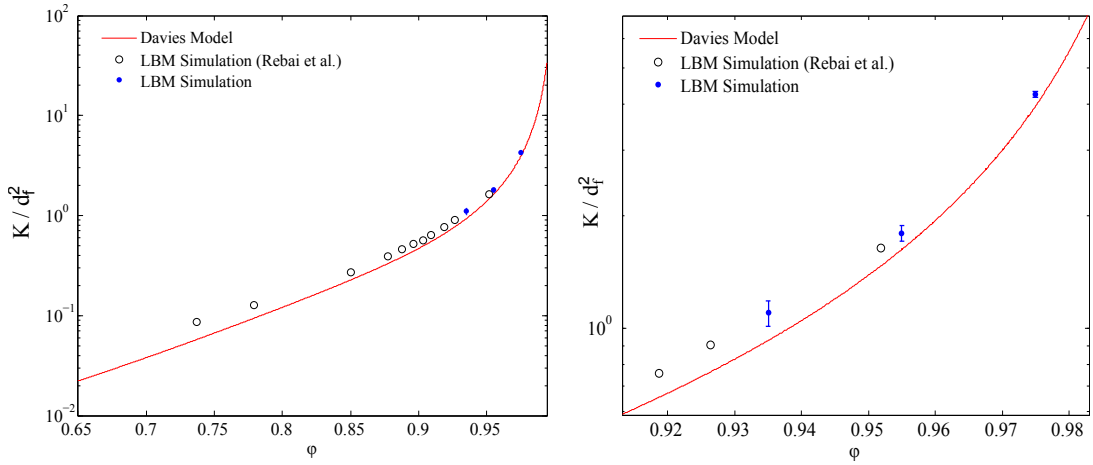

Figure 4.14: Normalized permeability vs. porosity (3D case).

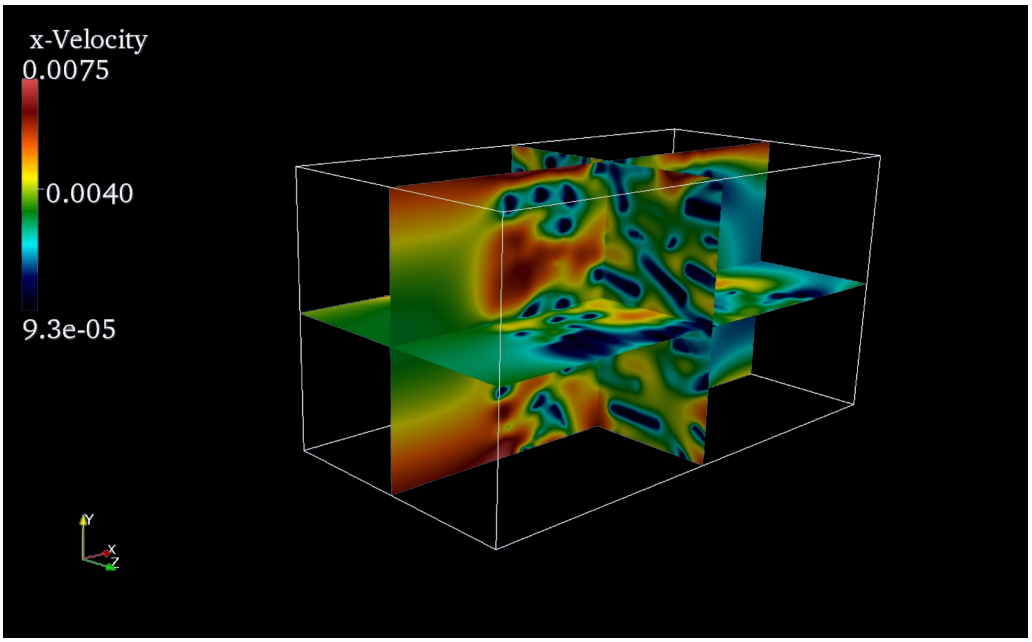

Figure 4.15: X-velocity: 3D uniform random fibrous media.

Figure4.15 shows the x-velocity in three different planes perpendicular to each other in order to show how the pattern of flow changes inside a grossly disordered geometry.

4.3.2 Simulation of flow inside model geometry of a foam-paper

To simplify the complexity of geometry and reduce the computational time of the simulations, a model based on random oriented cylinders are proposed to be used instead of simulating the mesh came out of the tomographic results. Since the geometry of foam-paper is a non-uniform porous geometry, the data for fibre concentration in the thickness of foam-papers is required. This data is provided by Micro X-ray tomography from the cross-sections of the samples as shown in Figure4.16. Figure4.16 actually shows the fibre concentration distribution in the thickness of a foam paper.

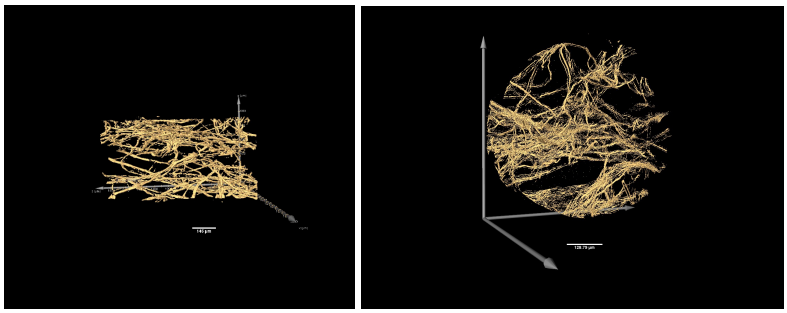

Figure 4.16: Tomographic images of side and top view of a foam-paper.

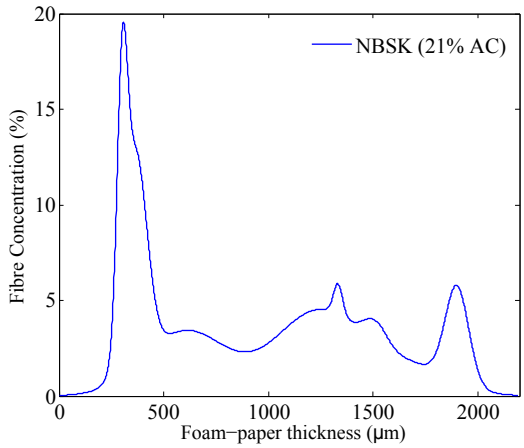

Figure 4.17: Fibre concentration frequency in the thickness of foam-paper.

The result of Figure4.17 is used to generate random numbers from this distribution function

instead of using the uniform random number generator in the thickness direction of the model geometry domain. Figure4.18 shows the random numbers which are generated from the distribution of fibre frequency in the thickness of a foam-paper (results of x-ray tomograph, Figure4.16). The geometry for the simulation is made from these random numbers in two different porosities as reported in Table4.2.

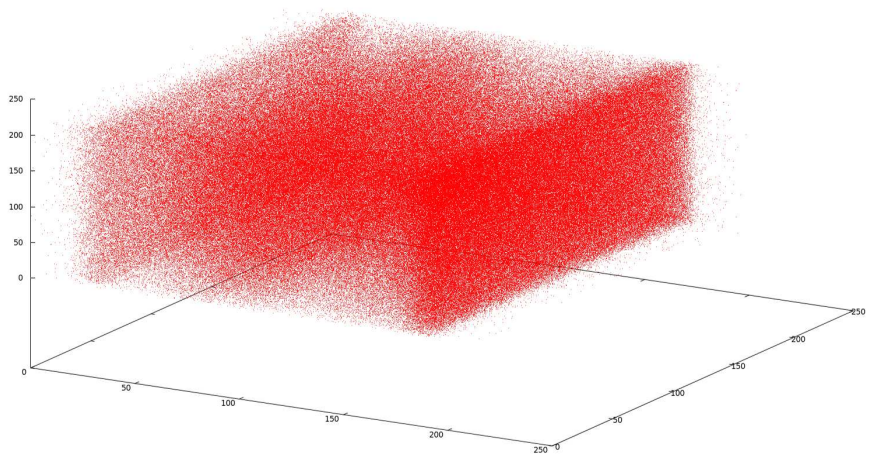

Figure 4.18: Random numbers generated from the distribution of fibre frequency in the thickness of a foam-paper.

Table 4.2: Foam-paper simulation cases.

Porosity	No. of cylinders	N_x	N_y	N_z
93.5	338	330	220	220
95.5	231	330	220	220

Figure 4.19a shows the residual plots for hydrodynamic parameters to illustrate the convergence of the simulations. Since the simulations are done by applying a pressure drop between the inlet and the outlet of the channel, the flowrate will evolve in the simulation. Since the simulations are in low Reynolds regime, the value for the average velocity at the inlet must converge to a constant

value. This condition is another criteria for the convergence of low Re number flows as shown in Figure4.19b. In order to guarantee the stability of simulations, the value of maximum Ma number is presented at each time-step as shown in Figure4.19c (Final value of $Ma_{max} = 0.024$). This value is lower than the critical Ma number value ($Ma_{max} < 0.3$) [79].

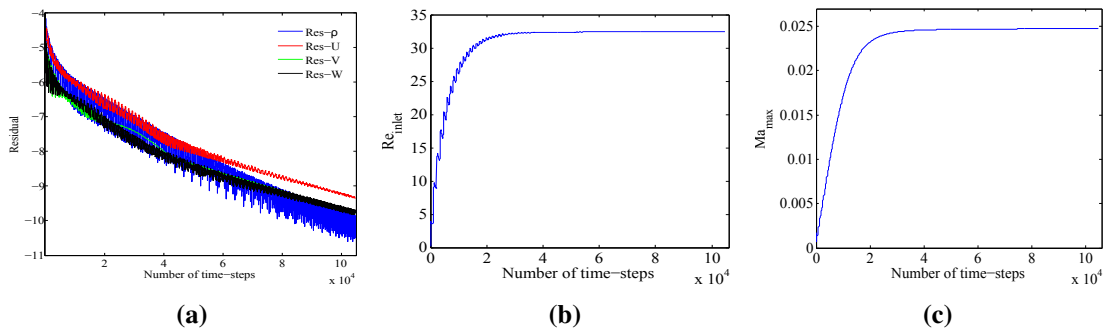

Figure 4.19: Convergence criteria (a) Residuals (b) Re_{inlet} (c) Ma_{max}.

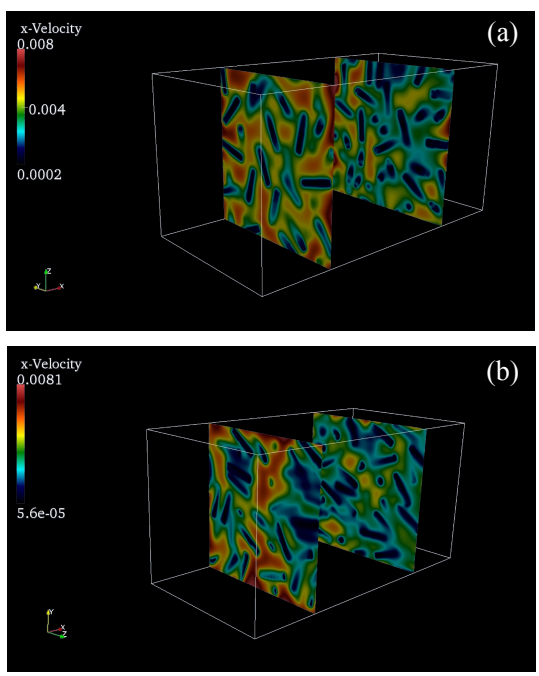

Figure 4.20: Comparing the x-velocity simulation of a foam-paper with a uniform 3D random fibrous media at same porosity.

Figure 4.20 compares the x-velocity simulation of a foam-paper with a uniform 3D random fibrous media at the same porosity. This qualitative result show the difference between the fibres frequency distribution of a foam paper and a uniform medium. The difference between the flow pattern in both geometries are also shown in Figure4.20.

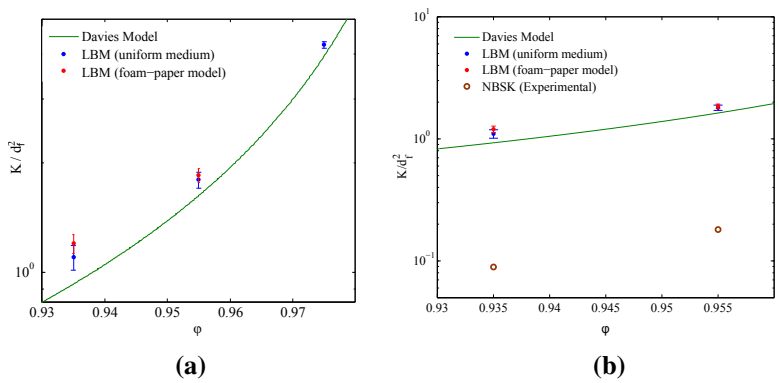

Figure 4.21: Convergence criteria (a) Residuals (b) Re_{inlet} (c) Ma_{max}.

Results of normalized permeability vs. porosity are presented in Figure4.21a. The results are compared to Davies empirical model[75] and the LBM simulations of a uniform 3D random fibrous media which is done by author. The results of foam-paper simulations are compared to the experimental results of actual NBSK foam-paper as shown in Figure4.21b.

Cylinders that are used here for the simulations are rigid bodies and have an aspect ratio of 5 which is much different from the actual foam-paper fibre strands which are flexible and have an aspect ratio range of 60 - 130. It may be said that since the cylinders are stiff as well as random in their arrangement, there are void spaces in between which cannot be occupied. The situation in the real case is much less stringent as the fibres can bend which, is assumed, also increases blockage in flow leading to high tortuosity and low permeability. Also, in the simulations, random generation of fibres is carried out in a way that no two cylinders intersect or are in tangential contact. This is not the case with foam-paper micro-structure as fibre strands are not completely spatially segregated and there may be a large number of points where one single strand is in contact with many other strands. This fact suggests that the flow around a real fibre strand is different in the vicinity of these contacts. A cylinder in simulation on the other hand is completely surrounded by a flow field. Hence there may be some flow leakage in simulations as the fibre-fibre contacts are not taken into account.

Now if there are two different foam-paper blocks both with the same length, cross-section and

average porosity, but one is uniform and the other has a distribution, that is, the local porosity varies along the length, the extent of difference in permeability values for the two different blocks will depend on the porosity distribution of the non-uniform block. If the minimum and maximum local porosities for the non-uniform block have a small difference, the resulting permeability will not be significantly different from that of the uniform block. It is assumed that this will not continue to hold true if there is a huge overall variation in the distribution or steep gradients in porosity along the length.

Chapter 5

Conclusions and final remarks

Since the total amount of paper consumption in the north America was diminished approximately 25% in the past five years, it is necessary to make new products with different applications from cellulose fibres. Foam-forming is one the potential ideas to make new products with various applications out of cellulose fibres. Foam-forming process can be simply implemented and attached to an automated paper-machine. The 3D, honeycomb structure of foam leads to making high porous materials out of cellulose fibres called foam-paper. The experimental tests show pretty reasonable results in aerosol filtration of sub-micron particles, heat insulation and sound absorption.

In the sub-micron air-filtration tests, foam papers made by NBSK and CTMP pulp can not be used as efficient filters because of their poor filtration properties. However, the results show that the key parameters for making efficient filters from cellulose fibres are crowding number and fibre specific surface. The experimental results show that having 10% to 30% weight ratio of NBSK valley beaten fibres in the structure of foam-papers improves both their mechanical properties and filtration characteristics compared to the commercial filters. Moreover, foam papers made by nanofibrillated fibres show excellent filtration properties at high foam air-contents. The only problem is that the process of making them (Freeze-drying) is not economically affordable. Moreover, at very high foam air-contents they show very poor mechanical properties. For the next step, the author recommends to do a research on filtration properties of air-dried foam-papers by adding different weight ratio of nanofibrillated fibres to their structure.

Comparing the results of thermal conductivity of NBSK foam-papers with commercial heat insulators show that the new products made in high foam air-content can be used as heat insula-

tors. Multilayer NBSK foam-papers also show reasonable acoustic properties. However, the best results are obtained from samples which are made by nanofibrillated fibres. Overall, based on the experimental data in the range of the experiments of this dissertation, there is a possibility to think about commercialization, however doing much more research is required.

Understanding the physics of the flow inside the disordered geometries of foam-papers is another aim of this research. Practically, it is hard to use regular Navier-Stokes solvers for these kind of geometries because of so many issues which has already been discussed in this thesis. An OpenMP parallel C/C++ code for handling large data structures is developed for multi-core machines in Linux platform. Since lattice Boltzmann method is a local numerical algorithm, it can be massively parallelized for parallel machines. In the modeling of foam-papers using the model geometries of cylinder, it should be noted that due to computational constraints, the number of fibres that is used in the simulations is less than what it actually is in the foam-paper geometry. Nevertheless, the simulations may be considered to be a preliminary step to numerically studying the flow through foam-paper media as they do provide ample amount of qualitative information about nature of flow through this kind of domains which have highly randomized geometries. More precise results may be obtained by carrying out the simulations for a larger ensemble of fibres as that is expected to be a better statistical approximation of the porous medium. Also the random fibre generator can be improved to mimic the real geometry. Aspect ratio of cylinders used in the simulations is kept at 5 whereas in reality it is in the rage of 60 - 130. Also the real fibres are present in bent and twisted shapes and are in contact with other fibres. This geometrical details should be analysed and taken into consideration for randomly generating the fibres.

Bibliography

[1] Jim Ford; Susan Kinsella; Gerard Gleason; Andrew Goldberg; Robin Averbeck. The state of the paper industry. 2011. → pages ix, 1, 2

[2] Timo Lappalainen and Jani Lehmonen. Determinations of bubble size distribution of foam-fibre mixture using circular hough transform. *NORDIC Pulp and Paper Research*, 27 (5):930–939, 2012. → pages 6, 10

[3] D. Weairea and R. Phelana. A counter-example to kelvin's conjecture on minimal surfaces. *Philosophical Magazine Letters*, 69(2):107–110, 1994. → pages 7

[4] Christopher James William Breward. *The Mathematics of Foam*. PhD thesis, The University of Oxford, 1999. → pages 7

[5] J.C.Isarin; A.D.J.Kaasjager and R.B.M.Holweg. Bubble size distribution during the application of foam to fabrics and its effects on product quality. *Philosophical Magazine Letters*, 65(2):61–69, 1985. → pages 8

[6] Samuel P. Gidoa; Douglas E. Hirta; Susan M. Montgomerya; Robert K. Prud'hommea and Ludwig Rebenfelda. *Journal of Dispersion Science and Technology*, (6):785–793. → pages 8

[7] A.B.J. Kroezen; J. Groot Wassink and C.A.C. Schipper. *Journal of the Society of Dyers and Colourists*, pages 393–400. → pages 8

[8] A.B.J. Kroezen and J. Groot Wassink. *Journal of the Society of Dyers and Colourists*, pages 397–401. → pages 8

[9] D. E. Hirt; R. K. Prud'homme and Ludwig Rebenfeld. *AIChE Journal*, (6):326–328. → pages 8

[10] R. C. Chang; H. M. Schoen and C. S. Grove. *Industrial and Engineering Chemistry*, (11): 4a–6a. → pages 8

[11] K. A. Brakke. *Experimental mathematics 1*, pages 141–165. → pages 8

[12] Yi Jiang. Extended large- q potts model simulation of foam drainage. *Philosophical Magazine Letters*, 74(2):119–128, 1996. → pages 8

[13] J.J.Bikerman. *Foams*. Springer-Verlag, 1973. → pages 9

[14] John P. Heller and Murty S. Kuntamukkula. Critical review of the foam rheology literature. *Industrial and Engineering Chemistry Research*, 26(2):318–325, 1987. → pages 9, 12, 14

[15] M.J. Rosen and J.T. Kunjappu. *Surfactants and interfacial phenomena*. John Wiley and Sons., 2012. → pages 10

[16] Liguang Wang and Roe-Hoan Yoon. Effects of surface forces and film elasticity on foam stability. *International Journal of Mineral Processing*, 85(4):101–110, 2008. → pages 10

[17] W. B. Russel; D. A. Saville and W. R. Schowalter. *Colloidal Dispersions*. Cambridge, 1989. → pages 11

[18] J. A. Krug. *Oil gas journal*, 73, 1975. → pages 11

[19] C. L. Wendorff and R. B. Ainley. *Presented at the Annual Fall Meeting of the Society of Petroleum Engineers*, 73, 1981. → pages 11

[20] J. D. Lincicome. *World oil*, 28, 1984. → pages 11

[21] J. O. Sibree. The viscosity of froth. *Trans. Faraday Soc*, 28:325–331, 1934. → pages 11

[22] C.S.Grove; G.E.Wise; W.C.March and J.B.Gray. Viscosity of fire fighting foam. *Ind. Eng. Chem.*, 43:1120–1122, 1951. → pages 11

[23] S.S.Marsden and S.A.Khan. The flow of foam through short porous media and apparent viscosity measurements. *Soc. Pertrol Eng.*, 6:17–25, 1966. → pages 12

[24] R. J.; Stelson T. E Wenzel, H. G.; Brungraber. The viscosity of high expansion foam. *J. Mater*, 5:396–400, 1970. → pages 12

[25] J.T. Patton; H. Belkin; S. Holbrook and M. Kuntamukkula. Rheology of mobility-control foams. *Soc. Petrol Eng.*, 23:456–460, 1983. → pages 12

[26] G.J.Hirasaki and J.B.Lawson. Mechanisms of foam flow in porous media: apparent viscosity in smooth capillaries. *Annual Technical Conference and Exhibition of the Society of Petroleum Engineers, San Francisco, CA*, 1983. → pages 12, 13, 14

[27] A. M. Kraynik. *Annual Meeting of the Society of Rheology, Evanston, IL*, 1982. → pages 13

[28] H.M.Princen. Rheology of foams and highly concentrated emulsions. i. elastic properties and yield stress of a cylindrical model system. *Journal of colloidal interface science*, 1983. → pages 13

[29] B Radvan and A.P.J Gatward. The formation of wet-laid webs by a foaming process. *TAPPI*, 55(5):748–751, 1972. → pages 15, 18

[30] M.K Smith and V.W Punton. The role of the forming process in determining the structure and properties of paper. *Pulp and Paper Canada*, 76(2):114–117, 1975. → pages 15, 18

[31] R.W. Tringham and M.A. Manager. New developments in Radfoam process. *Paper Technology*, pages 288–294, 1974. → pages 15

[32] V.W Smith, M.K; Punton and A.G Rixson. The structure and properties of paper formed by a foaming process. *TAPPI*, 57(1):107–111, 1974. → pages 15, 18

[33] T. Lappalainen and J. Lehmonen. Determinations of bubble size distribution of foam-fibre mixture using circular hough transform. *NORDIC Pulp and Paper Research*, 27(5): 930–939, 2012. → pages 15

[34] H.; Salmela J.; Poranen, J.; Kiiskinen and J. Asikainen. Breakthrough in papermaking resource efficiency with foam. *TAPPI journal*, pages 1688–1695, 2013. → pages 16

[35] W.C.Hinds. *Aerosol Technology: Properties, Behavior and Measurement of Airborne Particles.* J. Wiley and Sons. New York. USA., 1982. → pages 27

[36] R.C.Brown. *Air Filtration*. Pergamon Press Inc., New York, USA., 1993. → pages 27, 31

[37] J. Seinfeld and P. Spyros. *Atmospheric Chemistry and Physics: From Air Pollution to Climate Change*. John Wiley and Sons, Inc., 2006. → pages 27, 28

[38] KW Lee and B.Y.H. Liu. On the minimum efficiency and the most penetrating particle size for fibrous filters. *Air Pollution Control Association Journal*, 30(4):337–381, 1972. → pages 28

[39] J.A. Pritchard. A guide to industrial respiratory protection. *National Institute for Occupational Safety and Health. Cincinnati, OH.*, pages 5–8, 1976. → pages 29

[40] Clarke A. Rodman and Richard C. Lessmann. Automotive nonwoven filter media: their constructions and filter mechanisms. *TAPPI*, pages 161–168, 1988. → pages 30

[41] Jingliang Mao, Biljana Grgic, Warren H. Finlay, John F. Kadla, and Richard J. Kerekes. wood pulp based filters for removal of submicrometer aerosol particles. *NORDIC Pulp and Paper Research*, 23(4):420–425, 2008. → pages 30

[42] Alan L. Macfarlane, John F. Kadla, and Richard J. Kerekes. High Performance Air Filters Produced from Freeze-Dried Fibrillated Wood Pulp: Fiber Network Compression Due to the Freezing Process. *Industrial and Engineering Chemistry Research*, 51(32): 10702–10711, 2012. → pages 30

[43] C. Tseng, M. Yamaguchi, and T. Ohmori. Thermal conductivity of polyurethane foams from room temperature to 20 K. *Cryogenics*, 37(6):305–312, 1997. → pages 40

[44] A.J. Loeb. Thermal conductivity: Viii, a theory of thermal conductivity of porous materials. *American Ceramic Soc.*, 37(2):96, 1954. → pages 40

[45] J.C. Maxwell. *A Treatise on Electricity and Magnetisim*. Dover, Newyork, 1954. → pages 40

[46] H.W.Russel. Principles of heat flow in porous insulation. *American Ceramic Soc.*, 18(1): 96, 1935. → pages 40

[47] G. Reichenauer; U. Heinemann and H.P. Ebert. Relationship between pore size and the gas pressure dependence of the gaseous thermal conductivity. *Colloids Surf.*, pages 204–207, 2007. → pages 40

[48] David S. Smith; Arnaud Alzina; Julie Bourret; Benoit Nait-Ali; Fabienne Pennec and Nicolas Tessier-Doyen. Thermal conductivity of porous materials. *Journal of Materials Research*, 28(17):2260–2272, 2013. → pages 41

[49] J.P. Arenas and M.J. Crocker. Recent trends in porous sound-absorbing materials. *Sound and Vibration, Materials Reference Issue*, 2010. → pages 47

[50] A.F. Seybert and D.F. Ross. Experimental determination of acoustic properties using a two microphone random excitation technique. *Journal of the Acoustical Society of America*, pages 1362–1370, 1977. → pages 48

[51] W. Lauriks; J. F. Allard and A. Cops. Inhomogeneous plane waves in layered media. *Physical Acoustics*, pages 425–431, 1991. → pages 48

[52] J.F. Allard. *Propagation of Sound in Porous Media: Modelling Sound Absorbing Materials*. Chapman and Hall, 1993. → pages 48

[53] Vigran T.E.; Kelders L.; Lauriks W.; Leclaire P. and Johansen T.F. Prediction and measurements on the in?uence of boundary conditions in a standing wave tube. *Acustica/Acta Acustica*, pages 419–423, 1997. → pages 48

[54] Yvan Champoux and Michael R. Stinson. *Journal of accoustical society of America*, (2), . → pages 48

[55] Yvan Champoux and Michael R. Stinson. *Journal of accoustical society of America*, (4), . → pages 48

[56] K. Attenborough. Acoustical characteristics of rigid fibrous absorbents and granular materials. *Journal of accoustical society of America*, 73:785–799, 1983. → pages 48, 49

[57] Y. Izumi; T. Iwase and R. Kawabata. A new measuring method for sound propagation constant by using sound tube without any air spaces back of a test material. *J. Internoise*, 98, 1998. → pages 48

[58] Y. Salissou and R. Panneton. Wideband characterization of the complex wave number and characteristic impedance of sound absorbers. *Journal of accoustical society of America*, 128, 2010. → pages 48

[59] O. Doutres; Y. Salissou; N. Atalla and R. Panneton. Evaluation of the acoustic and non-acoustic properties of sound absorbing materials using a three-microphone impedance tube. *Journal of Applied Acoustics*, 71(6):506–509, 2010. → pages 48

[60] M. Delany and E. Bazley. Acoustical properties of fibrous absorbent materials. *Journal of Applied Acoustics*, 24(1):63–70, 1988. → pages 49

[61] Y. Miki. Acoustical properties of porous materials: modifications of delany-bazley models. *J.Acoust. Soc. Jp.*, 11(1):19–28, 1990. → pages 49, 53

[62] M.A. Biot. Theory of propagation of elastic waves in a fluid-saturated porous solid. i. low frequency range, ii. higher frequency range. *Journal of accoustical society of America*, 28, 1956. → pages 49

[63] D.L. Johnson; J. Koplik and R. Dashen. Theory of dynamic permeability and tortuosity in fluidsaturated porous media. *Journal of Fluid Mechanics*, 176:379–402, 1987. → pages 49

[64] J.F. Allard and Y. Champoux. New empirical equations for sound propagation in rigid frame fibrous materials. *Journal of accoustical society of America*, 9:3346–3353, 1992. → pages 49

[65] T.; N. Tsujiuchi Koizumi and A. Adachi. The development of sound absorbing materials using natural bamboo fibers. *WIT Press*, 2002. → pages 49, 50

[66] Y.E. Lee and C.W. Joo. Sound absorption properties of recycled polyester fibrous assembly absorbers. *AUTEX Research Journal*, 3(2), 2003. → pages 49

[67] M. Ren and F. Jacobsen. A method of measuring the dynamic flow resistance and reactance of porous materials. *Applied Acoustics*, 39(4):265–276, 1993. → pages 49

[68] J. Conrad. *Engineering Acoustics and Noise Control*. Prentice-Hall, 1983. → pages 50

[69] Y. Shoshani and Y. Yakubov. Use of nonwovens of variable porosity as noise control elements. *I.N.J*, 2003. → pages 50

[70] M.A. Ibrahim and R.W. Melik. Physical parameters affecting acoustic absorption characteristics of fibrous materials. *Proceedings of the mathematical and physical society of Egypt*, 1978. → pages 50

[71] M. Coates and M. Kierzkowski. Technical-textiles-international. *Acoustic Textiles - Lighter, Thinner and More Absorbent*, 2002. → pages 50

[72] A. Tamayol and M. Bahrami. Analytical determination of viscous permeability of fibrous porous media. *International Journal of Heat and Mass Transfer*, 52(9):2407–2414, 2009. → pages 56

[73] F. E. Teruel. Characterization of a porous medium employing numerical tools: Permeability and pressure-drop from darcy to turbulence. *International Journal of Heat and Mass Transfer*, 52(25):5878–5888, 2009. → pages 56

[74] D. Shou; J. Fan and F. Ding. Hydraulic permeability of fibrous porous media. *International Journal of Heat and Mass Transfer*, pages 4009–4018, 2011. → pages 56

[75] C.N. Davies. The separation of airborne dust and particles. *Proceedings of Institute of Mechanical Engineers, London*, 1952. → pages 56, 82, 83, 88

[76] J. Drummond and M. Tahir. Laminar viscous flow through regular arrays of parallel solid cylinders. *International Journal of Multiphysics Flow*, 1984. → pages 82

[77] A. Sangani and A. Acrivos. Laminar viscous flow through regular arrays of parallel solid cylinders. *International Journal of Multiphysics Flow*, pages 193–206, 1982. → pages 56, 82

[78] C. Cercignani. *The Boltzmann equation and its applications*. Springer-Verlag, New York, 1988. → pages 60

[79] S. Succi. *The Lattice Boltzmann Equation for Fluid Dynamics and Beyond*. Oxford Science Publications. → pages 60, 62, 63, 65, 66, 68, 69, 74, 87

[80] M. Kardar. *Statistical Physics of Particles*. Cambridge University Press, 2007. → pages 60

[81] D.A. Wolf-Gladrow. *Lattice-gas cellular automata and lattice Boltzmann models: an introduction*. 2000. → pages 61, 62

[82] E. R. Berlekamp; J. H. Conway and R. K. Guy. *Winning ways for your mathematical plays*. Academic Press, New York, 1984. → pages 62

[83] M. Garder. The fantastic combinations of conway's new solitaire game of "life". *Science America*, 1970. → pages 62

[84] M. Garder. Geometric fallacies: hidden errors pave the road to absurd conclusions. *Science America*, 1971. → pages

[85] M. Garder. On cellular automata, self-reproduction, the garden of eden and the game "life". *Science America*, 1971. → pages 62

[86] G.D. Doolen; U. Frisch; B. Hasslacher; S. Orszag and S. Wolfram. *Lattice Gas Methods for Partial Differential Equations*. Academic Press, New York. → pages 62

[87] G. McNamara and G. Zanetti. Use of the boltzmann equation to simulate lattice gas automata. *Physical Review Letter*, 61:2332, 1988. → pages 62

[88] F. Higuera and J. Jimenez. Boltzmann approach to lattice gas simulations. *Europhys. Lett.*, 9:663, 1989. → pages 62, 63

[89] P. Bhatnagar; E. Gross and M. Krook. A model for collision process in gases i: Small amplitude processes in charged and neutral one component system. *Phys. Rev.*, 94:511, 1954. → pages 63

[90] Y. Qian; D. d'Humieres and P. Lallemand. Lattice bgk models for the navier-stokes equation. *Europhys. Lett.*, 17:479, 1992. → pages 63

[91] Martin Hecht and Jens Harting. Implementation of on-site velocity boundary conditions for d3q19 lattice boltzmann simulations. *Journal of Statistical Mechanics: Theory and Experiment*, 10:1018, 2010. → pages 64

[92] S. Chapman and T. Cowling. *Mathematical Theory of Non-Uniform Gases*. Cambridge University Press. → pages 65

[93] X. Shan and H. Chen. Lattice boltzmann model for simulating flows with multiple phases and components. *Phys. Rev. E*, 47:1815–1819, 1993. → pages 67

[94] Martin Hecht and Jens Harting. Lattice boltzmann method for fluid flows. *Annual Review of Fluid Mechanics*, 30:329–364, 1998. → pages 67

[95] M Rebai, F Drolet, and D Vidal. A Lattice Boltzmann approach for predicting the capture efficiency of random fibrous media. *Asia Pacific Journal of Chemical Enginering*, pages 29–37, 2011. → pages 67, 82, 83

[96] O. Filippova and D. Hanel. Lattice-bgk model for low mach number combustion. *Int. J. Mod. Phys. C*, 9:1439, 1998. → pages 67

[97] S. Chen; H. Chen; D. Martinez and W. Matthaeus. Lattice boltzmann model for simulation of magnetohydrodynamics. *Phys. Rev. Lett.*, 67:3776–3779, 1991. → pages 67

[98] O. Filippova; S. Succi; F. Mazzocco; C. Arrighetti; G. Bella and D. Hanel. Multiscale lattice boltzmann schemes with turbulence modeling. *Int. J. Mod. Phys. C*, 170:812829, 2001. → pages 67

[99] M.L.R; D.B. Bingham Thomas and M. Pourkashanian. Prediction of the permeability of fibrous porous media using the lattice boltzmann method in conjuction with coarse numerical lattices. *Open Transport*, pages 80–89, 2010. → pages 67

[100] R. Przekop and L. Gradon. Non-steady-state aerosol filtration in nanostructured fibrous media. *Philosophical transactions. Series A, Mathematical, physical, and engineering sciences*, 369:2476–2484, 2011. → pages 67

[101] O. Filippova and D. Hanel. Grid refinement for lattice-bgk models. *Journal of Computational Physics*, 14:219–228, 1998. → pages 68

[102] D. Yu; R. Mei; L. Luo and W. Shyy. Viscous flow computations with the method of lattice boltzmann equation. *Progress in Aerospace Sciences*, 39:329–367, 2003. → pages 68, 69, 75

[103] Urpo Aaltosalmi. *Fluid flow in porous media with the Lattice-Boltzmann method.* PhD thesis, University of Jyvaskyla, 2005. → pages 68

[104] Chen Peng. The lattice boltzmann method for fluid dynamics: Theory and applications., 2013. → pages 68

[105] Q. Zou and X. He. On pressure and velocity boundary conditions for the lattice boltzmann bgk model. *Physics of Fluids*, 9:1591, 1997. → pages 68, 72, 73, 74, 75

[106] T. Inamuro; M. Yoshina and F. Ogino. A non-slip boundary condition for lattice boltzmann simulations. *Physics of Fluids*, 7:2928–2930, 1995. → pages 68

[107] P. A. Skordos. Initial and boundary conditions for the lattice boltzmann method. *Phys. Rev. E*, 48:4823–4842, 1993. → pages 69

[108] J. Verschaeve and B. Muller. A curved no-slip boundary condition for the lattice boltzmann method. *Journal of Computational Physics*, 2010. → pages 69

[109] C. Zheng Z. Guo and B. Shi. An extrapolation method for boundary conditions in lattice boltzmann method. *Phys. Fluids*, 14:2007–2010, 2002. → pages 69

[110] D. Hanel O. Filippova. Boundary setting and local grid refinement for lattice-bgk models. *International Journal of Modern Physics C*, 9:1271–1279, 1998. → pages 69, 71, 72

[111] R. Mei; L.S. Luo and W. Shyy. An accurate curved boundary treatment in the lattice boltzmann method. *Journal of Computational Physics*, 155:307–330, 1999. → pages 69, 71, 72

[112] M. Bouzidi; M. Firdaouss and P. Lallemand. Momentum transfer of a lattice boltzmann uid with boundaries. *Phys Fluids*, 2001. → pages 69

[113] James D. Sterling and Shiyi Chen. Stability analysis of lattice boltzmann methods. *Journal of Computational Physics*, 123(1):196–206, 1996. → pages 74, 75

[114] D. DHumieres; I. Ginzburg; M. Krafczyk; P. Lallemand and L. Luo. Multiple relaxation time lattice boltzmann models in three dimensions. *Philosophical transactions*, 360: 437–51, 2002. → pages 75

[115] P. Lallemand and L.S. Luo. Theory of the lattice boltzmann method: Dispersion, dissipation, isotropy, galilean invariance, and stability. *Physical Review E*, 61:6546–6562, 2000. → pages 75